MICROCOPY RESOLUTION TEST CHART
NATIONAL BUREAU OF STANDARDS-1963

DTIC FILE COPY

DTIC
SELEC
MAR 3 1 1988
S
D

A STUDY OF FAILURE CHARACTERISTICS IN

THERMOPLASTIC COMPOSITE MATERIAL

THESIS

Robert John Martin
First Lieutenant, USAF

AFIT/GA/AA/88M-2

DEPARTMENT OF THE AIR FORCE

AIR UNIVERSITY

# AIR FORCE INSTITUTE OF TECHNOLOGY

Wright-Patterson Air Force Base, Ohio

LECTE

A STUDY OF FAILURE CHARACTERISTICS IN

THERMOPLASTIC COMPOSITE MATERIAL

THESIS

Robert John Martin
First Lieutenant, USAF

AFIT/GA/AA/88M-2

A STUDY OF FAILURE CHARACTERISTICS IN

THERMOPLASTIC COMPOSITE MATERIAL

THESIS

Presented to the Faculty of the School of Engineering

of the Air Force Institute of Technology

Air University

In Partial Fulfillment of the

Requirements for the Degree of

Master of Science in Astronautical Engineering

Robert John Martin

First Leiutenant, USAF

March 1988

x-rays and providing facilites for analyzing the videotape;
and to Ed Porter of the Materials Lab for producing the
x-rays in such a short amount of time.  Thanks also goes to
the Technical Photographic Division of the 4950th Test Wing
for printing the photographs in this thesis and to Jack
Smith for helping with the logistics of ordering the
numerous photos.  And at AFIT's School of Engineering, I
extend much thanks to Mr. Nick Yardich for providing
equipment support.

Lastly, I wish to dedicate this thesis to my parents,
Bob and Patty Martin.  I am ultimately indebted to them for
their long distance support during this study and for their
influence on me to pursue such a career.  My father
published his thesis 25 years ago this month, and I always
seem to follow in his footsteps....

# Table of Contents

# List of Figures

ix

# List of Tables

## Abstract

Space facilities of the next decade will require
applications of highly advanced materials which have
properties exhibiting excellent fracture toughness and high
strength-to-weight ratios. The recently introduced
thermoplastic composite material, graphite polyetherether-
ketone (Gr/PEEK) APC-2, promises lower costs, lower part
weight, and higher operating temperatures. This new class
of organic material has fracture toughness properties
superior to those of graphite epoxy. This thesis examines
the failure characteristics of Gr/PEEK through an
experimental investigation and through the application of a
fully nonlinear ply-by ply finite element technique.
Laminates investigated were $[0_{16}]$ and $[90_{16}]$ unidirectional
lay-ups and $[\pm 45]_{4S}$ angle-ply lay-ups. An experimental
investigation was also done on $[0/45/90/-45]_{2S}$ and
$[0/\pm 45/90]_{2S}$ quasi-isotropic lay-ups to study failure
characteristics.

The experimental investigation of Gr/PEEK APC-2
involved the testing of 34 tension and compression coupons
to derive basic material properties for use with the finite
element program. To investigate failure characteristics
experimentally, 78 tensile specimens were manufactured with

0.4-inch diameter holes. A portion of these unidirectional, shear, and quasi-isotropic specimens where tested at room temperature to ultimate strength. The remaining specimens were tested to percentages of average failure stress to investigate the initiation and progression of laminate failure. To supplement the test results, two post-failure analyses were conducted. Videotapes were made of each test to ultimate strength. Also stereo x-rays were taken of each test specimen subjected to a percentage of failure load.

For comparison to experimental results, a fully nonlinear progressive-ply-failure finite element program was employed. The models of stress-strain responses and growth of failure were found to closely approximate the results of the experimentation.

This investigation provided futher data on the application of tensile loads to Gr/PEEK containing circular discontinuities. This study also proved that a nonlinear finite element program can closely approximate progressive ply failure in a Gr/PEEK laminate. The excessive nonlinearity of this material proved the need for using nonlinear techniques when analyzing laminates of Gr/PEEK. Furthermore, this research reinforced the proposition that the thermoplastic matrix does produce a reliable composite that should be considered for use on aircraft, spacecraft, and space facilities.

# A STUDY OF FAILURE CHARACTERISTICS IN
# THERMOPLASTIC COMPOSITE MATERIAL

## I.   Introduction

Man has studied materials and their failure mechanisms
since he began building facilities, seeking transportation,
and manufacturing goods.  Knowing how a material fails under
given loading conditions leads to improvements in material
capabilities.  The study over time of earth, wood, metals,
and plastics has led to more advanced materials;  and often
materials have been combined to produce optimum effects.
Over the past few decades, this idea of combination has led
researchers to develop advanced composite materials.

In the next decade, space facilities and spacecraft
will require application of highly advanced materials that
have properties which exhibit high fracture toughness, high
strength-to-weight ratio, and low thermal expansion.  The
recently introduced polyether-based thermoplastic composite
material, graphite polyetherether-ketone (Gr/PEEK) promises
lower costs, lower part weight, and higher operating
temperatures.  This new class of organic material has a
fracture toughness much higher than that of graphite epoxy
(Gr/Ep) [1].  In general, thermoplastics promise lower
production costs and improved maintainability over similar
thermosets such as Gr/Ep [2].

1

By studying the stress-strain response to ultimate strength and the initiation and progression of failure in this new composite material, this thesis contributes to the vigorous research effort being conducted by many groups to evaluate Gr/PEEK thermoplastic composite material for practical applications.

A.  Purpose

The purpose of this thesis is to investigate the initiation and progression of failure in Gr/PEEK containing a circular discontinuity and subjected to tensile loading. With this purpose in mind, the objectives of this study were:

(1)  To determine basic material properties for the Gr/PEEK at room temperature (RT),

(2)  To determine the experimental stress-strain response of $[0_{16}]$ and $[90_{16}]$ unidirectional laminates, $[\pm 45]_{4s}$ angle-ply laminates, and $[0/+45/90/-45]_{2s}$ and $[0/\pm 45/90]_{2s}$ quasi-isotropic laminates of Gr/PEEK specimens containing a 0.4-inch diameter circular discontinuity and loaded to ultimate strength at RT,

(3)  To experimentally investigate the initiation and progression of failure in similar specimens containing a hole and loaded to percentages of average failure stress,

(4)  To analytically model the failure process of the unidirectional and angle-ply laminates using a fully

nonlinear, progressive-ply-failure finite element program, and

(5) To compare experimental results of the quasi-isotropic specimens and to investigate their potential for delamination by comparison to Gr/Ep.

These objectives were accomplished; and the report of all theories, procedures, results, and conclusions is contained in this thesis.

## B. Background and Overview

A composite material, as defined in this thesis, is a material consisting of reinforcements, such as fibers, in a continuous matrix, such as a polymer. These two constituents are combined on a macroscopic scale to form a useful material.

Composites have a long history of use. Prehistoric civilizations used straw in mud bricks; plywood existed in early Egyptian construction; and medieval knights used combinations of various metals in their swords [3]. In the last century, reinforced concrete began to give engineers greater applications in construction.

Conventional composite materials, or "reinforced-plastic" (RP), was first commercialized as fiberglass in 1939. Fiberglass still accounts for 90% of the RP market [4]. But the emphasis on research in the past few decades has been on advanced composite materials.

The adjective `advanced` is used to distinguish between composites of new ultrahigh strength and stiffness fibers and composites of familiar fibers such as glass. The matrix of these new composites can be either a plastic, such as epoxy, or a metal, such as aluminium. These advanced composites have two major advantages among many others: (1) improved strength-to-weight and stiffness-to-weight ratios and (2) the ability to tailor a composite to meet design requirements.

Composite components can be made that have the same strength and stiffness as high strength steel components but are 70% lighter. Some advanced composites are up to three times stronger than aluminum but are 60% lighter. These advanced composite materials are ideal for weight-sensitive structural applications such as space structures and space vehicles. Some examples of current use include the motor casings on the space shuttle solid-fuel rockets [4] and the wings of the X-29 forward-swept-wing developmental aircraft. The F-15 and F-16 have proven the value of composites in their use as horizontal and vertical stabilizers.

Tailoring a composite to meet strength and stiffness requirements in particular directions leads to economy of manufacturing. Because fibrous composites are anisotropic, i.e., material properties are different in all directions, components can be designed for strength and stiffness in a particular direction. There is little waste. Part

consolidation and reduction of post-fabrication machining provide up to 50% cost savings over analogous machined-metal assemblies [3]. Conventional isotropic materials must be designed for the worst case, resulting in excess strength, stiffness, and weight in all other directions [3]. These advantages of composite materials promise to lead to new aircraft and spacecraft designs that significantly depart from past efforts based on conventional isotropic materials.

In the composite industry, the dominant reinforcement of composite materials is continuous fibers (as opposed to whiskers, filaments, or spheres of reinforcing material). Throughout this thesis, reference to composites will imply continuous-fiber-reinforced composite materials. Also throughout this thesis, reference to composites will imply the use of a polymer-based matrices, such as epoxy or PEEK.

In applications of composite materials, the conventional problems of design and analysis arise. As in any structure, composite components, or laminates, have to have holes to serve various purposes. In practice, composite components are connected through adhesively bonded joints, through bolted joints, or through a combination of each. Whether caused by bolts, or in hostile environments by bullets or even meteorites, holes in laminates lead to analysis and design problems in composites that are unique from conventional isotropic metals. Loads are not easily redistributed around a hole in the non-homogeneous material,

and discontinuous fibers cause shear lag effects which lead to design difficulties [3].

The numerous difficulties in determining the tensile strength of notched composite laminates involve the consideration of an infinite number of parameters which include:

(1)  The infinite number of possible ply lay-ups, or stacking sequences,

(2)  The great variety of fibers, matrices, and fiber/matrix combinations,

(3)  The uncertain and inconsistency of failure criteria,

(4)  The infinite variety of geometries (thicknesses, notch size and shape, width-to-hole size, etc.), and

(5)  The great variety of environmental conditions influencing the behavior of composites.

The techniques available for the prediction of strength reduction or ultimate strength in a material with a hole are almost as numerous.  In general, the techniques include finite element methods [5, 6, 7, 8] and fracture mechanics approaches [3, 9, 10, 11, 12].

Fracture is caused by higher stresses around holes, cracks, or flaws in the material.  Fracture has a new dimension in composite materials because of the presence of two or more constituents.  In analyzing the failure of composites, one can consider fracture of the individual

constituents or the separation of the interface between the constituents [3]. In analyzing the effects of a hole, the classical approaches to analysis that are used with metals and other isotropic materials do not work in general with a composite. The differences exist because the stress concentration factors (SCF's) for composites have not been characterized successfully [13]. Isotropic SCF's are based on the conditions at the hole boundary, while the strength of composite laminates seems related to the in-plane elastic stress region adjacent to the hole boundary. The measure of strength for composites containing circular disconti-nuities must be based on a more complete description than simply stress concentration factors [13].

Early attempts at predicting the strength of composites containing notches involved the application of a linear fracture mechanics concept. These attempts evolved into the two-parameter fracture theories that became popular in the early 1970's [8]. Some particular fracture mechanics models include the linear elastic fracture mechanics (LEFM) approach [9], the point stress criterion [9], the average stress criterion [9], a "three parameter model" [13], and a first-ply-failure (FPF) model [11]. But, from further review, it was seen that the fracture mechanics approaches confine themselves to particular ranges of parameters, such as geometry, notch size, etc. In general, these theories

required the use of crack length corrections to reflect the presence of damage zones.

Awerbuch [10] reviews several fracture models for predicting notch strength of composite laminates, and notes that emphasis is placed on semi-empirical techniques which are simple to use. But as References [5-8] point out,

> with the development of accurate non-destructive evaluation methods, it became apparent that the damage zone corrections (of fracture theories) were arbitrary and subject to question. As a result, attempts were made to develop analysis methods that model the actual damage accumulation process [8].

Thus, to obtain a satisfactory design incorporating the use of fiber-reinforced composite laminates, one must know the entire stress-strain behavior to ultimate strength of the component. Although experimentation and repeated testing will yield this knowledge, it is both expensive and inconvenient considering the large variety of parameters listed above. As an alternative, another technique would be to analytically relate the properties of the individual plies, or laminas, to the laminate. With this technique, one would have to know the material biaxial properties of the laminas for various load combinations, which can easily be obtained by experimentation [5].

To obtain these biaxial properties of individual lamina under simple loading conditions (uniaxial tension, uniaxial compression, and pure shear), one may estimate these properties from the properties of the constituent materials.

The 'Rule of Mixtures' is a well known estimation scheme
[3]. Fan and Knapp [14] provide an alternative to the rule
of mixtures in the estimate of composite properties.
Starting with the Second Law of Thermodynamics, and leading
the development through a heat balance equation, they use
variational calculus to derive an ultimate strength equation
that incorporates nonlinearity present in the material.
However, this approach is advocated for advanced design
purposes; and verification testing is still necessary [14].
These estimation procedures were not effective for this
study so mechanical properties of the laminas were obtained
by experiment.

Even if the behavior of the lamina can be accurately
predicted, the problem of determining the performance of
laminas in a laminate still remains. The degradation of
strength of individual laminas may not precipitate the
failure of the laminate. For example, in the case of a
cross-ply laminate (a composite laminate with alternating
layers of $0°$ and $90°$ orientations of plies) subjected to
normal stresses $(\sigma_1, \sigma_2)$ acting in the direction of the
fibers, the degradation of strength of laminas in the
transverse direction does not result in the failure of the
laminate; the laminate is capable of sustaining stresses
higher than those causing transverse degradation of the
individual laminas [5]. In general, the behavior of the
lamina under complex stress states is predicted by using a

9

criterion to relate the parameters of strength obtained from the simple tests to the states of stress in the laminate [6].

This lamina-laminate response has been the subject of many theoretical and experimental studies [5]. Noyes and Jones modified Hill's failure criterion [3, 9] to determine the onset of failure in a ply or plies. Chiu modified this approach to reduce the affected stiffnesses and strengths gradually, instead of instantaneously [5].

These early attempts assumed linearity of stress-strain response, even though tests indicated significant nonlinear behavior of the composite lamina under transverse and shear loadings. Petit and Waddoups relaxed this linearity assumption. They used properties of unidirectional laminae in conjunction with a piece-wise linear approach to determine response of the laminate. In their method, the loading is proportional and is applied in small increments to compute the current stress-strain states. Biaxial strains are used to obtain tangent moduli from stress-strain data generated under simple load conditions [6]. However, this method does not consider that strains in the stress-strain curves are simple, while the lamina strains in the laminate are not. (This aspect will be discussed in more detail in Section II F.) Additionally, stress-strain curves of laminates obtained by this method are very much

dependent upon the size of the increment used in the applied loads [5].

Hahn and Tsai [15] proposed a method which allows only for the nonlinearity of the shear stress-strain response by the equation

$$\varepsilon_6 = S_{66}\, \sigma_6 + S_{6666}\, \sigma_6^{\,3} \qquad\qquad (1)$$

where $\sigma_6$ and $\varepsilon_6$ are shear stress and shear strain, respectively, and $S_{66}$ and $S_{6666}$ are constants. This approach does not distinguish between tensile and compressive behaviors of the lamina, and it does not deal with the problem of failure [5, 6].

In the composite industry, at least 30 failure theories exist for laminated composites (as of late 1986) [16]. Some of these theories are applied directly to the laminate, while the others are applied to the individual laminas. In addition, at least 12 theories exist of post-failure behavior of laminated composites [16]. Nahas concludes that some failure theories are special cases of the maximum stress theory. He also found that some theories are based on assumptions that are not always true for composite materials. Some of the more general theories have been used only for special cases, which reduce them to the Tsai-Wu theory. For theories such as Sandhu's strain energy failure criterion, theory-experiment correlation coefficients are included which make calculated and test results agree closely. Although such coefficients must be determined for

each material [16], once they are obtained, the finite element method using Sandhu's criteria may be used for a variety of geometries. Rowlands [17] remarks in his survey in the Handbook of Composites that

whereas most of the strength predictions assume a linear stress-strain relationship in the associated lamination analysis, those by Sandhu and Petit-Waddoups provide for nonlinear lamina material response [17].

The composite strength analysis proposed by Sandhu differs from the more conventional formulations in the following respects [17]:

(1) The nonlinear lamina stress-strain responses to failure are represented analytically by cubic-spline functions. The tangent moduli of these functions are employed to evaluate lamina and laminate stiffnesses and compliances during load increments.

(2) In keeping with the nonlinear provision, ply degradation is based on an energy to failure criterion.

(3) Equivalent strain increments are defined. (See Section II F.)

Thus considering the above justifications, this study uses Sandhu's fully nonlinear progressive-ply-failure finite element method to analyze the damage accumulation process in Gr/PEEK tension specimens containing a circular discontinuity. This study uses the technique of Sandhu for predicting the response to failure. Previous works have described this technique in detail [5, 6], and others have used this technique for predicting behavior in Gr/Ep [6, 7,

8, 18, 19]. In applying this technique to predict the behavior of Gr/PEEK, no previous work could be found.

As a general description of this analytical technique, cubic spline interpolation functions are used to represent basic stress-strain curves obtained from simple tests [5]:

1. Longitudinal tension and compression.

2. Transverse tension and compression.

3. Shear.

Cubic spline functions yield smooth composite stress-strain curves (from sets of three data points) from which the computer program can determine accurate moduli of elasticity over the entire range of the curves [6].

This functional form of stress-strain curves provides an accurate representation of stresses, strains, and moduli over the entire range of curves. This representation is used in conjunction with an incremental constitutive law. This law, which relates the increments of stresses and strains, is used to generate the response of Gr/PEEK laminates subjected to tensile loads. The basic data and constitutive relations are then used to determine the ultimate load-carrying capacity of the laminates under incremental loading by a plywise application of Sandhu's failure criterion using strain energy under longitudinal, transverse, and shear loadings as independent parameters [5,6]. The theory behind this technique is discussed in detail in Chapter II, and the procedure used in this thesis

for accomplishing the analysis is described in Chapter III. The results obtained by this technique are compared with experimental results of this study.

The laminates studied through both analysis and experimentation were the $[0_{16}]$ and $[90_{16}]$ unidirectional lay-ups and the $[\pm45]_{4s}$ angle-ply lay-up. The two quasi-isotropic lay-ups, $[0/+45/90/-45]_{2s}$ and $[0/\pm45/90]_{2s}$, were only studied experimentally for comparison to similar Gr/Ep laminates. All test specimens contained 16 layers and were symmetric about their mid-plane. Also, they all contained a 0.4˝ diameter hole at their centers. Thus the laminate geometry represented a finite-width plate containing a stress concentrator subjected to uniaxial tension. Furthermore, bending was not induced in the specimens by tension because of the symmetry of the lay-ups.

Basic properties were first derived with the experimentation process, and then the five types of laminates with holes were tested to their ultimate loads and to percentages of ultimate load. Testing to ultimate yielded the laminate stress-strain responses for the entire range of strength. Testing to percentages of failure load yielded partially failed specimens which could be examined by stereo x-ray.

In addition to the x-rays, one other medium allowed for a post-failure analysis. A video camera filmed each test to ultimate strength. Through repeated viewing of the tape and

14

through stills, or photographs, taken off the tape, one could deduce further results from the experimentation.

A description of the procedures used in the experimentation phase of this thesis is presented in Chapter IV. Results of both experimentation and analysis are presented and discussed in Chapter V. Conclusions on the entire study are reported in Chapter VI.

## C. Material Choice

A polyaromatic resin, such as polyetheretherketone (PEEK), combined with a continuous fiber is known as an aromatic polymer composite (APC) [13]. The Gr/PEEK chosen for this study is refered to as APC-2, an improved laminate over APC-1. Whereas APC-1 contained Courtauld XAS graphite fibers, APC-2 contains Hercules AS-4 graphite fibers. The AS-4 fibers make a better bond with the PEEK matrix [13]. Gr/PEEK can be converted into a range of component shapes and sizes by a full spectrum of fabrication technologies [2, 4, 13].

Demuts and Sharpe [1] found APC-2 to be 25% tougher than graphite/epoxy (Gr/Ep) in static post-impact residual compression strength. They further found that the fatigue life of thermoplastic laminates is twice that of comparable thermosets. They conclude that thermoplastic matrix composites have the potential for more efficient wing skins at lower fabrication and maintenance costs as compared to the more brittle thermosets. Carpenter [20] reiterates

15

these findings, praising the potential of thermoplastics for lowering production costs and improving maintainability.

Ramey [13] conducted a comparison study of strength reduction in APC-2, APC-1, and Gr/Ep using tension and compression specimens with circular holes at their centers. He found APC-2 to be superior in its strength properties over the others. His comparisons included microphotographs of each failed specimen, and an analysis using a fracture mechanics approach. He found that the failure surfaces of APC-2 were combinations of different failure modes, and he concluded that there was "no general failure prediction model" that covered a range of temperatures or a broad range of hole sizes. He also suggested that a continuum mechanics approach would be advisable in analyzing the behavior of APC-2 [13]. Thus, the logic is reinforced of using the progressive-ply-failure finite element analysis in this study. The strain energy failure criterion used in this analysis exhibits the characteristics of a continuum mechanics approach.

D.  Progression of Study

This thesis began with a simple abstract and test plan, and evolved into producing further information about Gr/PEEK and its nonlinear behavior. The planning of this thesis required a large logistic effort on a local level. Several organizations at Wright-Patterson AFB aided in the completion of this thesis. The process of seeking the help

16

of these organizations and communicating to them a research
problem had not been documented.  For completeness, the
logistics efforts of this thesis are included in Appendix A.
The author hopes that this appendix may help streamline the
research efforts of future AFIT students.

## II. Theory

This chapter discusses theories used to describe
stresses, strains, and failure in fiber/polymer composite
materials. First considered is the behavior of the
composite on a micromechanical level, and then the
discussion turns to one of macromechanics. Micromechanics
examines the interaction of the constituent materials,
defining the behavior of the heterogeneous composite
material. But in an engineering approach to composite
materials, one chooses to view the entire material
macroscopically. Macromechanics examines the effects of the
constituent materials as averaged apparent properties,
defining the behavior of the homogeneous composite material.

Following this review of mechanics of composite
materials, this chapter presents a brief formulation of
linear finite element theory, which is then expanded to
handle multiple-layered composite materials. Further
development leads to nonlinear finite element methods.
Finally, the failure criteria used to match analytical
results to experimental findings concludes this chapter.

### A. Micromechanical Behavior of Composite Material.

Although a designer is generally interested in the
resultant properties of the fiber/matrix combination, it is
often useful to know the micromechanical behavior of the
material to determine optimum resultant properties. For

example, toughness or resistance to temperature and humidity can be maximized in a material by starting at the molecular level and designing outward. To better understand the failure of the composite, the specific composition of each constituent must be known. This section discusses the nature of polymer matrices and organic fibers.

Polymers are formed as a collection of long-chain molecules. Elemental units, or monomers, linked together form the long-chain molecules. The units in a chain can vary in element and size, yielding an infinite number of possible polymers [13]. Organic or carbon-based polymers have chains based on a unit of carbon. The PEEK polymer is formed from the carbon-based repeat unit shown in Figure 1 [2].

The polymer chains can take many shapes. In rubber, for example, the carbon-based units form a spiral, thus
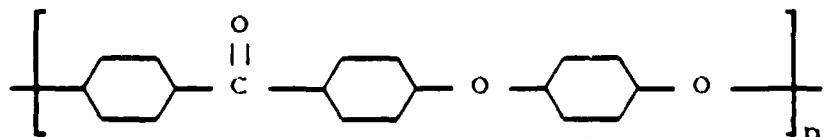


Figure 1. Repeat Unit of the PEEK Polymer

yielding a highly deformable material. In other materials, the carbon chain may be a zig-zag and yield a material which is less deformable.

When units in the main chain are linked to other similar chains by side chains, a network polymer is formed. This dense cross-linked polymer is referred to as thermo-setting because it does not soften upon heating once it is formed. A thermosetting material remains hard and eventually disintegrates under extreme temperatures [13]. The matrix epoxy of Gr/Ep is formed from this type of material.

Linear polymers with small to no amount of cross-links form viscous fluids. These fluids exist as tangled masses of molecular segments sliding over one another. The viscosity of these fluids varies greatly with temperature. These thermally activated fluids are called thermoplastic polymers. Below their glass transition temperature, $T_g$, they are typical glass. Above their $T_g$, they range from fluids to deformable solids, depending on their amount of cross-links between molecular chains [13]. Polyetherether-ketone (PEEK) is a thermoplastic material exhibiting these properties.

The strain in a thermoplastic, as well as in any material, is a combination of elastic strain plus creep, or time-dependent strain. The rate of chain straightening (tension strain) or crumbling (compression strain) depends

on viscosity. When a material is unloaded, elastic strain is recovered instantly; but strain due to creep recovers gradually because of the viscous drag on the molecular chains [13]. According to the creep data provided in Reference [2], for the duration of each test, creep is negligible for each type of ply arrangement. Therefore, one assumption of this study is that creep, or visco-elasticity, can be ignored.

In the manufacturing of thermoplastics, one must control the crystallinity of PEEK to optimize the performance of the polymer. This is done by controlling the rate at which the composite is cooled down from its melted state at $720°F$-$750°F$ to its $T_g$ at $300°F$ [2]. In crystalline regions, the chains are parallel; in non-crystalline regions they are tangled. A single molecular chain may exist in both crystalline and non-crystalline regions [13]. If APC-2 is cooled at rates less than $18°F$ per minute, crystallinity will increase beyond optimum, which will result in reduction of composite toughness. If cooling rates exceed $1260°F$/minute, the polymer's 'spherulitic growth' will not achieve completion and the optimum level of crystallinity will not be reached. This may cause reduction in stiffness and resistance to solvents' [2]. Reheating and recooling (annealing) the composite can correct any errors in cooling so that optimum crystallinity can be achieved.

In APC-2, the PEEK matrix surrounds and chemically bonds to AS4 carbon fibers to form the composite material. As alluded to in Chapter I, this combination of fiber and matrix form a thin lamina when continuous fibers are laid in a single direction or woven in various directions. Figure 2 shows two principal types of laminae [3].

The fibers are the principal reinforcing or load-carrying agent. Advanced carbon fibers, such as AS4 fibers, are produced from precursor fibers in three steps. The first step involves controlled oxidation of carbon filaments. Complex reactions between the aligned polymer chains of the precursor form crosslinks, and an extended carbon

LAMINA WITH
UNIDIRECTIONAL FIBERS

LAMINA WITH
WOVEN FIBERS

(a.)          (b.)
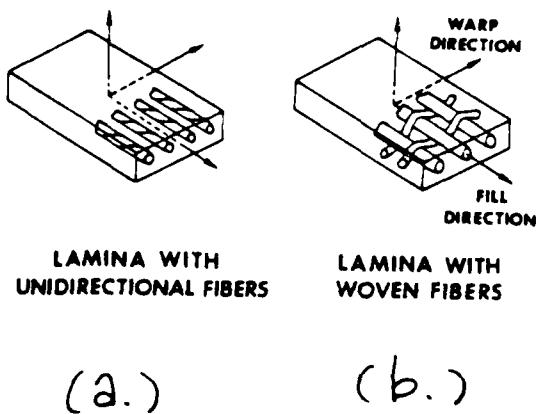
Figure 2.  Two Principal Types of Laminas

Note: APC-2 laminates follow the pattern of Figure (a).

network is formed which is aligned along the fiber axis
[21]. Individual filaments range in diameter from six to
nine micrometers [2]. In the second step pyrolysis under
an inert atmosphere drives off most non-carbonaceous atoms.
Finally, the third step exposes the carbon filament to high
temperature to form extended graphite ribbons aligned along
a fiber axis [21]. In this graphitization of carbon, a
layered hexagonal crystal structure is formed under heat.
Graphite fibers may also be subjected to surface treatment
to improve their compatibility with the matrix. [21].

With the fibers carrying the load, the matrix acts to
support and protect the fibers and to provide a way of
distributing the load among the fibers and transmitting the
load between fibers. As shown in Figure 3 [3], this
distribution and transmission of load is especially
important if a fiber breaks. The load is transferred to the
matrix and then to the other side of the broken fiber, as
well as to adjacent fibers. The shearing stress developed
in the matrix is the mechanism for the load transfer. This
shearing stress resists the pulling out of the broken fiber
[3]. This description of mechanical action between fiber
and matrix accounts for much of the explanation of failure
progression in composite materials.

To determine the stiffness properties of composite
materials, many analytical approaches are possible. One can
use the mechanics of materials approach, or the Rule of
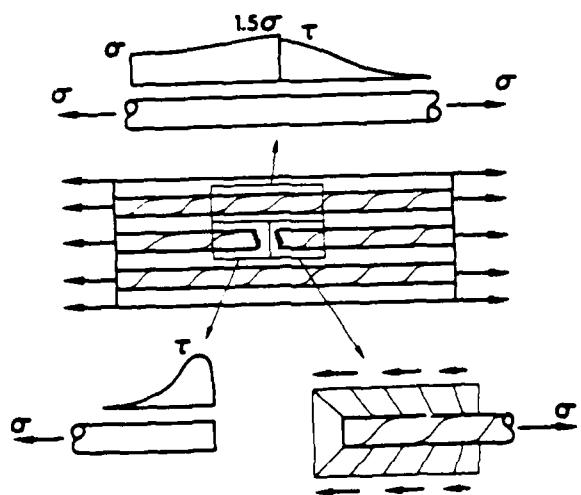
FIGURE 3. EFFECT OF A BROKEN FIBER
ON MATRIX & FIBER STRESSES

Mixtures, in which simple approximations to the engineering constants are derived by averaging the properties of each constituent material over the composite cross-section. Another approach is that of elasticity. This approach includes bounding techniques, exact solutions, and concepts of contiguity.

Halpin and Tsai developed an interpolation procedure that is an approximate representation of more complicated micromechanics results [3]. According to Jones, Tsai gives expressions for $E_1$, $E_2$, $\nu_{12}$, and $G_{12}$ that are in good agreement with experimental data for a glass reinforced resin composite, but a "contiguity factor" [3] is the key to the agreement. Tsai found that the constituent material properties have the following effect on the properties of the composite:

(1) Young's modulus, E, of the fiber makes a significant contribution to $E_1$ of the lamina,

(2) E of the matrix makes a significant contribution to $E_2$ and $G_{12}$ of the lamina, and

(3) The Poisson ratios for both the fiber and the matrix have little effect on $E_2$ and $G_{12}$ and have no effect on $E_1$ of the lamina.

Although engineering properties could be derived with these micromechanical approaches, this study conducted experiments to find these properties. Not only was accuracy

desired, but nowhere did these methods accurately and easily take into account the nonlinearity of material properties.

B.  Macromechanical Behavior of Composite Materials

A lamina is the basic building block in a laminated fiber-reinforced composite.  In this section, the behavior of a lamina and a laminate will be considered from a macromechanical approach.  A laminate is two or more laminas bonded together to act as an integral structural element.  This stack of laminas may have plies of various orientations of principal material directions as shown in Figure 4 [3].  Note that the laminate is shown under uniaxial loading, and the orientations of the plies are measured with respect to this axis of loading.

Fiber-reinforced composites are usually treated as linear elastic materials since the fibers provide the majority of the strength and stiffness.  This thesis attempts to refine that approximation by considering nonlinearity.  Although most theories are based on linear assumptions, repeated experimentation has shown that fiber-reinforced composites exhibit nonlinearity, and the experimentation in this thesis also displays this phenomenon.  (See Chapter V, Results and Discussion.)  To treat the nonlinearity problem, the linear elastic theories presented in this section have been employed such that if a given load increment is small enough, linear elastic theory

$\mathcal{J}_x$

0° PLY

+45° PLY

90° PLY

-45° PLY

0° PLY

$\mathcal{T}_x$
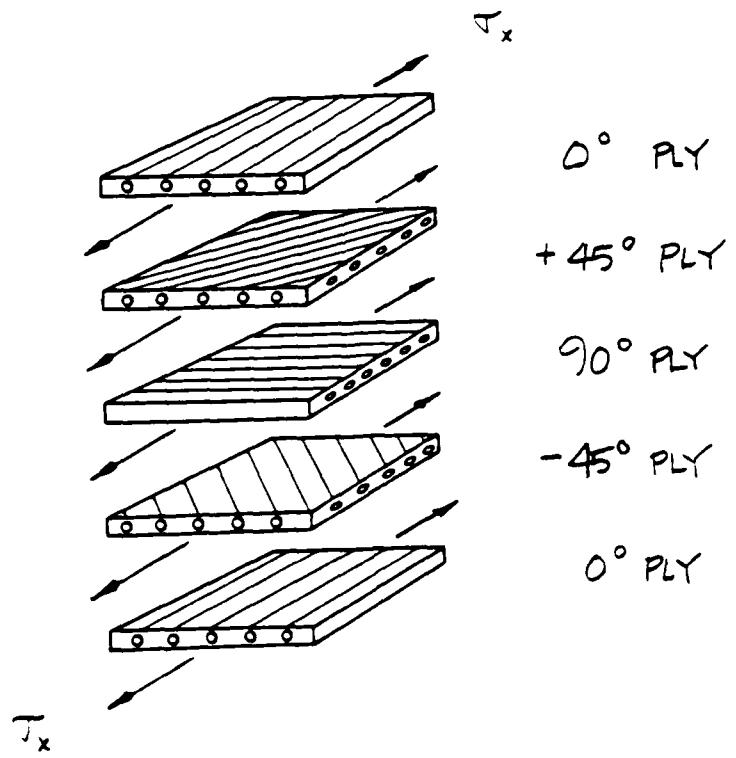
FIGURE 4.   LAMINATE CONSTRUCTION.

applies. As will be shown in Sections F and G of this chapter, linear elastic theory is applied incrementally while the basic properties of the material vary with each increment.

A potential problem in the construction of laminates is the introduction of shearing stresses between layers. The shearing stresses arise due to the tendency of each layer to deform independently of its neighbors because all may have different orientations and thus different properties in the direction of loading. Such shearing stresses are largest at the edges of a laminate and may cause delamination there. The transverse and normal stresses resulting from uniaxial loading can also cause delamination [3].

Whitney discusses this subject of interlaminar stresses in Reference [9], and he discusses the influence of stacking sequence on interlaminar stresses. The most influential of the interlaminar stresses is the normal stress, i.e., the stress attempting to separate the plies. Sandhu [22, 23] describes the tendency for a composite to delaminate through the use of a `delamination moment coefficient` (DMC), which is based on the stacking sequence. For Gr/Ep specimens identical in geometry to those of this thesis, the critical DMC is approached for the [0/±45/90] laminate under tensile loading. A ply-by-ply plane stress analysis, such as the one used in this thesis (see Chapter III), does not take into consideration stacking sequence. Thus, reductions in

strength caused by delaminations would cause unwanted
disagreement between analysis and experimentation.
Therefore, the [0/+45/90/-45] laminate was also chosen to
evaluate in this study for comparison to the [0/±45/90]
laminates.

In describing the behavior of a single lamina, the
basic restriction of the macromechanical approach is to
linear elastic behavior. This assumption is appropriate in
this thesis because nonlinear behavior is modeled as a
series of increments which deduce the varying material
properties from smooth curves of stress-strain data.
Summarizing the linear elastic theory for a lamina, the
generalized Hooke's law relating stresses to strains can be
written in contracted notation as

$$\sigma_i = C_{ij}\varepsilon_j \qquad i,j = 1,\ldots,6 \qquad\qquad (2)$$

where $\sigma_i$ are the stress components, $C_{ij}$ is the stiffness
matrix, and $\varepsilon_j$ are the strain components [3]. The
components of the stiffness matrix, and the terms of its
inverse the compliance matrix, $S_{ij}$, will be referred to as
elastic constants (keeping in mind the incremental
assumption of the above paragraph).

A unidirectional reinforced lamina in the macro-
mechanical approach is considered orthotropic, i.e., there
are three mutually orthogonal planes of material property
symmetry. These planes of symmetry are described by the set

28
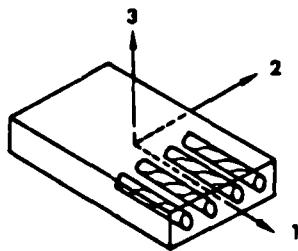
Figure 5.    The Principal Material Axes for a
             Unidirectionally Reinforced Lamina

of axes in shown above in Figure 5 [3] as the principal

material directions.

Taking the inverse of Hooke's law above, the

strain-stress relations become

$$\varepsilon_i = S_{ij} \sigma_j \qquad i,j = 1,\ldots,6 \qquad (3)$$

For an orthotropic material with body coordinate axes X and

Y aligned with principal material directions, Eq. 2 becomes

$$\begin{Bmatrix} \varepsilon_1 \\ \varepsilon_2 \\ \varepsilon_3 \\ \gamma_{23} \\ \gamma_{31} \\ \gamma_{12} \end{Bmatrix} = \begin{bmatrix} S_{11} & S_{12} & S_{13} & 0 & 0 & 0 \\ S_{12} & S_{22} & S_{23} & 0 & 0 & 0 \\ S_{13} & S_{23} & S_{33} & 0 & 0 & 0 \\ 0 & 0 & 0 & S_{44} & 0 & 0 \\ 0 & 0 & 0 & 0 & S_{55} & 0 \\ 0 & 0 & 0 & 0 & 0 & S_{66} \end{bmatrix} \begin{Bmatrix} \sigma_1 \\ \sigma_2 \\ \sigma_3 \\ \tau_{23} \\ \tau_{31} \\ \tau_{12} \end{Bmatrix} \qquad (4)$$

where $\gamma_{ij} = 2 \varepsilon_{ij}$. The terms $\gamma_{ij}$ ($i \neq j$) represent engineering shear strain, whereas $\varepsilon_{ij}$ ($i \neq j$) represent tensor shear strain [3].

For the study conducted in this thesis, the tension specimens representing finite-width thin plates were subjected to plane stress. For a lamina in the 1-2 plane, a state of plane stress is defined by setting

$$\sigma_3 = 0, \quad \tau_{23} = 0, \quad \tau_{13} = 0 \tag{5}$$

in the three dimensional strain-stress relation given in Eq. (4) above. Thus, the strain-stress relations in Eq. (4) above reduce further to

$$\begin{Bmatrix} \varepsilon_1 \\ \varepsilon_2 \\ \gamma_{12} \end{Bmatrix} = \begin{bmatrix} S_{11} & S_{12} & 0 \\ S_{12} & S_{22} & 0 \\ 0 & 0 & S_{66} \end{bmatrix} \begin{Bmatrix} \sigma_1 \\ \sigma_2 \\ \tau_{12} \end{Bmatrix} \tag{6}$$

where the compliance terms are:

$$S_{11} = \frac{1}{E_1} \qquad\qquad S_{22} = \frac{1}{E_2}$$

$$S_{12} = S_{21} = -\frac{\nu_{12}}{E_1} = -\frac{\nu_{21}}{E_2} \tag{7}$$

$$S_{66} = \frac{1}{G_{12}} \quad .$$

$$S_{16} = S_{26} = S_{61} = S_{62} = 0$$

The stain-stress relations in Eq. (6) are inverted to obtain the stress-strain relations:

30

$$\begin{Bmatrix} \sigma_1 \\ \sigma_2 \\ \tau_{12} \end{Bmatrix} = \begin{bmatrix} Q_{11} & Q_{12} & 0 \\ Q_{12} & Q_{22} & 0 \\ 0 & 0 & Q_{66} \end{bmatrix} \begin{Bmatrix} \varepsilon_1 \\ \varepsilon_2 \\ \gamma_{12} \end{Bmatrix} \qquad (8)$$

where the $Q_{ij}$ are called the "reduced stiffnesses," are defined as [3]:

$$Q_{11} = \frac{E_1}{1 - \nu_{12}\nu_{21}} \qquad\qquad Q_{22} = \frac{E_2}{1 - \nu_{12}\nu_{21}}$$

$$Q_{12} = Q_{21} = \frac{\nu_{21}E_1}{1 - \nu_{12}\nu_{21}}$$

$$\qquad\qquad\qquad\qquad\qquad\qquad\qquad\qquad (9)$$

$$Q_{66} = G_{12}$$

$$Q_{16} = Q_{26} = Q_{61} = Q_{62} = 0$$

The preceding stress-strain and strain-stress relations are the basis for the stiffness and stress analysis of an individual lamina subjected to forces in its own plane. Note that the stiffness and compliance terms are based on four general independent material properties:

$$E_1 , E_2, \nu_{12}, \text{ and } G_{12}$$

where subscripts 1 and 2 refer to principal material axes. Note also that these four properties are expanded to seven specific properties when considering tension and compression. These properties are designated as:

$$E_1^T, E_1^C, E_2^T, E_2^C, \nu_{12}^T, \nu_{12}^C, \text{ and } G_{12}$$

31

where the superscripts T and C represent tension and compression basic properties. The shear modulus $G_{12}$ is not affected by the change of unidirectional load.

Often the principal directions of a lamina do not coincide with the coordinate directions of the component, the X and Y directions, that is, axes 1 and 2 are oriented at an angle $\theta$ from the X and Y axes. This rotation of principal material axes is shown in Figure 6 [3]. To handle this problem, first a transformation relation is needed between the stresses in the principal material directions and those in the body coordinates. Second, a method is needed to transform stress-strain relations from one coordinate system to another.

Through this procedure of transformations, the stress-strain relation of Eq. (8) can be written that will account for any orientation of the lamina [3]:

$$\left\{ \begin{array}{c} \sigma_x \\ \sigma_y \\ \tau_{xy} \end{array} \right\} = [\bar{Q}] \left\{ \begin{array}{c} \varepsilon_x \\ \varepsilon_y \\ \gamma_{xy} \end{array} \right\} = \left[ \begin{array}{ccc} \bar{Q}_{11} & \bar{Q}_{12} & \bar{Q}_{16} \\ \bar{Q}_{12} & \bar{Q}_{22} & \bar{Q}_{26} \\ \bar{Q}_{16} & \bar{Q}_{26} & \bar{Q}_{66} \end{array} \right] \left\{ \begin{array}{c} \varepsilon_x \\ \varepsilon_y \\ \gamma_{xy} \end{array} \right\} \tag{10}$$

where the terms $\bar{Q}_{ij}$ denote transformed reduced stiffnesses, as opposed to the reduced stiffnesses of $Q_{ij}$. The values of $\bar{Q}$ are given as [3]:
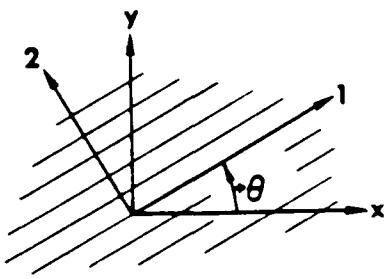
FIGURE 6. ROTATION OF PRINCIPAL AXES (1,2) FROM BODY AXES (X,Y).

$$\bar{Q}_{11} = Q_{11}m^4 + 2(Q_{12} + 2Q_{66})n^2m^2 + Q_{22}n^4$$

$$\bar{Q}_{12} = (Q_{11} + Q_{22} - 4Q_{66})n^2m^2 + Q_{12}(n^4 + m^4)$$

$$\bar{Q}_{22} = Q_{11}n^4 + 2(Q_{12} + 2Q_{66})n^2m^2 + Q_{22}m^4$$

$$\bar{Q}_{16} = (Q_{11} - Q_{12} - 2Q_{66})n\,m^3 + (Q_{12} - Q_{22} + 2Q_{66})n^3m$$

$$\bar{Q}_{26} = (Q_{11} - Q_{12} - 2Q_{66})n^3m + (Q_{12} - Q + 2Q_{66})n\,m^3$$

$$\bar{Q}_{66} = (Q_{11} + Q_{22} - 2Q_{12} - 2Q_{66})n^2m^2 + Q_{66}(n^4 + m^4)$$

where the values of $Q_{ij}$ were given in Eq. (9). Note that there are still only four general independent constants which characterize an orthotropic lamina.

Alternatively, the strains can be expressed in terms of the stresses in body coordinates by inversion of Eq. (10),

$$\left\{ \begin{array}{c} \varepsilon_x \\ \varepsilon_y \\ \gamma_{xy} \end{array} \right\} = [\bar{S}]^{-1} \left\{ \begin{array}{c} \sigma_x \\ \sigma_y \\ \tau_{xy} \end{array} \right\} = \left[ \begin{array}{ccc} \bar{S}_{11} & \bar{S}_{12} & \bar{S}_{16} \\ \bar{S}_{12} & \bar{S}_{22} & \bar{S}_{26} \\ \bar{S}_{16} & \bar{S}_{26} & \bar{S}_{66} \end{array} \right] \left\{ \begin{array}{c} \sigma_x \\ \sigma_y \\ \tau_{xy} \end{array} \right\} \quad (11)$$

where values of the transformed reduced compliance terms, $\bar{S}_{ij}$, are given as [3]:

$$\bar{S}_{11} = S_{11}m^4 + (2S_{12} + S_{66})n^2m^2 + S_{22}n^4$$

$$\bar{S}_{12} = S_{12}(n^4 + m^4) + (S_{12} + S_{66} - S_{66})n^2m^2$$

$$\bar{S}_{22} = S_{11}n^4 + (2S_{12} + S_{66})n^2m^2 + S_{22}m^4$$

$$\bar{S}_{16} = (2S_{11} - 2S_{12} - S_{66})n\,m^3 - (2S_{22} - 2S_{12} - S_{66})n^3m$$

$$\bar{S}_{26} = (2 S_{11} - 2 S_{12} - S_{66})n^3 m - (2 S_{22} - 2 S_{12} - S_{66})n m^3$$

$$\bar{S}_{66} = 2 (2 S_{11} + 2 S_{22} - 4 S_{12} - S_{66}) n^2 m^2 + S_{66}(n^4 + m^4)$$

where the values of $S_{ij}$ were given in Eq. (7).

## C.  Strength of Composite Laminates

In describing strength of composite materials, deter-
mination of the strength of laminate is built upon the
strengths of its laminas.  Because of the anisotropic
and hetergeneous nature of composite materials, failure
modes are often quite different from those of isotropic
homogeneous materials.  In particular, the failure of one
layer in a composite material does not necessarily mean the
entire laminate will fail.  The laminate may be capable of
sustaining higher loads despite a significant change in
stiffness [3].  This concept was introduced in Chapter I and
is shown graphically in Figure 7 [3].

Because of the various characteristics of composite
materials, it is difficult to determine a strength theory in
which all failure modes and their interactions are taken
into account.  Strength theories presented in Reference [3]
are based on a macroscopic analysis in which the strengths
of each lamina must be assessed as it relates to the whole
laminate.  They include maximum stress, maximum strain, and
maximum distortional energy approaches.  As described in the
following sections, this thesis uses a finite element
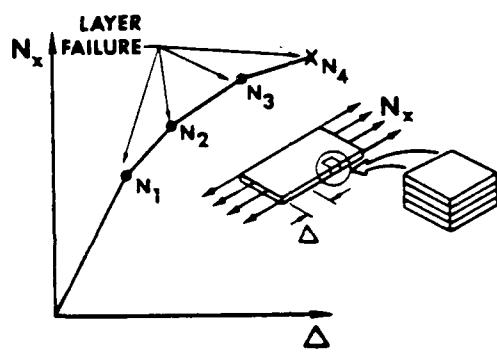
FIGURE 7. LAMINATE LOAD-DEFORMATION BEHAVIOR

approach to the overall failure of the laminate, but its
inherent strain energy failure criterion for individual
elements is not unlike the other analytical approaches
mentioned above.  See Section II F.

In any method of strength analysis, the designer is
striving to determine either (1) the maximum loads a given
laminate can withstand or (2) the laminate characteristics
necessary to withstand a given load. [3].  The overall
procedure of determining laminate strength is straight-
forward, but extremely tedious; thereby implying the
need for computer techniques.  A general procedure is shown
schematically in Figure 8 [3], and the computer application
used in this thesis is a specific version of this general
procedure.

## E.  Holes in Laminates

For the problems of holes in laminates, one of the
first solutions to the difficult problem of stresses around
a hole was given by Lekhnitskii in 1936, 1963, and 1968.
[3].  Greszczuk plotted the circumferential stress around
the hole for an isotropic material and several unidirec-
tional materials.  See Figure 9 [3].  The usual stress
concentration for an isotropic material is 3, i.e.,
$\sigma_\theta / \sigma_x = 3$ at $\theta = 90°$.  For composite materials such as
graphite epoxy, the stress concentration factor depends on
laminate construction.

37

- LAMINAE PROPERTIES
- PROPORTIONS BETWEEN APPLIED LOADS

CALCULATE LAMINATE STIFFNESSES A, B, D

IF NO LAMINAE HAVE FAILED

IF LAMINAE HAVE FAILED

CALCULATE LAMINAE STRESSES RELATIVE TO LOAD FACTOR
$(\sigma_x^k, \sigma_y^k, \tau_{xy}^k)/L$

CALCULATE LAMINAE STRESSES AT LAST LOAD LEVEL
$\sigma_x^k, \sigma_y^k, \tau_{xy}^k$

DETERMINE RELATIVE LAMINAE STRESSES IN PRINCIPAL MATERIAL DIRECTIONS
$(\sigma_1^k, \sigma_2^k, \tau_{12}^k)/L$

DETERMINE LAMINAE STRESSES IN PRINCIPAL MATERIAL DIRECTIONS
$\sigma_1^k, \sigma_2^k, \tau_{12}^k$

COMPARE RELATIVE LAMINAE STRESSES WITH FAILURE CRITERION

COMPARE LAMINAE STRESSES WITH FAILURE CRITERION

CALCULATE LOAD FOR A LAMINA FAILURE

IF NO LAMINA FAILS, INCREASE LOAD FACTOR UNTIL A LAMINA FAILS

IF A LAMINA FAILS

IF NO LAMINAE LEFT, GROSS LAMINATE FAILURE OCCURRED AT LAST LOAD (TERMINATE PROCEDURE)

ELIMINATE LAMINA FROM LAMINATE BY ASSIGNING IT ZERO PROPERTIES

CALCULATE LAMINATE DEFORMATIONS $\epsilon_x, \epsilon_y, \gamma_{xy}$

FIGURE 8. GENERAL PROCEDURE FOR DETERMINATION OF STRENGTH IN COMPOSITE LAMINATES.
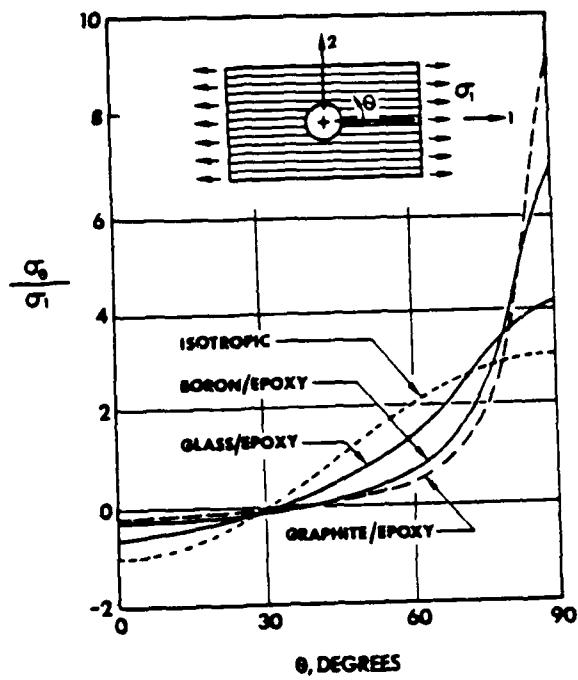
FIGURE 9. EFFECT OF MATERIAL PROPERTIES ON CIRCUMFERTIAL STRESS, $\sigma_\theta$, AT THE EDGE OF A CIRCULAR HOLE IN AN ORTHOTROPIC PLATE SUBJECTED TO $\sigma_1$.

39

The circumferential stress at $\theta = 0°$ is reduced for composites relative to isotropic materials. Because of isotropy of material properties, the key factor in failure of isotropic plates with holes is the magnitude of the stress concentration factor from which the maximum (failure) stress is obtained. However, for orthotropic materials, a combined stress failure criterion instead of a maximum stress failure criterion is more accurate since failure of a lamina is a function of the strengths in various directions. Thus, stress concentration factors alone are insufficient for failure prediction of orthotropic (and anisotropic) plates. Moreoever, for laminated plates, the comparison of stress states with failure stress states must be done on a layer-by-layer basis [3].

Extending the analysis to a laminate, Figure 10 [3] shows stress concentrations around a circular hole in a cross-ply and an angle-ply laminate. The stress shown is a gross stress on the laminate, and the stresses in each layer must be found by classical lamination theory or some other method. Failure is determined by application of failure criterion to each layer. The interlaminar stresses are ignored, and thus predicted stresses are not accurate within about one laminate thickness from the edge.

These first sections have presented an overview of some theories and approaches used in studying the mechanics of composite materials. The next three sections describe the

40
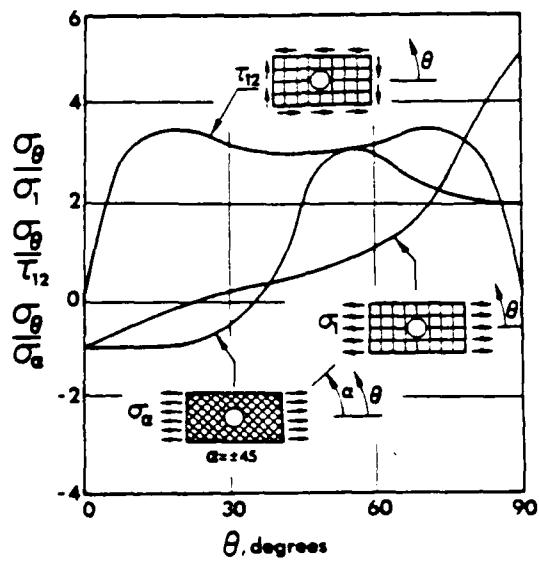
FIGURE 10.  STRESS CONCENTRATIONS AT THE
EDGE OF A CIRCULAR HOLE IN
CROSS-PLY AND ANGLE-PLY LAMINATES.

specific theories behind the analysis accomplished in this thesis.

E. Linear Finite Element Theory

For the convergence study described in Section III C, this study used a linear finite element program called PLSTR, written by Dr. R.S. Sandhu, that is a simplificaion of his nonlinear program PLSTREN, which is described in detail in References [5] and [6]. Both programs are a ply-by-ply analysis of finite element meshes representing the laminas of a composite material. The program takes into account the number and orientation of orthotropic plies in the model, and it can model an infinite number of geometries and discontinuities. This section describes the theory behind the analysis, beginning with linear finite element theory and extending the theory for use with multiple-layered meshes.

PLSTR is based on the constant strain triangle as shown in Figure 11, which implies a two-dimensional elasticity problem. Quadrilateral elements in this program are assemblages of four constant strain triangles, which then resemble linear elements [24]. The assumed displacement field is linear in the x and y directions:
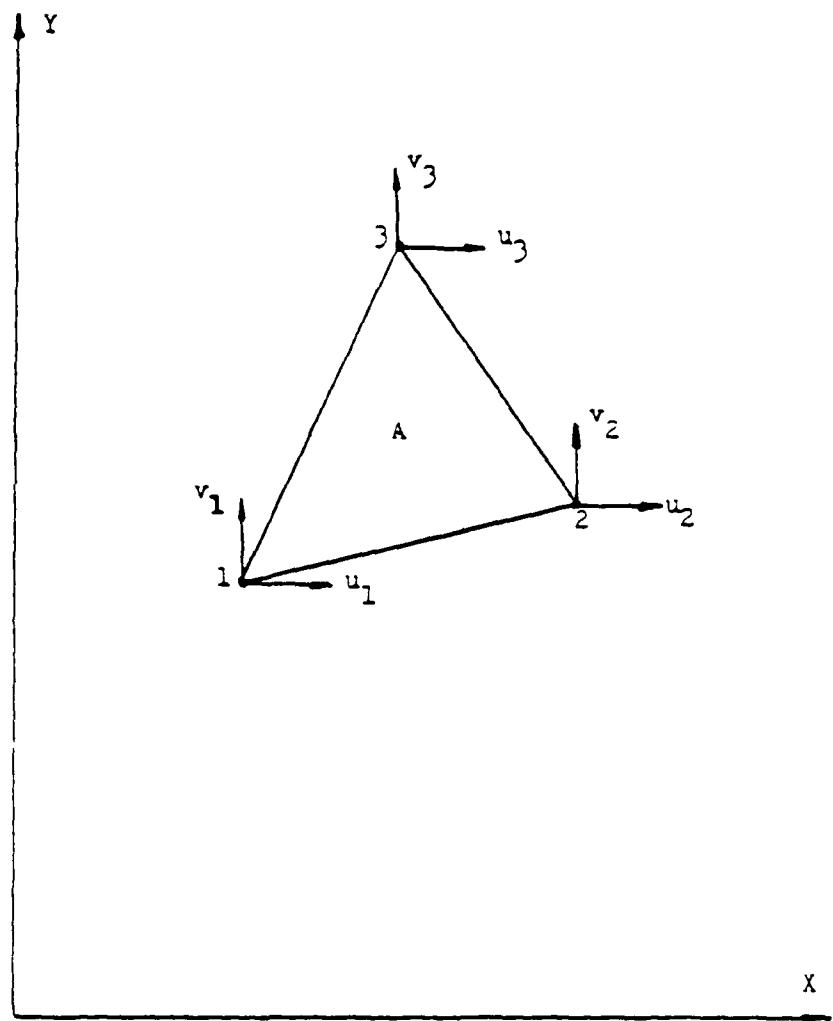
FIGURE 11.  CONSTANT STRAIN TRIANGLE ELEMENT.

43

$$
\left\{ \begin{array}{c} u(x,y) \\ v(x,y) \end{array} \right\} = \left[ \begin{array}{cccccc} 1 & x & y & 0 & 0 & 0 \\ 0 & 0 & 0 & 1 & x & y \end{array} \right] \left\{ \begin{array}{c} a_1 \\ a_2 \\ a_3 \\ a_4 \\ a_5 \\ a_6 \end{array} \right\} \qquad (12)
$$

Thus $\varepsilon_x = a_2$, $\varepsilon_y = a_6$, and $\gamma_{12} = a_3 + a_5$ [24]. The constant strain triangle assumes no variance of strain through the thickness of the element, i.e., no bending.

Through operations on the shape factors (See Reference [24]), the strains are expressed by,

$$
\underline{\varepsilon} = \left\{ \begin{array}{c} \varepsilon_x \\ \varepsilon_y \\ \gamma_{xy} \end{array} \right\} = [ B ]\{ d \} = [ B ] \left\{ \begin{array}{c} u_1 \\ v_1 \\ u_2 \\ v_2 \\ u_3 \\ v_3 \end{array} \right\} \qquad (13)
$$

where { d } is the nodal displacement vector and,

$$
[ B ] = \frac{1}{2A} \left[ \begin{array}{cccccc} (y_2-y_3) & 0 & (y_3-y_1) & 0 & (y_1-y_2) & 0 \\ 0 & (x_3-x_2) & 0 & (x_1-x_3) & 0 & (x_2-x_1) \\ (x_3-x_2) & (y_2-y_3) & (x_1-x_3) & (y_3-y_1) & (x_2-x_1) & (y_1-y_2) \end{array} \right]
$$

$$(14)$$

where A is the area of the triangle and $x_i$ and $y_i$ are the x and y coordinates of the $i^{th}$ node [19].

44

Developing an equation for the stiffness of an element,
the differential volume of an element for constant thickness
is dV = t·dA, where t is the element thickness. (Note that
this thickness is that of a ply.) The matrix [B] is
constant, and the material property matrix, defined in
general as [D], is assumed constant over the element.

The above assumptions yield the equation for the
element stiffness matrix [k],

$$[k] = \int_A [B]^T [D] [B] \, t \, dA = [B]^T [D] [B] \, t \, A \qquad (15)$$

For an orthotropic lamina whose material axes are
oriented at an angle $\theta$ to the X and Y directions, the
material property matrix [D] becomes [$\bar{Q}$], of Section II B;
i.e., the stresses are related to the strains by

$$\begin{Bmatrix} \sigma_x \\ \sigma_y \\ \tau_{xy} \end{Bmatrix} = [\bar{Q}] \begin{Bmatrix} \varepsilon_x \\ \varepsilon_y \\ \gamma_{xy} \end{Bmatrix} \qquad (16)$$

Since [$\bar{Q}$] is constant for each increment, it follows
that

$$[k] = [B]^T [\bar{Q}] [B] \, t \, A \qquad (17)$$

Now to account for n number of plies through the
thickness of the material, an equivalent element stiffness
matrix is formed as

$$[k_{eq}] = A \sum_{i=1}^{n} [B]^{T} [\bar{Q}]_i [B] \, t_i \qquad (18)$$

where $i$ denotes the $i^{th}$ layer, and here $n = 16$ plies. Thus, loads are related to displacement on an element basis by the finite element equation:

$$\{f\} = [k_{eq}] \{d\} \qquad (19)$$

Note that even though multiple layers have been allowed through the thickness of the element, the layers have common nodes. Thus strain or displacement gradients are not permitted through the thickness of the laminate [Cron]. Thus, 16 elements stacked together all deform in the same way under a given load. Whether or not an element fails depends on its own material properties and on its orientation to the given load.

F.  Nonlinear Finite Element Theory

As discussed in Chapter I, a more accurate analysis of composites must include the effects of nonlinearity in the material. The computer analysis portion of this thesis was accomplished using a nonlinear finite element technique, which is based upon the concepts of the previous two sections. Sandhu gives a complete development of this technique in References [5] and [6].

This progressive-ply-failure finite element computer program (called PLSTREN) was written by Sandhu to predict

(1) the damage initiation and accumulation process
in composite laminates containing stress concentrations and

(2) the static strength of composite laminates
containing stress concentrations.

The program combines a nonlinear point stress analysis
procedure [5, 6], with a damage accumulation approach [25].
The program is modular in structure to permit the use of
various finite elements, ply failure criteria, and
post-ply-failure unloading models. The present version of
the program uses constant strain elements, a "total strain
energy" failure criterion [5, 6], and two different
post-ply-failure unloading models [8]. This section
develops an incremental stress-strain law, discusses the
nonlinear material basic properties, describes a biaxial
stress state correction, and presents the finite element
procedure used in PLSTREN.

To account for nonlinearity of material behavior, an
incremental form of the constitutive law of Eq.(3) is
needed to define the response of the laminate under general
states of stress. In formulating this incremental
constitutive relationship it is assumed that [5]

   a. The increment of strain depends, upon the strain
state and the increment of stress; and

   b. The increment of strain is proportional to the
increment of stress.

With these assumptions, and with the assumption that
the strain-displacement relation (matrix [B]) remains
linear, for orthotropic laminas under generalized plane
stress, the incremental constitutive law can be written as

$$d\varepsilon_i = S_{ij}(\varepsilon_i)\, d\sigma_j \qquad (i,j = 1,2,6) \qquad (20)$$

where $d\varepsilon_i$, $d\sigma_j$ are strain and stress increments and $S_{ij}$ is
a function of the current strains, $\varepsilon_i$. Assuming that the
lamina remains orthotropic at all load levels, Eq. (20) is
expanded to become [8]

$$\begin{Bmatrix} d\varepsilon_1 \\ d\varepsilon_2 \\ d\varepsilon_6 \end{Bmatrix} = \begin{bmatrix} S_{11} & S_{12} & 0 \\ S_{12} & S_{22} & 0 \\ 0 & 0 & S_{66} \end{bmatrix} \begin{Bmatrix} d\sigma_1 \\ d\sigma_2 \\ d\sigma_6 \end{Bmatrix} \qquad (21)$$

which is the incremental version of Eq. (6). Since the
lamina is assumed to remain orthotropic at all load levels,
for each increment [8]

$$S_{16} = S_{26} = S_{61} = S_{62} = 0 \qquad (22)$$

For clarity, in Eq. (21)

$d\sigma_1$, $d\varepsilon_1$ = normal stress and strain increments in the
fiber direction,

$d\sigma_2$, $d\varepsilon_2$ = normal stress and strain increments in the
transverse direction,

$d\gamma_6 = d\sigma_{12}$ = shear stress increments,

$d\varepsilon_6 = d\varepsilon_{12}$ = shear strain increments,

$S_{ij}$ = terms of the compliance matrix representing
average values during an increment of
stress; defined by Eqs. (7).

Equation (19) can be inverted to yield the incremental version of Eq. (2):

$$d\sigma_i = C_{ij}(\varepsilon_j) \, d\varepsilon_j, \qquad (i,j = 1,2,6) \qquad (23)$$

where $C_{ij}$ is the inverse of $S_{ij}$.

In the application of the incremental constitutive law to multidirectional laminates, Eq. (23) for the $k^{th}$ ply is written in matrix notation as

$$\{d\sigma\}_k = [C]_k \{d\varepsilon\}_k \qquad (24)$$

where

$$[C]_k = [S]_k^{-1} = \text{Stiffness matrix of the } k^{th} \text{ ply}$$

$$\{d\sigma\}_k = \qquad \text{Stress increment in the } k^{th} \text{ ply}$$
relative to the material axes 1 and 2

$$\{d\varepsilon\}_k = \qquad \text{Strain increment in the } k^{th} \text{ ply}$$
relative to the material axes 1 and 2

Extending Eq. (24) to the general case of multidirectional and angle-ply laminates, the incremental constitutive law for the $k^{th}$ ply becomes:

$$\{d\sigma\}_k = [\bar{Q}]_k \{d\varepsilon\}_k \qquad (25)$$

where the terms of $[\bar{Q}]$ are given following Eq. (10).

To obtain the incremental stress-strain relations for a lamina, the definitions of the $S_{ij}$ terms from Section II B are substituted into Eq. (21), yielding

$$d\varepsilon_1 = \frac{d\sigma_1 (1 - \nu_{12}^{(3)})}{E_{11}}$$

$$d\varepsilon_2 = \frac{d\sigma_2 \left(1 - \frac{\nu_{21}}{\beta}\right)}{E_{22}} \tag{26}$$

$$d\varepsilon_6 = \frac{d\sigma_6}{G_{12}}$$

where $\beta = \dfrac{d\sigma_2}{d\sigma_1}$, and provided that $d\sigma_1$ and $d\sigma_2 \neq 0$ [5].

The incremental elastic constants in $[\bar{Q}]$ (or $[\bar{S}]$) are obtained from the basic lamina stress-strain data by an iterative procedure [8]. In general, the finite element equation, Eq. (19), presented in the last section is also written on an incremental basis:

$$d\{f\} = [k(\varepsilon)_{eq}] \, d\{d\} \tag{27}$$

where $d\{f\}$, $d\{d\}$, and $[k(\varepsilon)_{eq}]$ are the increments of load and displacement and the current stiffness matrix, respectively. Note that the stiffness matrix depends on the current level of strain. This dependence exists through the transformed reduced stiffnesses, $[\bar{Q}]$ [19]. From the previous section,

$$[k_{eq}] = A \cdot \sum_{i}^{n} [B]^{T} [\bar{Q}]_{i} [B] \, t_{i} \tag{28}$$

and one can see that $[k_{eq}]$ is calculated using the $i^{th}$ $[\bar{Q}]$. If the analyzed material exhibits nonlinearity, the basic properties of the laminas:

$$E_1^T, \; E_1^C, \; E_2^T, \; E_2^C, \; G_{12}, \; \nu_{12}^T, \; \nu_{12}^C$$

50

will vary with strain. It follows that $[\bar{Q}]_i$ and hence $[k_{eq}]$ will vary with strain as well [19].

Since material properties are not linear, material property curves must be used for this analysis. For this thesis these curves were obtained from stess-strain experiments on unidirectional lamina. The tests and their corresponding curves and material properties are shown in Table 1. These tests are described in Chapter IV of this thesis

To make the experimental curves usable by the computer code, they are entered in tabular form and are represented analytically by a piecewise cubic spline interpolation

---

Table 1.   Basic Property Tests, Curves, and
Corresponding Basic Properties

---

| Test | Curve | Basic Property |
|------|-------|----------------|
| $0°$ Tension | $\sigma_1$ vs. $\varepsilon_1$ | $E_1^T$ |
| $0°$ Compression | $\sigma_1$ vs. $\varepsilon_1$ | $E_1^C$ |
| $90°$ Tension | $\sigma_2$ vs. $\varepsilon_2$ | $E_2^T$ |
| $90°$ Compression | $\sigma_2$ vs. $\varepsilon_2$ | $E_2^C$ |
| $\pm45°$ Tension | $\tau_{12}$ vs. $\gamma_{12}$ | $G_{12}$ |
| $0°$ Tension | $\nu_{12}$ vs. $\varepsilon_1$ | $\nu_{12}^T$ |
| $0°$ Compression | $\nu_{12}$ vs. $\varepsilon_1$ | $\nu_{12}^C$ |

---

function [8]. The use of the spline function renders smooth stress-strain curves, which are desirable for determination of elastic moduli under incremental and iterative computations [8]. With the stress-strain curves thus represented by simple polynomials, the tangent moduli of $E_1$, $E_2$, and $G_{12}$ can be readily obtained as functions of strain by differentiating the appropriate cubic spline functions with respect to strain.

To satisfy the numerical nature of the computer, the loads must be applied incrementally on the finite element model, as implied by Eq. (27). However, $[k_{eq}]$ may vary within a load increment. To overcome this dilemma, a "predictor-corrector and iterative technique"[6] is employed in the program.

In this procedure, $[k_{eq}]$ is initially calculated in the first increment using engineering linear elastic constants, which are equal to the initial slope of the basic property curves. For the subsequent increments, $[k_{eq}]$ is calculated using material properties that correspond to the state of strain existing at the end of the previous load increment. Having calculated $[k_{eq}]$ from the $n^{th}$ load increment, a new increment of load is applied and an increment of displacement is calculated using Eq. (27). Thus Eq. (27) will take the form

$$d\{f\}_{n+1} = [k(\varepsilon)_{eq}]_n \, d\{d\}_{n+1} \qquad (29)$$

where n denotes the $n^{th}$ load increment [19].

The new displacements, $d\{d\}_{n+1}$, can then be used to calculate an increment of strain using

$$d\{\varepsilon\} = [B] \, d\{d\} \qquad (30)$$

The incremental stress can then be calculated from

$$d\{\sigma\}_\iota = [\bar{Q}]_\iota d\{\varepsilon\} \qquad (31)$$

where $\iota$ denotes the $\iota^{th}$ layer as defined previously [19].

Given the current levels of stress and strain, new increments of stress and strain are computed and added to the end of the current level to obtain a new level. A mean level of strain is then computed by averaging the new level of strain with the previous level at the end of the increment. These mean strains are then used to determine a new set of material properties since they are readily obtainable as functions of strain through the cubic spline functions [19].

Given the new elastic properties, [Q], [$\bar{Q}$], and hence $[k_{eq}]$ are recalculated. The same load increment, not an additional one, is then reapplied; and the increment of displacement and strain is recalculated. This procedure is continued for a given load increment until the change of the strain increment converges to less than a specified value, i.e., until

$$\frac{d\varepsilon_{n+1} - d\varepsilon_n}{d\varepsilon_n} < 0.001 \qquad (32)$$

where n denotes the $n^{th}$ reapplication of a given load increment. When Eq. (32) is satisfied, a new load increment is applied. The repetitive use of the procedure outlined above generates the predicted stress-strain response of the laminate under consideration [19].

Graphically, this procedure is shown in Figure 12. [19]. A one-dimensional case of shear loading is shown for clarity, but the program recalculates elastic properties using all seven curves during a load increment. Stepping through the example, the initial strain $\gamma_o$ exists due to a previous load increment. A new increment of the load is then applied and the resulting strain, $\gamma_1$, is calculated based on $G_{12}$ at point 0. A new modulus is now determined, corresponding to the average of $\gamma_1$ and $\gamma_o$, point A. With new moduli, the load is then reapplied and a new strain, $\gamma_2$, is calculated using the modulus at point A. Again, a new modulus corresponding to the average of $\gamma_2$ and $\gamma_o$, point B, is calculated and a reapplication of the load yields $\gamma_3$. This procedure is repeated until [19]

$$\frac{\gamma_{n+1} - \gamma_n}{\gamma_n} < 0.001 \qquad (33)$$

Note that superposition principles do not apply in the iterative procedure that begins with Eq. (29). The
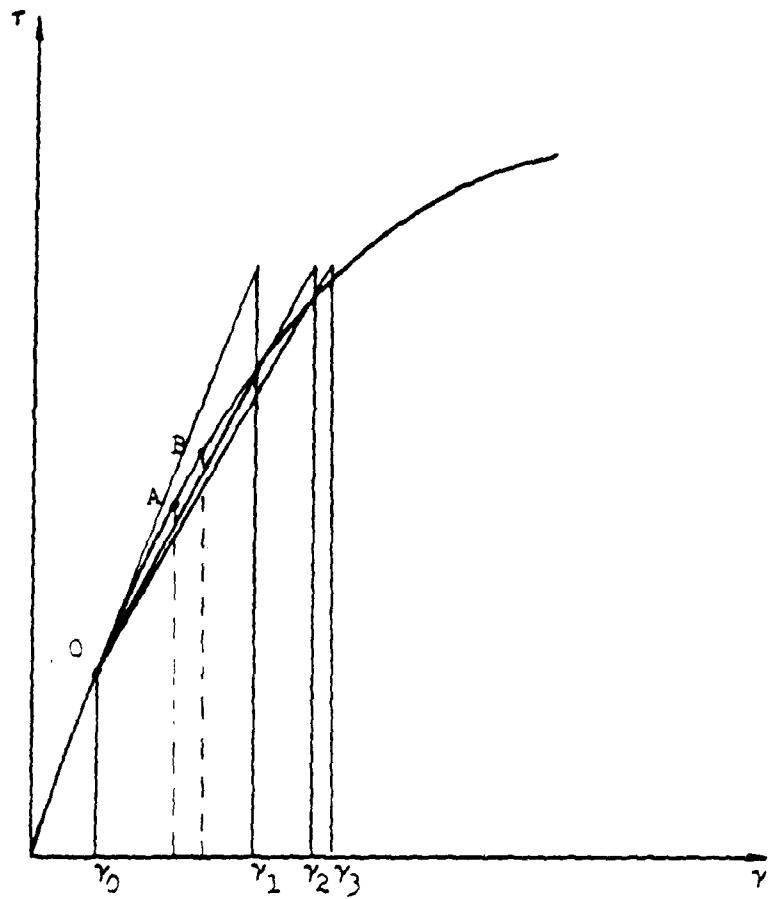
FIGURE 12. GRAPHICAL ILLUSTRATION OF ONE-
DIMENSIONAL NONLINEAR RESPONSE.

stiffness matrix [k] is an assemblage of element stiffnesses
built upon the (assumed) independent basic material
properties. Thus Figure 12 cannot be applied directly to
Eq. (29).

During the determination of the incremental elastic
constants, direct use of the lamina stress-strain curves may
be incorrect. For the off-axis laminas, uniaxial loads
create a biaxial stress state in the lamina. For plies
under biaxial stress, the biaxial strains $\varepsilon_1$ and $\varepsilon_2$ must be
modified before they can be used to determine the elastic
constants from the cubic spline stress-strain curves. It
would be erroneous to use these strains to determine $E_1$ or
$E_2$ from stress-strain curves obtained under simple loading
conditions. Recalling Eqs. (26), $d\varepsilon_2$ corresponds to the
curve $\overline{ON}$ in Figure 13 [5] on the plane $\overline{OEHG}$. The simple
stress-strain curve $\overline{OM}$ lies on the plane $\overline{OEDC}$.
Stress-strain data similar to ON is not avialable;
therefore, it is assumed that simple equivalent strain
increments can be computed from the following expressions
[5]:

$$d\varepsilon_1 \bigg|_{eq} = \frac{d\sigma_1}{E_1} = \frac{d\varepsilon_1}{1 - \nu_{12} \dfrac{d\sigma_2}{d\sigma_1}} \quad , \quad (34)$$

$$\varepsilon_2 = \sigma_2(1 - \nu_{21}\sigma_1/\sigma_2)/E_2$$
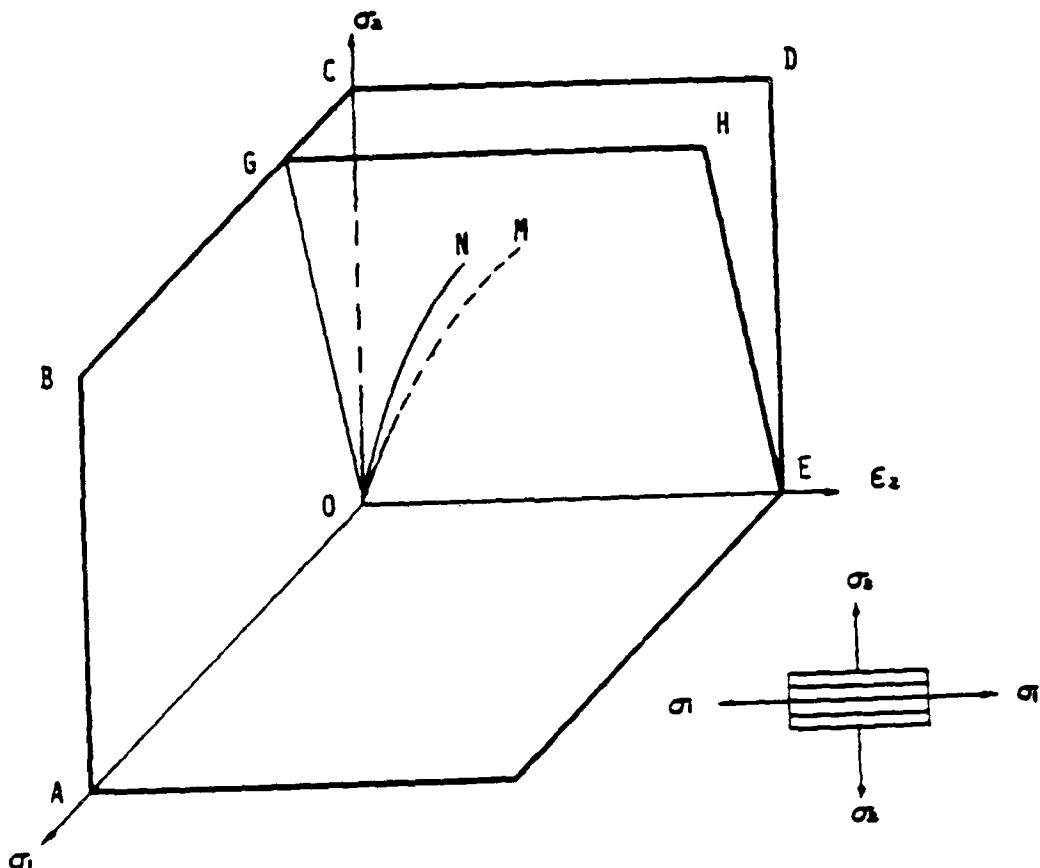
FIGURE 13. STRAIN, $\varepsilon_2$, UNDER A BIAXIAL STRESS FIELD $(\sigma_1, \sigma_2)$.

$$d\varepsilon_2\Big|_{eq} = \frac{d\sigma_2}{E_2} = \frac{d\varepsilon_2}{1 - \nu_{21}\dfrac{d\sigma_1}{d\sigma_2}} \tag{35}$$

Note that the error that would result from using $d\varepsilon_1$ and $d\varepsilon_2$ instead of their equivalent strain would be $\nu_{12}\beta$ for $d\varepsilon_1$ and $\nu_{21}/\beta$ for $d\varepsilon_2$, where $\beta = d\sigma_2/d\sigma_1$.

Specifically, the nonlinear finite element analysis in this thesis uses the foregoing methods to accomplish the following process. Assuming that stresses are uniformly distributed through the thickness of each ply, stress resultant increments, [dN], in the X, Y coordinate system are given by

$$[dN] = \sum_{k=1}^{P} [d\bar{\sigma}]_k t_k \tag{36}$$

where

$d\bar{\sigma}$ = the (transformed) stress increments in the X, Y coordinate system

$t_k$ = thickness of the $k^{th}$ ply

$p$ = number of plies in a laminate

Paralleling the development of Section II, B and substituting the incremental constituitive law, Eq. (25), into Eq. (36), the stress resultants become

58

$$[dN] = \sum_{k=1}^{P} t_k \, [\bar{Q}]_k \, [d\bar{\varepsilon}]_k \qquad 37$$

where $[d\bar{\varepsilon}]$ are (transformed) strain increments in the X, Y coordinate system.

Noting that the strain increments $[d\bar{\varepsilon}]_k$ are the same for all plies in the laminate, Eq. (38) becomes

$$[dN] = [A] \, [d\varepsilon] \qquad (38)$$

where

$$[A] = \sum_{k=1}^{P} t_k \, [\bar{Q}]_k \qquad (39)$$

Inversion of Eq. (39) yields

$$[d\varepsilon] = [A]^{-1} \, [dN] \qquad (40)$$

where $[A]^{-1}$ represents the average compliance properties of the laminate during the $(n+1)^{th}$ load increment. However, $[A]^{-1}$ is not known when the $(n+1)^{th}$ increment is applied. To overcome this difficulty, the elastic properties at the end of the $n^{th}$ load increment are used in Eq. (40), i.e.,

$$[d\varepsilon]_{n+1} = [A]^{-1}_n \, [dN]_{n+1} \qquad (41)$$

The strain increments $[d\varepsilon]_{n+1}$ obtained from Eq. (41) are used in Eqs. (25), (34), and (35) to calculate $[d\sigma]_k$, $[d\varepsilon]_k$, $d\varepsilon_1\big|_{\oplus q}$, and $d\varepsilon_2\big|_{\oplus q}$. These stress and strain increments are added to stresses and strains at the $n^{th}$ load increment to obtain the current stresses and strains in all plies. The

current stresses and strains are employed to determine the
average elastic properties of the plies and a new $[A]^{-1}$ is
computed.  This procedure is repeated, in the manner of
Figure 12, until the difference between two values of
$[d\varepsilon]_{n+1}$ is less than 0.1 percent.  Eq. (41) then becomes

$$[d\varepsilon]_{n+1} = [A]^{-1}_{n+1} [dN]_{n+1} \qquad (42)$$

The repetitive use of the procedure outlined above generates
the stress-strain response of unidirectional, angle-ply, or
multidirectional laminates [8].

## G.  Failure Criterion

The incremental loading procedure outlined in the
preceding section cannot continue indefinitely.  The
prediction of the response of the laminate should culminate
with the incremental failure of elements and the eventual
failure of the laminate.  A level will be reached where a
lamina or laminas can no longer sustain additional loads.
Thus, the failure state of a lamina under general stress
states is determined by a criterion relating the behavior of
the ply in the laminates to the behavior of the ply under
simple load conditions.  Various criteria have been
proposed which formulate criteria for the failure of
anisotropic materials [26].  This section describes one
criterion, developed by Sandhu [5, 6], which accounts for
nonlinear material behavior.

Following the development found in References [5] and
[6], a scalar function, f, defining the failure condition of
materials exhibiting nonlinear behavior can be written as

$$f(\sigma, \varepsilon, K) = 1 \qquad (43)$$

where $\sigma$ and $\varepsilon$ are the stress and strain states and K
describes the material characteristics.

A simple scalar function dependent upon both stress and
strain states is the strain energy of the material. In the
case of orthotropic materials, strain energies that are due
to uniaxial tension and compression along and transverse to
the material axes, and due to shear are independent
parameters. To measure the level of the effect of both
stress and strain states on the orthotropic materials under
a combined stress state, a simple scalar function is a
linear combination of functions of different strain
energies. Thus, an explicit form of Eq. 43) can be written
as

$$\sum_{i=1}^{3} \sum_{j=1}^{3} K_{ij} \left[ \int_{\hat{\varepsilon}_{ij}} \sigma_{ij} \, d\varepsilon_{ij} \right]^{m_{ij}} = 1 \qquad 44$$

where $\hat{\varepsilon}$ are the current strain components and $m_{ij}$ are the
parameters defining the shape of the failure surface in the
strain energy space [5]. The strain energy failure
criterion is based upon total strain energies. By being a
function of both stress and strain states, this criterion

81

helps to account for the nonlinear strains that occur prior to failure [19] in composites such as Gr/PEEK.

Specialized for the plane stress condition and using contracted notation, Eq. (44) becomes [5]

$$K_1 \left[ \int_{\hat{\varepsilon}_1} \sigma_1 \, d\varepsilon_1 \right]^{m_1} + K_2 \left[ \int_{\hat{\varepsilon}_2} \sigma_2 \, d\varepsilon_2 \right]^{m_2} + K_6 \left[ \int_{\hat{\varepsilon}_6} \sigma_6 \, d\varepsilon_6 \right]^{m_6} \tag{45}$$

or, using nonrepeating summation notation

$$K_i \left[ \int_{\hat{\varepsilon}_i} \sigma_i \, d\varepsilon_i \right]^{m_i} = 1, \qquad (i = 1, 2, 6) \tag{46}$$

Using results of tests under simple load conditions,

$$K_i = \left[ \int_{\varepsilon_{iu}} \sigma_i \, d\varepsilon_i \right]^{-m_i}, \qquad (i = 1, 2, 6) \tag{47}$$

where $\varepsilon_{iu}$ are the ultimate normal (tensile or compressive) and shear strains. Combining Eqs. (46) and (47), the following equation is obtained [5]:

$$\left[ \frac{\int_{\hat{\varepsilon}_i} \sigma_i \, d\varepsilon_i}{\int_{\varepsilon_{iu}} \sigma_i \, d\varepsilon_i} \right]^m = 1, \qquad i = 1, 2, 6 \tag{48}$$

This equation states that a lamina will fail in a particular direction (1, 2, or 6) when the corresponding area under the stress-strain curve, due to the incremental loading by the finite element program, reaches a combined maximum area, i.e., the area which corresponds to failure.

The shape of the failure surface in the strain energy space (Eq. 48.) is determined by the shape factor, m. For three values of m (1/2, 1, 2), this criterion is compared with some of the other failure theories for a boron-epoxy material system in Figure 14 [19]. While a value of m ≠ 1 may make the analysis more accurate than with m = 1, there is no biaxial strain energy failure data available to fix m to a specific value. Therefore, this study took m to to be unity. This reduces the criterion to a simple linear relationship i.e., when the sum of the three ratios equals unity, the lamina degrades completely. The three ratios at that time are contributions to degradation made by longitudinal, transverse, and shear stress acting in the lamina [6].

In a study of composites, two failure phenomena are assumed to be possible. These are matrix failure, due to tension, compression, or shear, and fiber failure due to tension or compression. Matrix failure occurs without necessarily precipitating fiber failure. In this case, the failed portion of the lamina is unloaded in transverse tension and shear, while continuing to carry loads in the
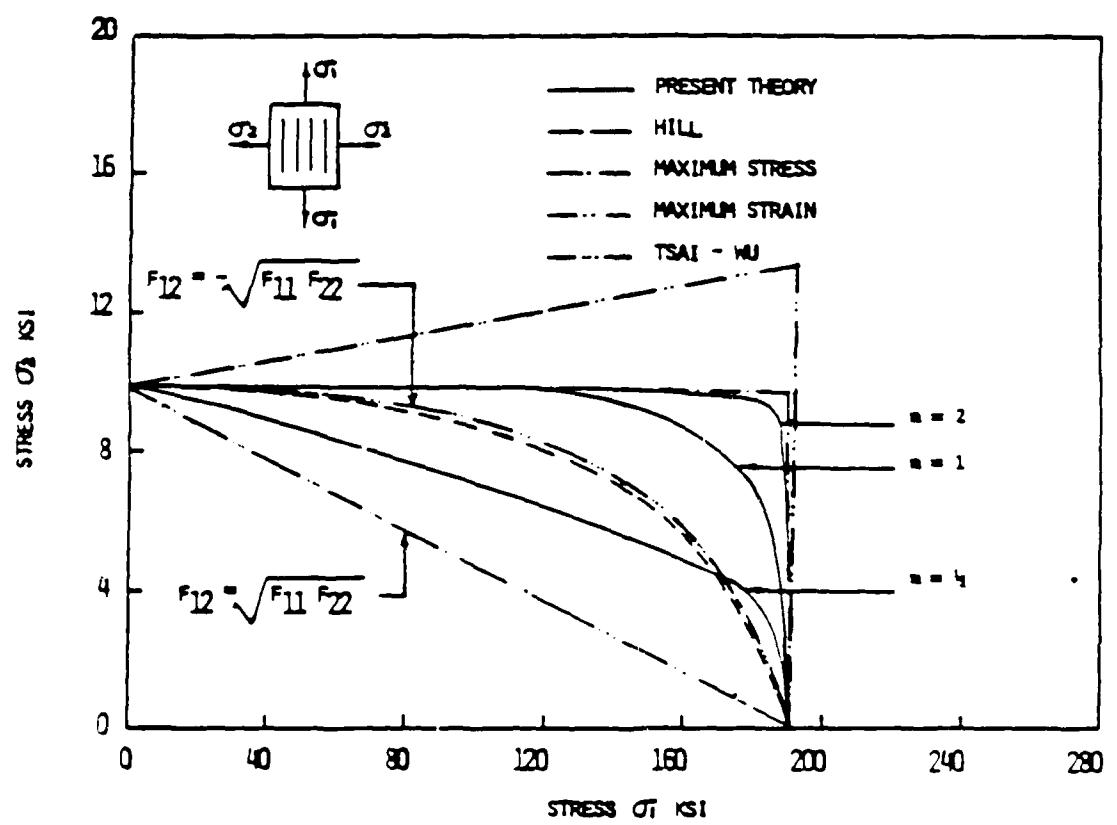
FIGURE 14. COMPARISON OF STRENGTH THEORIES

fiber direction. (Unloading schemes for the computer program are described subsequently.) If the fiber failure mode occurs, the lamina is assumed to be completely failed, and the loads are transferred to the adjacent lamina. The occurrence of either lamina failure mode is determined by using the strain energy failure criterion [8].

Fiber failure is assumed to occur if

$$\frac{K_1 \left\{ \int_{\varepsilon_1} \sigma_1 \, d\varepsilon_1 \right\}}{\sum\limits_{\iota=1,2,6} K_\iota \left\{ \int_{\varepsilon_\iota} \sigma_\iota \, d\varepsilon_\iota \right\}} \geq 0.1 \qquad (49)$$

and the criterion of Eq. (48) is satisfied. Matrix failure occurs when Eq. (48) is satisfied and inequality (49) is not. It is further assumed that the delamination moment coefficient [22] is below the critical value for delamination to occur.

A final point to present is the modeling of the progressive-ply-failure [8]. Once lamina failure occurs in one or more elements, the failed elements have to be unloaded. The following two failed-ply unloading schemes are possible in the program PLSTREN.

In the case of multidirectional laminates, it is assumed that the failed element(s) unload gradually. This is reasonable since as areas of laminas fail, adjacent

65

areas and laminas pick up the extra stresses. Thus, the analysis attempts to model interlaminar stresses. But according to Petit [25],this action of the laminate is "not so easily postulated." It is not known what proportion of the load the lamina retains nor what happens to the modulus after degradation. The of unloading is done by assigning negative values to the affected moduli, which determined on the basis of the failure mode. This scheme is shown for transverse tension in Figure 15. Note the slope of the negative tangent modulus. This slope varies for all simple loads, and its value in this analysis is assumed to be the negative of the initial slope of the respective basic property curves.

The incremental loading is continued on the modeled laminate until the stresses in the affected element(s) are reduced to zero. The moduli are then set to nominally small values. This failed-ply unloading scheme was used in Reference [23] and was found to give excellent results for stress-strain curves of multidirectional laminates. The scheme attempts to model the progressive nature of the matrix cracking process within the elements. But while reasonable for multidirectional laminates, this failed-ply unloading scheme gives results that are too high for unidirectional laminates.

In the case of unidirectional laminates, it should be assumed that the failed elements unload rapidly. This idea
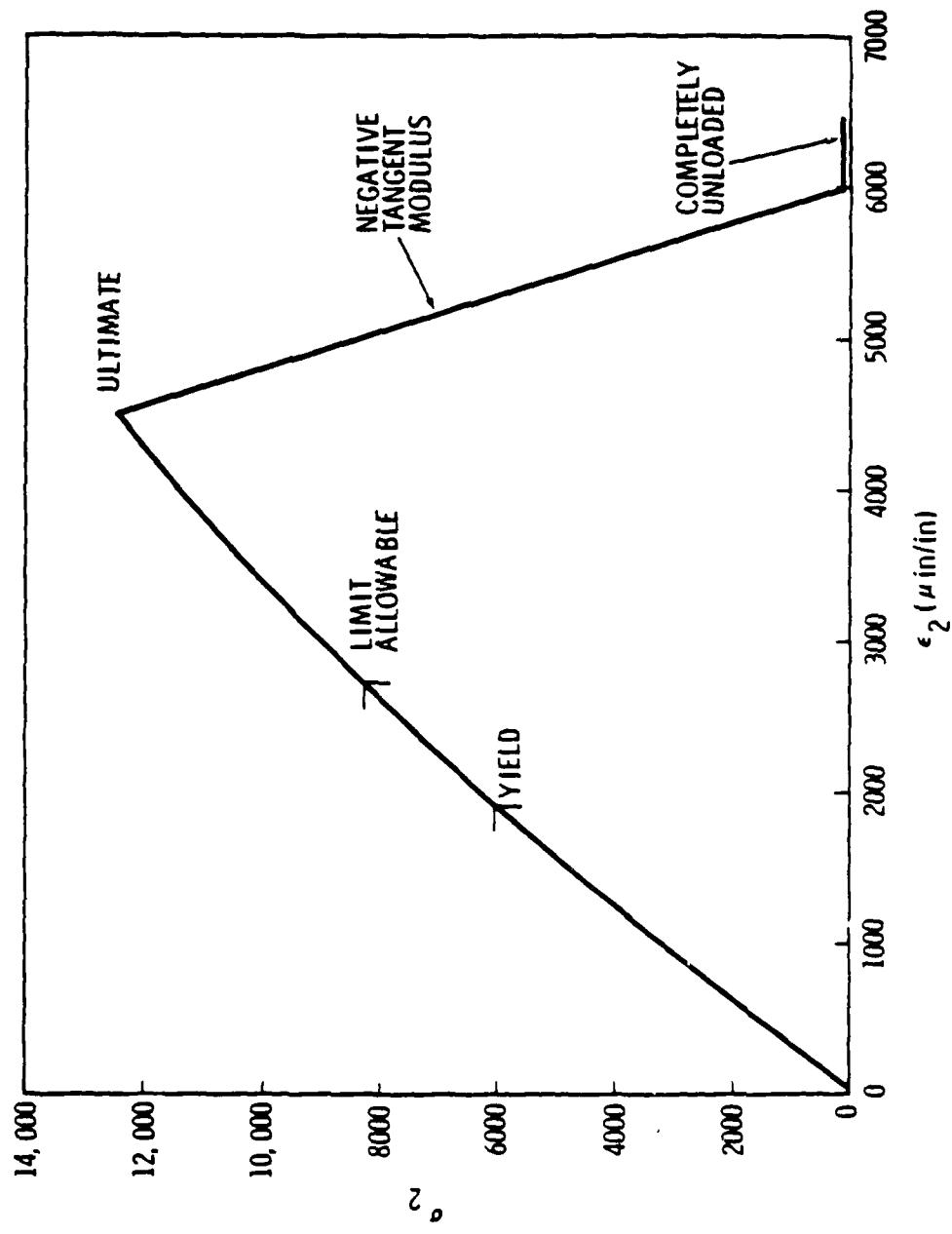
FIGURE 15. POST ULTIMATE BEHAVIOR.

is reasonable since failure in a unidirectional laminate occurs through the thickness and is usually sudden; theoretically, no interlaminar stresses exist. The affected moduli of a failed element are set to nominally small values (100 psi) and the same load increment is applied again. This reapplication of the load increment can cause failure of additional elements. These failures are secondary in that they are caused by load redistribution without an increase in load. If secondary failures occur, the load increment is repeated until no further secondary failures occur. The load is then increased to the next higher level. Generally, this unloading scheme gives lower strength predictions than the gradual unloading scheme [8].

As a summary of the development presented for the program PLSTREN, a diagram of Sandhu's program is shown in Figure 16. The chart shown is not a typical flowchart, but instead shows the complexity of a nonlinear progressive-ply-failure finite element program.

This chapter has presented the theory behind the analytical and experimental investigations of this thesis. The following two chapters describe procedures used in the analysis and experimentation phases. Results and conclusions are presented in subsequent chapters.

COMPUTER PROGRAM "PLSTREN"
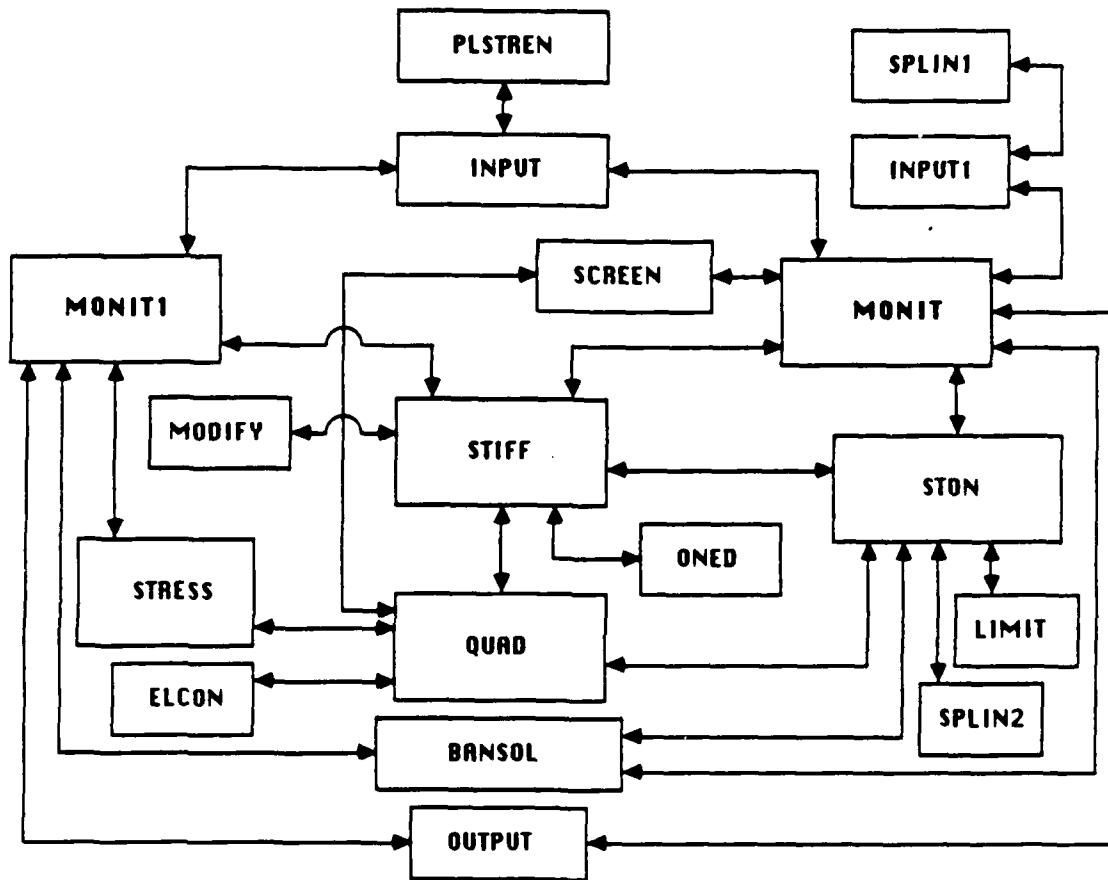
FIGURE 16. DIAGRAM OF SANDHU'S PROGRAM "PLSTREN."

# III. Analysis

As discussed in Chapter I, the analysis of composite laminates to predict the onset, progression, and completion of failure has been accomplished by many methods. These range from numerous fracture mechanics approaches to several finite element techniques. In this thesis, the nonlinear incremental finite element technique described in Chapter II was used on three stacking sequences of Gr/PEEK laminates. The purpose of this effort was to study the initiation and progression of failure at or near a circular discontinuity in a material which is subjected to tension. With a particular specimen geometry chosen, a suitable finite element mesh developed, and finally with experimentally derived data, a nonlinear analysis was accomplished for the composite material Gr/PEEK.

## A. Specimen Geometry

To analyze the failure characteristics of Gr/PEEK, the specimen geometry shown in Figure 17 was chosen for this study. Note that the diameter of the hole is one-third the width of the specimen. As mentioned previously, this 6" X 1.2" X 0.084" specimen represents a thin composite plate of finite width. These tensile coupons were manufactured with 16 layers of laminas with the prescribed orientations, or

0.4" DIA

1.2"

0.084"

6.0"
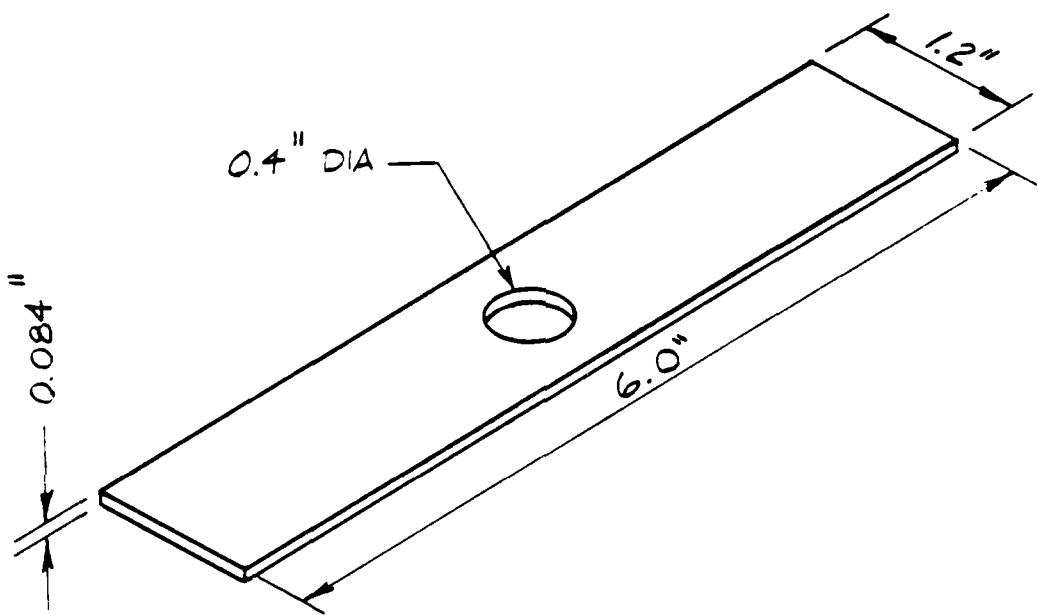
FIGURE 17.   SPECIMEN GEOMETRY.

|  | Stacking Sequence | Symbol | Type |
|---|---|---|---|
| Table 2. | Modeled Stacking Sequences. | | |
| | $[0_{16}]$ | 0T | Unidirectional |
| | $[90_{16}]$ | 90T | Unidirectional |
| | $[\pm45]_{4S}$ | SH | Angle-Ply |

stacking sequences.  The stacking sequences which were modeled and analyzed are listed above in Table 2.  Note that 'S' implies a symmetric laminate, and that all laminates are symmetric about their middle surfaces.

One reason for choosing these lay-ups was to investigate the reaction of unidirectional and angle-ply laminates under tension.  It is hoped that these results can be related to a future analysis of quasi-isotropic laminates under tension.  Of course interlaminar stresses would play a major role in the reaction of the plies in a quasi-isotropic laminate.  It is hoped that by studying individual orientations, one could draw conclusions about the quasi-isotropic specimens.

B.  Finite Element Modeling

An acceptable finite element model of a structure should accurately predict the displacement and stress fields

of the actual structure under a given load. To obtain such a model, the analyst must accurately model the size, shape, loads (or displacements), and boundary conditions of the actual structure. Furthermore, he must provide for adequate refinement of the element mesh in areas where gradients in the displacement field or the stress field are known or expected to be high. In describing the finite element modeling carried out in this thesis, each of these requirements will be discussed in this section.

The size and shape of the finite element mesh obviously modeled the rectangular thin plate analogy that was shown in Figure 17. Each of the sixteen layers of laminas were specified in thickness, $t_k$ of Eq. (36), and in orientations, $\theta$ in the transformed reduced stiffnesses of Eq. (10).

Because of the specimen and laminate symmetry, only a quarter of the specimen could have been modeled to minimize analysis time and computer costs. However, in the program, the stresses and strains in an element are output for the center of the element. Therefore, to acquire the stresses and strains at the transverse centerline of the specimen, half of the specimen was modeled as shown in Figure 18. In this way, output at the centerline is easily rendered without the need for extrapolation.

The model of Figure 18 was used for all three types of specimens. Note the coordinate axes relative to the model, the diagrammed constraints, and the listed information in
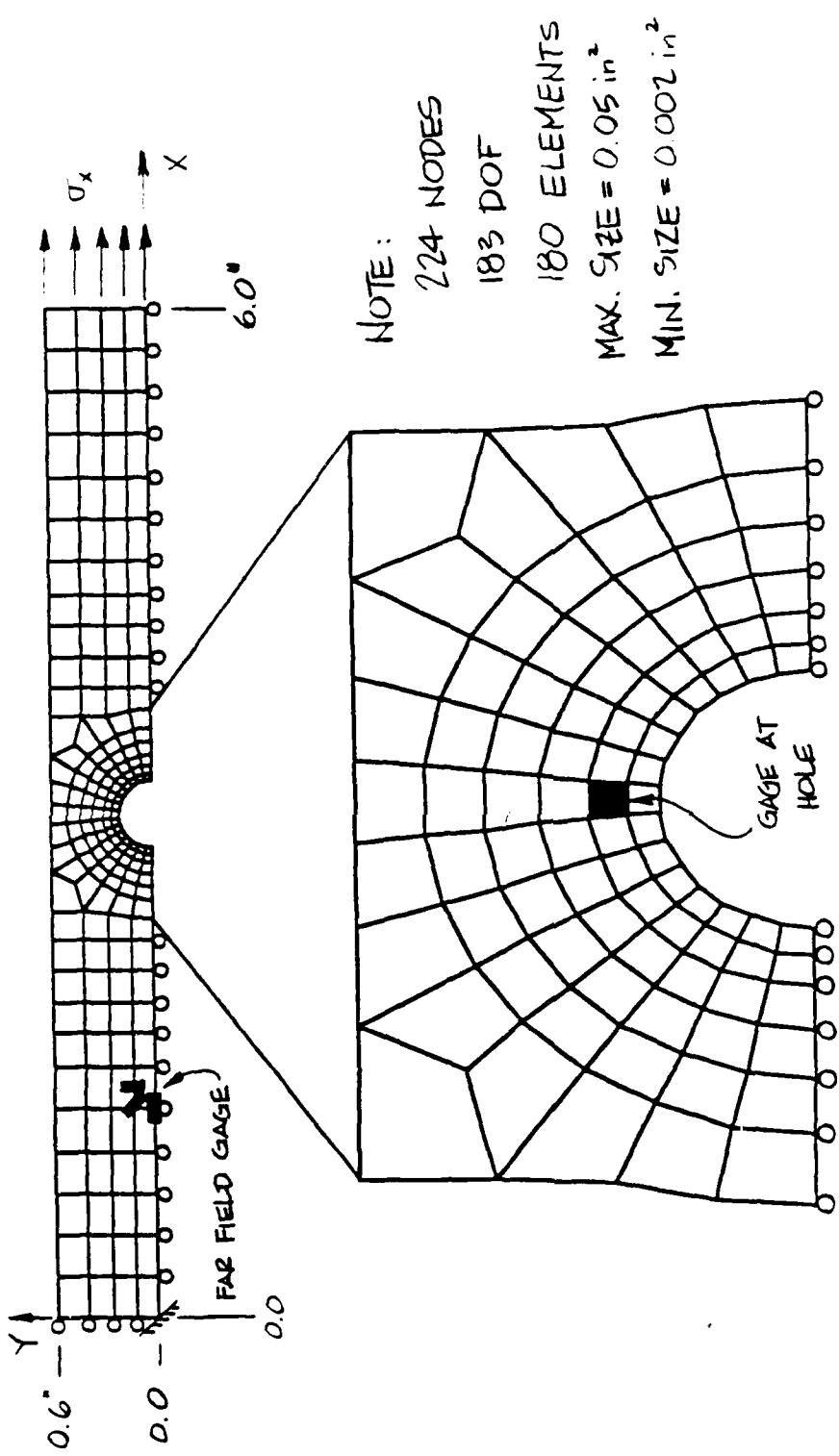
FIGURE 18. FINITE ELEMENT MESH USED IN ANALYSIS

NOTE:
224 NODES
183 DOF
180 ELEMENTS
MAX. SIZE = 0.05 in$^2$
MIN. SIZE = 0.002 in$^2$

$\sigma_x$

X

6.0"

0.6"

0.0

0.0

Y

GAGE AT HOLE

FAR FIELD GAGE

the figure. Also note that the elements are finer
surrounding the hole. Because of higher stress
concentrations nearer the hole, finer discretization of the
specimen will yield more accurate results. Note further
that no transition elements (such as triangular elements or
elements with five or more nodes) are used in this mesh.
According to Sandhu (in a conversation with him), the
program works best if the elements are as square as
possible. This has been accomplished with the quadrilat-
erals gradually increasing in size away from the hole until
they match the rectangular grid of the rest of the specimen.

To simulate the tension field on the specimen in the
test machine (See Chapter IV), the model was subjected to
tension by constraining the left end of the model and
displacing the other end. Another method of this program
applies "negative pressure" on the nodes at each end of the
specimen. This pressure is a force per unit length acting
on each end and creating tension in the specimen. This
method was not used because one of the nodes on which
pressure would have been applied was fixed in this model.
Thus, pressure on that node would have been meaningless.
Since its counterpart on the other end of the model was not
fixed, an asymmetrical stress field would have been set up
in the specimen, and the model would not have simulated the
actual structure.

As shown in Figure 18, the modeled boundary conditions
were such that the node at coordinate (0.0, 0.0) was fixed
in both the x and y directions to prevent rigid body motion
of the model. The longitudinal centerline of the specimen
dictated that the rest of the nodes along the line y = 0.0
were free to move in the x-direction but were fixed in the
y-direction. At the ends, the nodes along the line x = 0.0
were fixed in the x-direction but were free to move in the
y-direction. The nodes along the line x = 5.0 were
prescribed with a given displacement and were free in the
y-direction. The rest of the nodes in the model were free
in both directions. The goal of this model was to simulate
the actual boundary condition caused by the tension grips of
the test machine.

2. Convergence Study

To determine the refinement of the finite element mesh,
two competing goals were sought: (1) to predict behavior
as accurately as possible and (2) to save CPU time and
expense as much as possible. Thus, a convergence study was
accomplished using the three models of various refinement
shown in Figure 19.

Since the comparative experimentation had not been
accomplished at this time in the study, another comparison
was needed to determine which model yielded the best
results. It was decided that modeling the isotropic
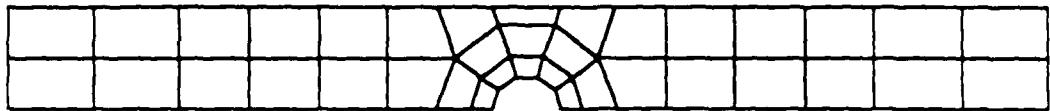
COARSE MODEL: 58 NODES, 37 ELEMENTS, 37 DOF.
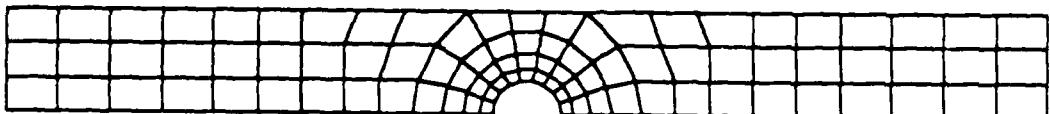
MEDIUM MODEL: 122 NODES, 90 ELEMENTS, 90 DOF.
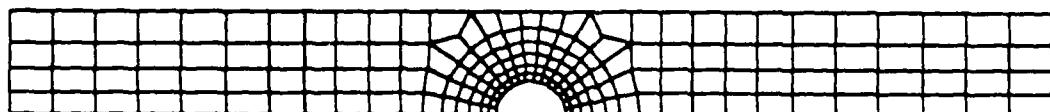
FINE MODEL: 224 NODES, 180 ELEMENTS, 183 DOF.

FIGURE 19. THREE MODELS FOR CONVERGENCE STUDY.

behavior of the coupon would yield a good basis for comparison. To model isotropic behavior, the 16 plies were all given a 0-degree orientation. The material properties were input as elastic engineering constants such that

$$E_1 = E_2 = 18.0 \times 10^6$$

$$G_{12} = \frac{E_1}{2(1 + \nu)}, \qquad \nu = 0.3$$

Using these isotropic properties, a stress concentration factor (SCF) could be used for the comparison of finite element models.

For a thin isotropic plate of finite width with a hole, the SCF was determined using Figure 20 [27]. A d/w ratio of 1/3 yielded a $K_t$, or SCF, of 3.46. Thus, the stress at the hole should be 3.46 times the 'far field' stress (the stress at least 2 diameters away from the hole and near the center of the specimen) for an isotropic material modeled by the meshes of Figure 19.

In the analysis, each mesh was given a displacement loading of 0.001 inch and stresses were calculated linear version of the program described in Another program was also used on the for greater accuracy with a lesser program used 'reduced built upon the program

The results

Table

MICROCOPY RESOLUTION TEST CHART
NATIONAL BUREAU OF STANDARDS - 1963
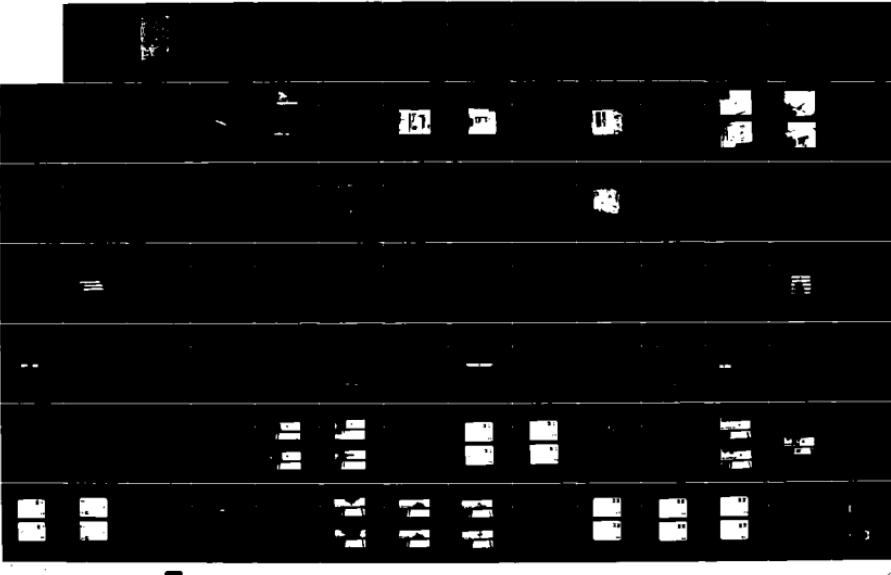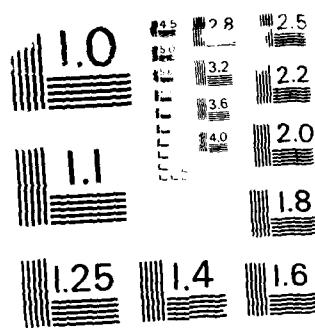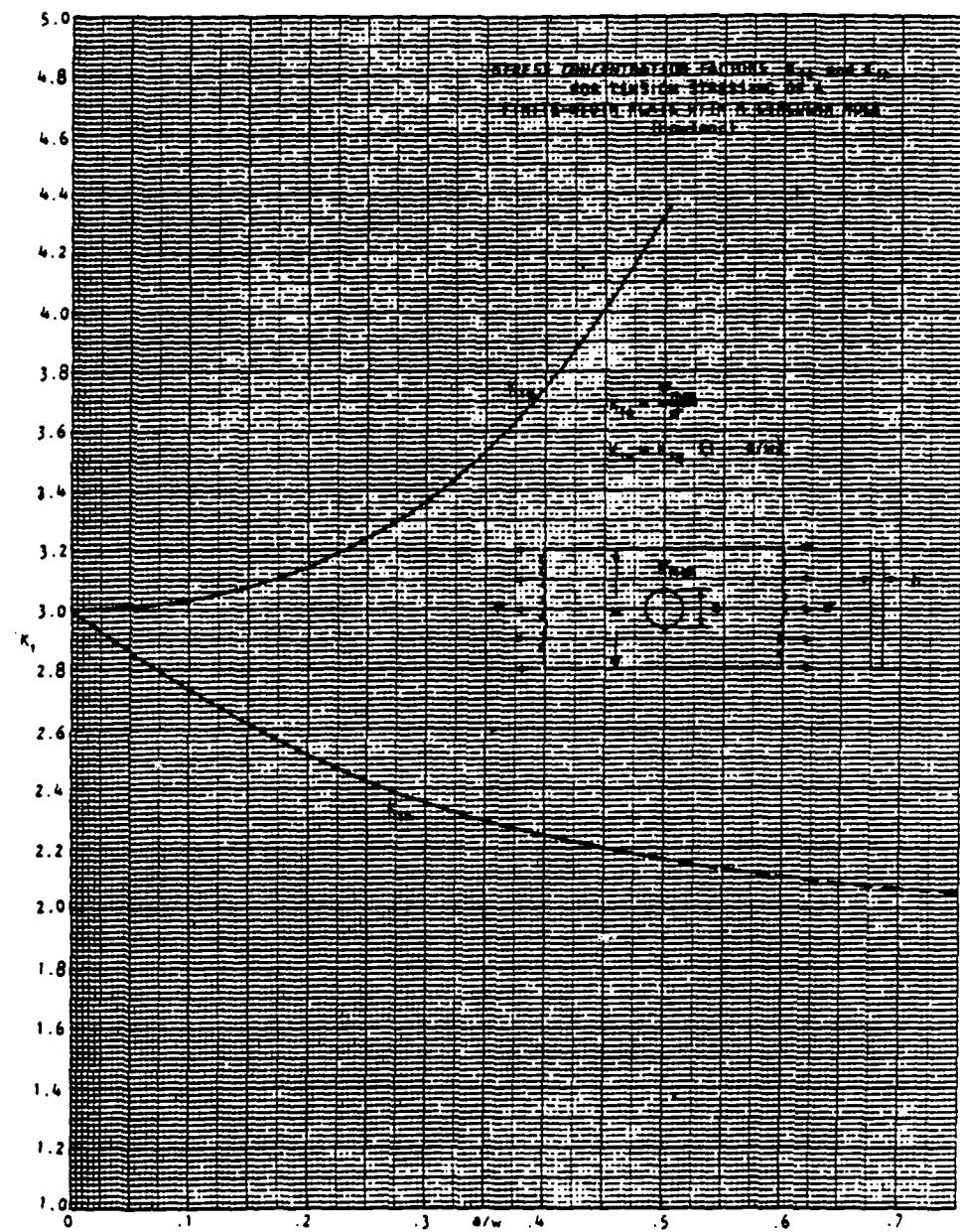
FIGURE 20. STRESS CONCENTRATION FACTORS FOR A FINITE-WIDTH PLATE WITH A CIRCULAR HOLE.
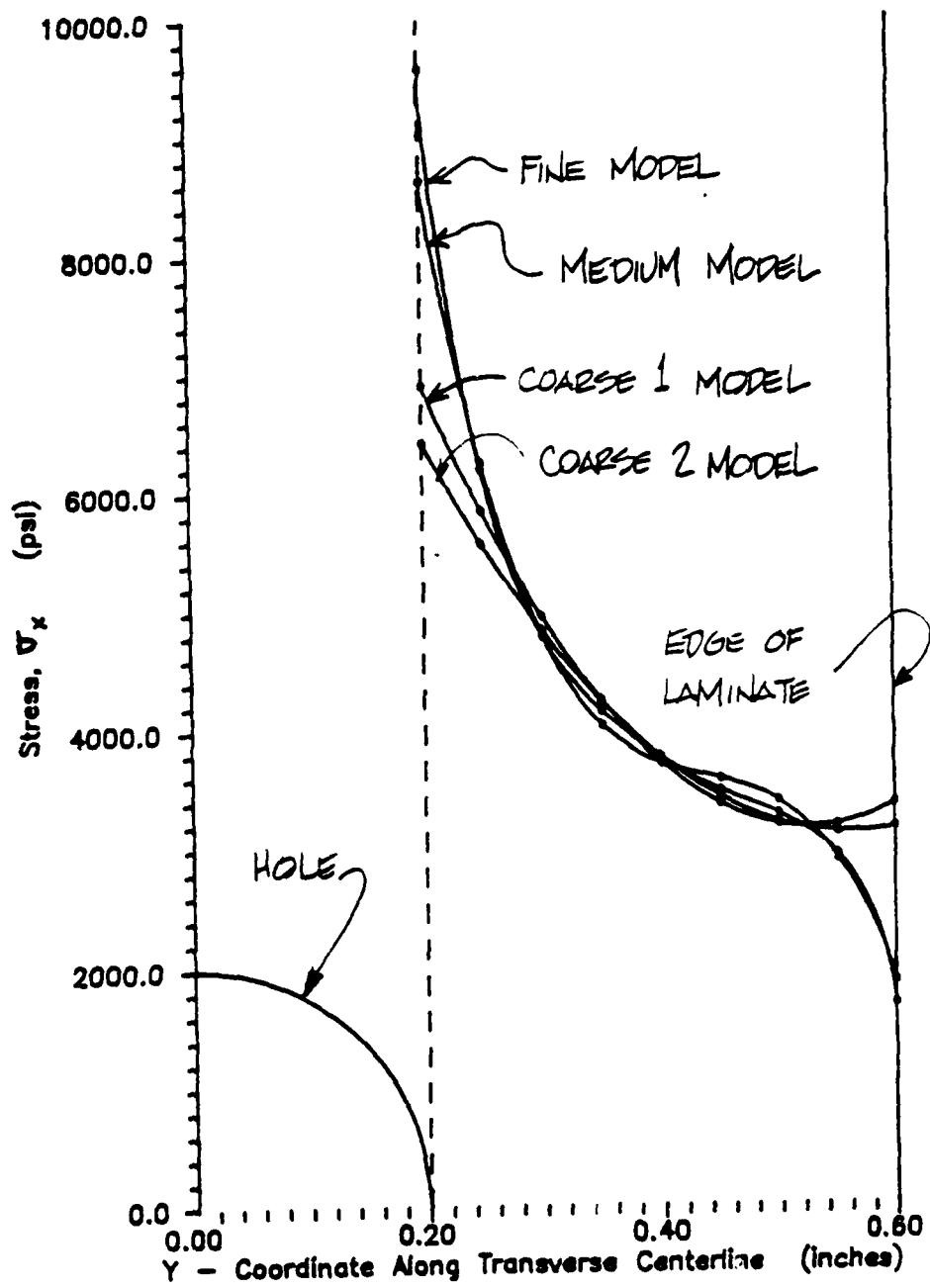
FIGURE 21. RESULTS OF CONVERGENCE STUDY.

| Model | Stress at y = 0.2 (psi) | Far Field Stress (psi) | Stress Concen. | Accuracy % | Time of Execution (sec.) |
|---|---|---|---|---|---|
| Coarse 1 | 6909. | 2890. | 2.39 | 69.1 | 9. |
| Coarse 2 | 6423. | 2865. | 2.23 | 64.5 | 200. |
| Medium | 8636. | 2865. | 3.01 | 87.0 | 34. |
| Fine | 9591. | 2855. | 3.36 | 97.1 | 46. |

Table 3. Results of Convergence Study

y = 0.2 were extrapolated using a computer algorithm based
on Lagrange's interpolating polynomial [29]. Note that the
fine model provides a highly accurate result with little
increase in CPU time over the others. Also note that the
second program did not provide increased accuracy and that
the time of execution was significantly higher than that of
the others. Thus, the fine model was used in this thesis to
carry out the analysis of Gr/PEEK under tension.

D.  Nonlinear Analysis

For comparison purposes, this study could have first
performed a linear analysis on all five laminates using
constant elastic engineering properties. But as past
studies have shown [5, 6, 7, 8, 19] and as the experimental
stress-strain curves of this study show (see Chapter V), a
nonlinear analysis is essential for an accurate study of

composite materials, especially Gr/PEEK. Due to these reasons, a nonlinear analysis was conducted in this thesis.

The nonlinear analysis began once the basic properties were determined experimentally (see Chapters IV and V). These properties were entered into each of the data files corresponding to each type of specimen. These types of input cards are included in the guide to the program in Appendix B.

Each run of the program was routed from a CYBER mainframe computer to a CRAY mainframe, where the program was executed. Although the CRAY performed the excutions at a higher expense per second than the CYBER, the time of execution was significantly faster, thus saving overall expense of this analysis. Once a run was completed, or a user-imposed time limit was reached, the CRAY routed the completed output files back to the CYBER. If a time limit had been reached, the run was restarted from the last increment of loading. This cycle of restarts was continued until the modeled specimen failed.

For each increment of loading during a run, the stresses, strains, and strain energy of each element and the displacements of each node were sent to an output file. As the loading increased, elements which reached their ultimate strain energy failed (see Section II G). The program output listed this sequence of element failure.

For each run of the laminates, tension stresses were set up in the model by displacing the free end a prescribed amount. In order to decide what increment would be appropriate, for simplicity data was taken from the experimental results of this study. The displacement applied was simply the total displacement of the failed specimen divided by ten and rounded up to the nearest $100^{th}$ of an inch. Precision was not critical because the program adjusts the increment to suit its needs in analyzing the failure process.

For each restart of the program, two output files from the previous start or restart were important. In an easily readable format, one output file contained the displacements of each node and the stresses, strains, and strain energy of each element. It also plainly stated if the element had failed. This output file was routed from the CYBER to a printer. And in the literally thousands of pages of output, one could read the analytical progression of failure in each of the specimen lay-ups.

The second output file contained only the displacements of each node for each increment of loading. This file was routed to a VAX mainframe where it became an input file to a plotting program. The VAX was used because it operated on a baud rate that was 8 times faster than the CYBER. Thus, for each increment of loading, a plot could be made of the distorted model. With the numerous plots of the distortions

caused by the load increments, one could see the gradual

analytical deformation of each specimen under tension.

While this analysis phase was taking place,

experimental tests on the specimens were being conducted as

well. Experimentation is discussed in the next chapter, and

the results of both analysis and experimentation are

presented in Chapter V.

## IV.  Experimentation

The purpose of experimentation in this thesis was to
determine the ultimate strength and failure progression in
Gr/PEEK, as well as to provide basic property data for the
computer analysis of the previous chapter.  The end result
was then a comparison of experimental and analytical
results.  Experimentation was conducted through the
Structures Division of the Air Force Flight Dynamics
Laboratory (FDL) of the Air Force Wright Aeronautical
Laboratories (AFWAL) at Wright-Patterson AFB, Ohio.  Prior
to testing, a test plan was submitted to the Structures
Division from the Air Force Institute of Technology (AFIT).
The test plan outlined the work to be done and was sent to
all organizations to be involved in this project.
Highlights of this test plan are presented in Appendix A,
along with an explanation of the logistics involved in
accomplishing experimentation through the Structures
Division of FDL.

Specifically, the objectives of this three-phase test
program were:

(1)  To determine basic properties for the thermoplasic
composite material Gr/PEEK at room temperature.

(2)  To determine the ultimate tensile strength of
Gr/PEEK tensile specimens containing a 0.4-inch diameter
circular discontinuity at room temperature.

(3) To investigate the progression of failure in
Gr/PEEK at a circular discontinuity at room temperature.

This chapter contains the description of fabricating,
instrumenting, and testing Gr/PEEK coupons; and it presents
the procedures followed in accomplishing the above test
objectives. Also discussed are the post-failure
examinations of the material, which were videotapes of the
ultimate strength tests and stereo x-rays of the failure
progression.

## A.  Specimen Fabrication

In accordance with the test plan, specimens were
fabricated from panels of Gr/PEEK composite panels. These
panels were supplied by the Fiberite Corporation, a
subsidiary of Imperial Chemical Industries of Great Britain.
The panels were supplied in the configurations listed in
Table 4. Note that all lay-ups contain 16 plies and are
symmetric about their midsurface. Out of these panels, 114
specimens were fabricated, instrumented, and tested. Some
surplus Gr/PEEK was used for destructive material analysis
to ensure that material specifications were met. The
remaining material was reserved for future testing.

Each panel was guaranteed by the manufacturer to be
APC-2 with Hercules AS4 graphite fiber in a Victrex® PEEK
matrix. The fiber content was 61% by volume and 68% by
weight. A random sampling of the panels showed that the
panels supplied met the material specifications of APC-2.

Table 4.  Configurations of Panels Supplied for Specimens

| Laminate Type | Stacking Sequence | Size (in. x in.) | Quantity |
|---|---|---|---|
| Uni-directional | $[0_{16}]$ | 10 x 14 | 5 |
| Uni-directional | $[90_{16}]$ | 10 x 14 | 5 |
| Angle-Ply | $[\pm45]_{4S}$ | 16 x 16 | 3 |
| Quasi-isotropic | $[0/+45/90/-45]_{2S}$ | 16 x 16 | 2 |
| Quasi-isotropic | $[0/+45/90]_{2S}$ | 16 x 16 | 2 |

A description of the manufacturing of APC-2 panels is contained in Appendix B.

When the panels first arrived from the manufacturer, they were subjected to a C-scan to determine flaws that might have disqualified the panel for fabrication of specimens. The Non-Destructive Evaluation Branch of the Air Force Materials Laboratory conducted the C-scan and found all panels to be free of significant flaws.

After the C-scan, specimens were fabricated for testing. Panels were cut into sub-panels; then sub-panels were 'tabbed.' By applying tabs to each end of the specimen, the testing machine was given an area to grip so that tensile and compressive forces were distributed evenly without damaging the specimen. The Beta Corporation, an in-house contractor of the Structures Division, supplied the

tabbing material, which consisted of 1/16-inch thick G-10

glass epoxy (0/90 woven). The tabbed subpanels were

cut into specimens according to the test plan. Also, the

specimens for the ultimate strength and failure progression

studies had 0.3970-inch holes drilled in their centers.

The final tension specimen geometries are shown in

Figure 22. These are ASTM standard tension specimens. Note

that the widths of the basic property specimens vary

according to lay-up. These widths were imposed so that the

ultimate strength of the specimen did not exceed the load

capacity of the test machine.

To experimentally derive compressive properties, there

are many compression specimen types from which to choose.

The one chosen for this study was the Rolfes compression

specimen [30], and its specimen geometry is shown in Figure

23. The tabbing procedure for the Rolfes compression

specimen is outlined in Figure 24. The end result of this

tedious process is a specimen covered mostly with tabbing

material. It is through this large area of tabbing material

that the compression fixture grips the specimen and through

shear applies compression to the coupon.

## B. Specimen Instrumentation

As fabrication of specimens was completed, the speci-

mens were instrumented. All specimens were instrumented

with appropriate sizes of strain gage rosettes. At all gage

locations, rosettes were placed back-to-back, i.e., they

10"

$\frac{1}{16}$" TYP.

2"   6"   2"

COMPOSITE COUPON

20° TYP.

TAB MATERIAL

(a.) PROFILE VIEW (TYP.)

WIDTH

10"

0.6"   0° TENSION

1.00"   90° TENSION

1.00"   SHEAR

(b.) BASIC PROPERTY SPECIMENS

10"

1.20"

0.400" DIA HOLE
DRILLED AT CENTER
OF SPECIMEN
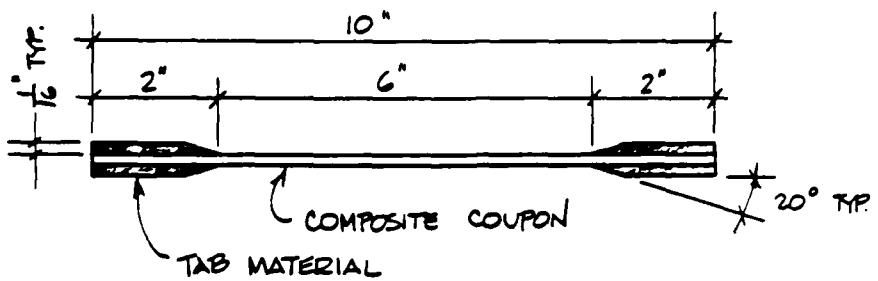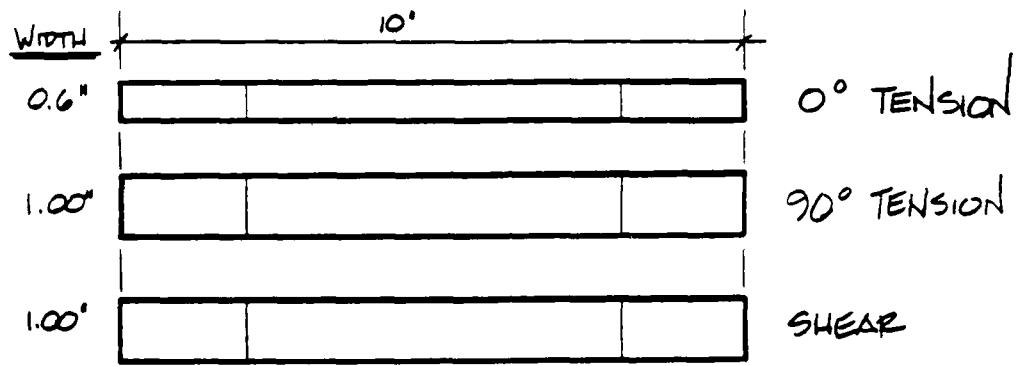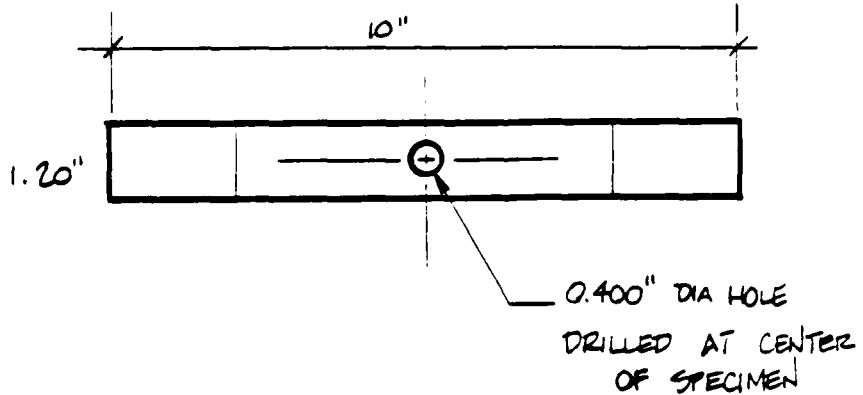
(c.) ALL OTHER SPECIMENS

FIGURE 22.   TENSILE SPECIMENS

FIGURE 23. ROLFES COMPRESSION SPECIMEN.

90
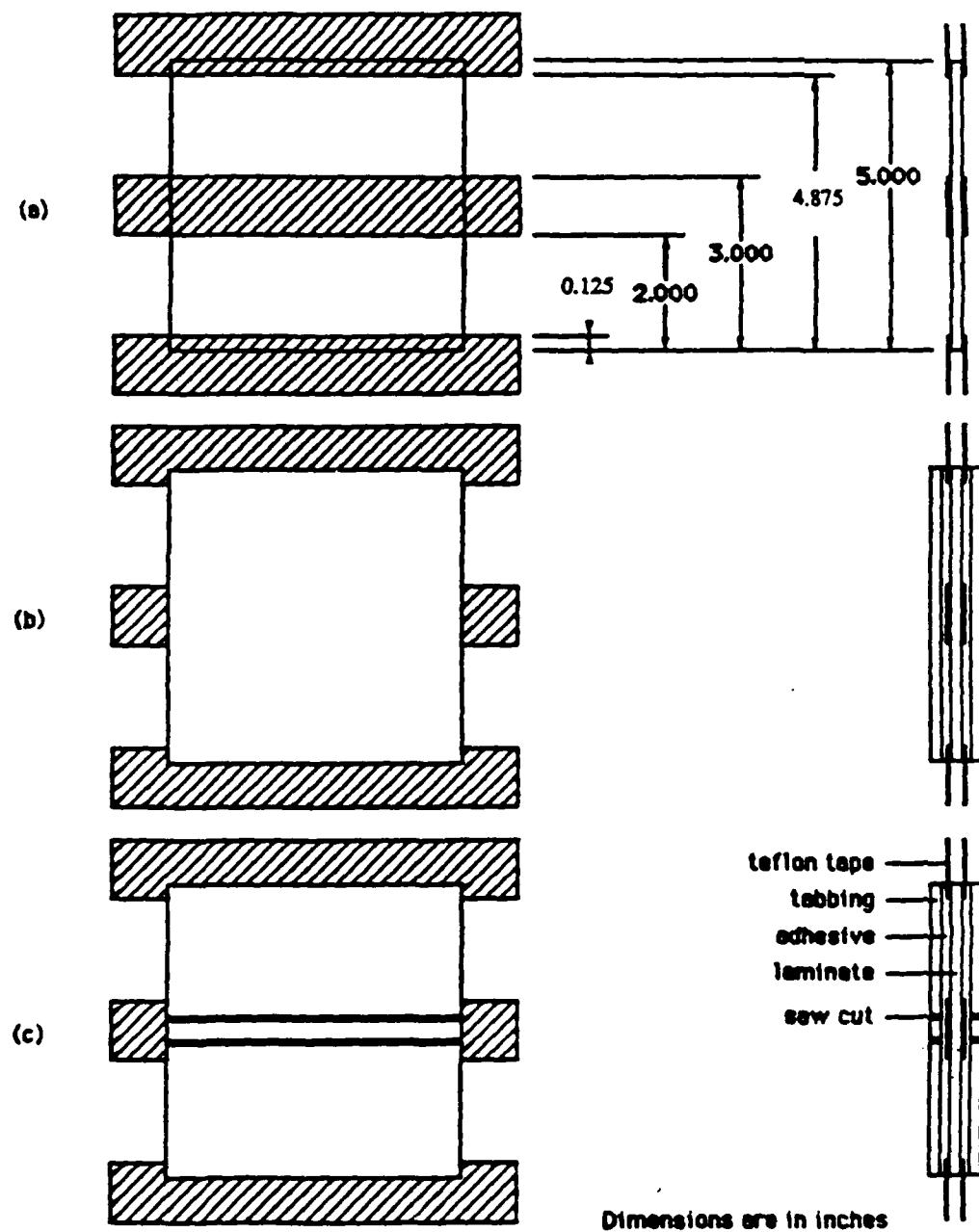
FIGURE 24. TABBING OF THE ROLFES
COMPRESSION SPECIMEN.

were adhered to each face. Figure 25 shows the strain gage

rosette configuration and numbering scheme for the front

face of a specimen. The rosette on the back face simply

mirrored the front gage.

Locations of each gage were a function of the type of

test conducted on the specimen. For basic property tests,

the strain gage was placed in the middle of the specimen. A

gaged compression specimen is shown in Figure 26. For the

specimens containing a hole, gages were placed both at the

hole and at the far field location for some specimens, as

shown in Figure 27. Other specimens had far field gages

only, as shown in Figure 28. The use of rosettes yields the

desired plane stress information: strain in the

longitudinal, transverse, and shear directions of the

specimen axis system.

C. Specimen Testing

In all tests, a 20-kip Instron universal test machine

was used to apply tension or compression to specimens under

an ambient environment. The specimens were loaded at a

constant crosshead travel rate of 0.05 inches per minute.

The crosshead is the component on the test machine which

provides displacement loading. This speed of displacement

was chosen as median speed between a faster impact type

loading and a slower creep type loading. For the duration

of all tests, it was assumed that creep was negligible (see

Section II A). Failure loads were measured using a

92
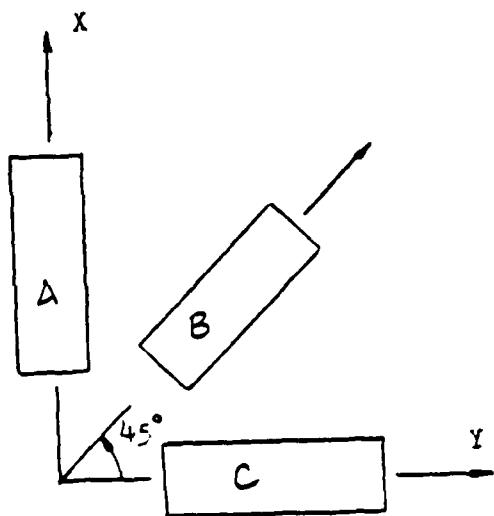
FIGURE 25.    STRAIN GAGE ROSETTE
CONFIGURATION & NUMBERING
SCHEME.

Figure 26.   Gaged Compression Specimen.
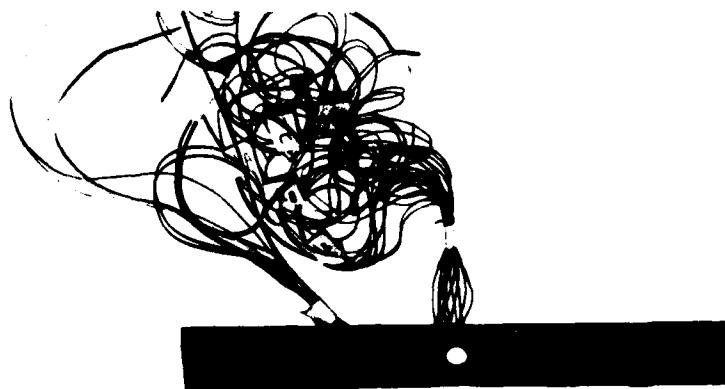
Figure 27.   Specimen with Gage at Hole and at Far Field.



Figure 28.   Specimen with Far Field Gage Only.

20-kip load cell, which consisted of permanent strain gages
which reacted to the displacement of the crosshead.
Videotapes of all the ultimate strength and failure
progression tests were made in an attempt to document the
failure process and provide for a post-failure analysis.

The Instron test machine is shown in the left half of
Figure 29 in a tension application mode. The specimen is
shown in the grips of the tension fixture, and the crosshead
is the horizontal member just below the test fixture. The
load cell is in the top of the machine, above the test
fixture. Also shown in this figure are the voltmeter, the
video camera (both shown in greater detail in subsequent
figures), and the data collection devices.

The voltmeter was used with the ultimate strength tests
to provide a visual measure of the load in the specimen
during tests. It measured load by measuring the resistance
across the load cell during the test. The amount of
resistance per pound of load varied with the range of load
for the test. In other words, if the machine's load range
for a particular test was 5000 pounds, the voltmeter read
1 volt per 1020 pounds. For a 20,000 pound load range, the
voltmeter output 1 volt per 4082 pounds. The voltmeter and
specimen are shown in Figure 30, with testing in progress.

The reason for the voltmeter was for use with the
videotape of the tests. With the videotape filming both
the failure process and the voltage reading (the load), one
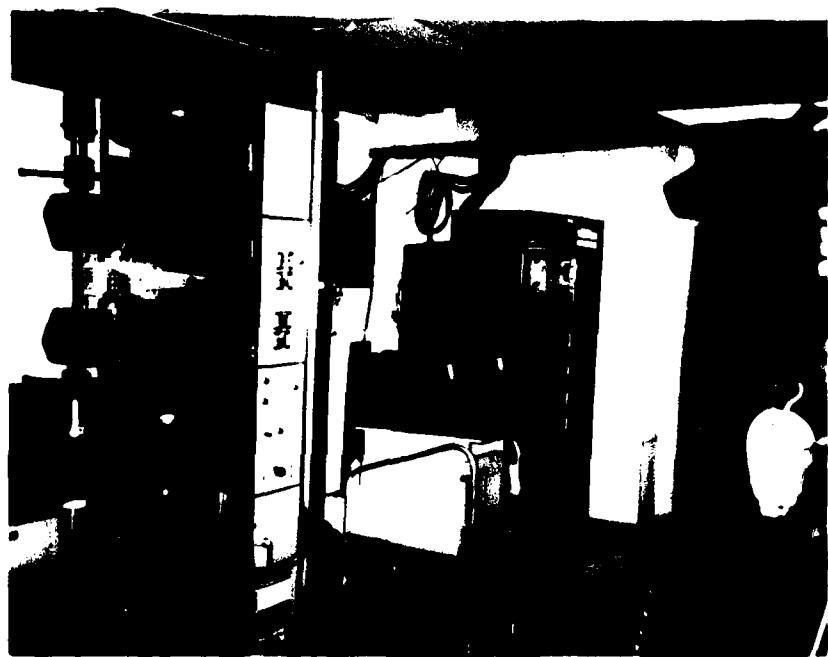
Figure 29.   Testing Area.

Figure 30.   Specimen and Voltmeter During Test.

could perform a repeated post-failure analysis on each test. Not only did visual occurrences reveal themselves after testing, but the failure in the specimen could be <u>heard</u> by the 'tinking' of individual fibers and the grating sound and sudden boom of the failed specimen. The video camera and its subject are shown in Figure 31, with testing in progress.

In the background of Figure 29, the data collection devices are shown. For each test, strain was read from all three elements of each strain gage and load was read from the load cell. For the strain, signals from each leg of the rosette were read by a strain gage conditioner, sent to an amplifier, then to a multiplexer (which combines the signals for the computer), and finally to a VAX mainframe computer. Load signals were sent in a similar path and combined with the strain information. The end result of each test was a great volume of data that could be output in any desired form.

The data collection devices were able to record test data in varying rates. For all specimens except the 90-degree tension coupons, the sampling rate was 2 data samples per second. The data sampling rate for the 90-degree tension test was increased to 4 data samples per second since these tests lasted a relatively short time. In this way, data collected was more reliable, and strain at failure was more precise.
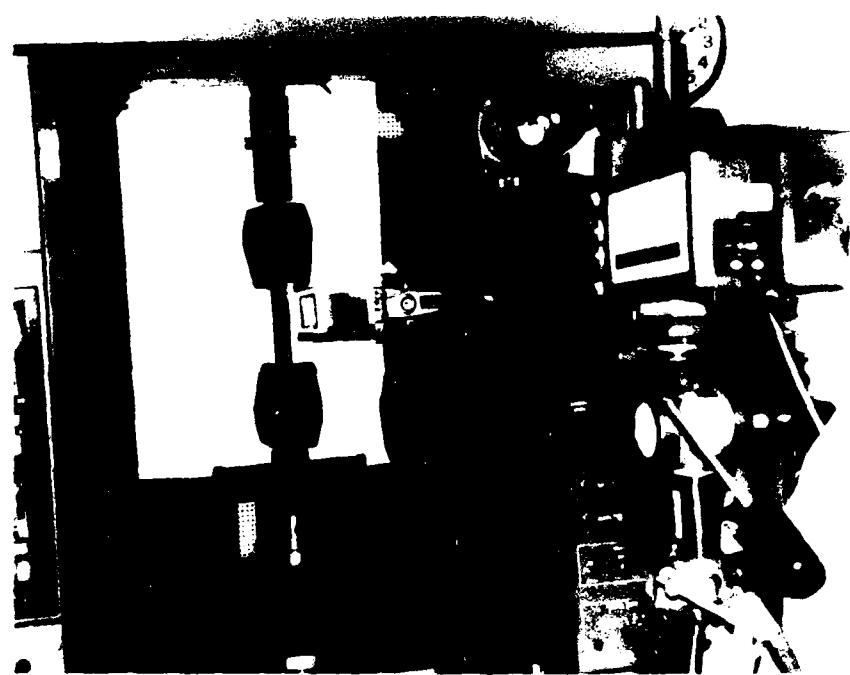
Figure 31.  Video Camera and Its Subject.

The Instron test machine is shown in Figure 32 in its
compression application mode. The specimen is in the Rolfes
compression fixture, and the crosshead is applying load by
moving down. Here, the load cell is under the fixture,
inside the rectangular box. Load cell data is fed through
the cable attached to the box and over to the data
collection devices. In this figure also note the plotter in
the upper left. Plotted for each test was a continuous load
versus displacement curve. A ball point pen simply traced
the load as the scroll moved with the displace of the
crosshead.

The Rolfes compression fixture is shown in the test
machine in Figure 33. One pair of wires for each leg of
each gage is extended from the gages to the terminal strip
at the left of the figure. From this terminal strip,
signals are sent to the data collection devices.

Further views of the compression fixture are shown in
Figure 34. Figure 34(a) shows the unassembled fixture with
one end of the specimen in the grips. Figure 34(b) shows
the assembled fixture. Note that the grip in the front
extends beyond the cover plates. It is on this grip that
the crosshead applies the displacement load.

The entire testing program is outlined in Table 5.
Note the test symbols listed. These will be used for
conciseness in the next chapter. Also note the quantities
of specimens required for each phase of the testing. For

Figure 32.   Instron Test Machine in Compression Mode.
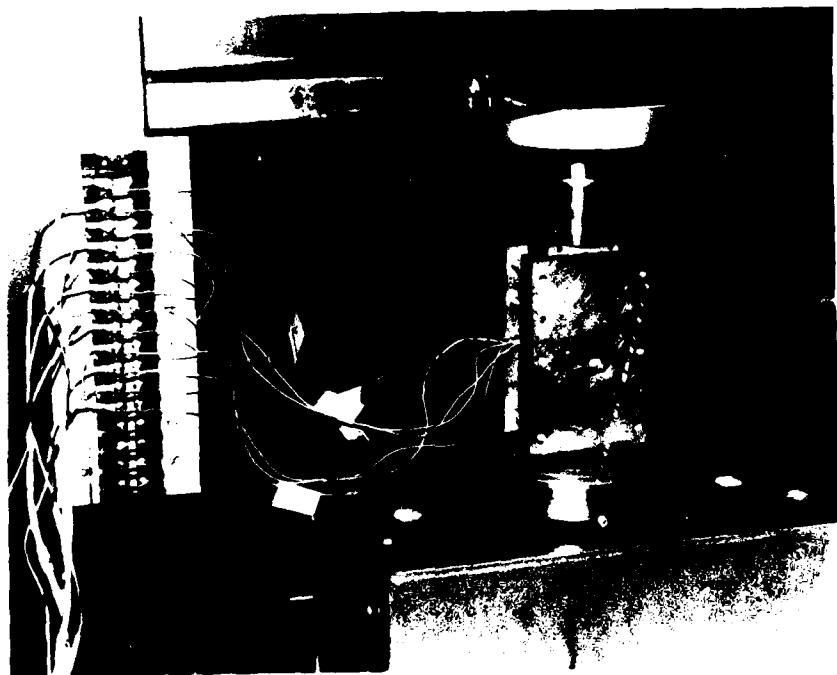


Figure 33.   Compression Specimen Wired for Test.
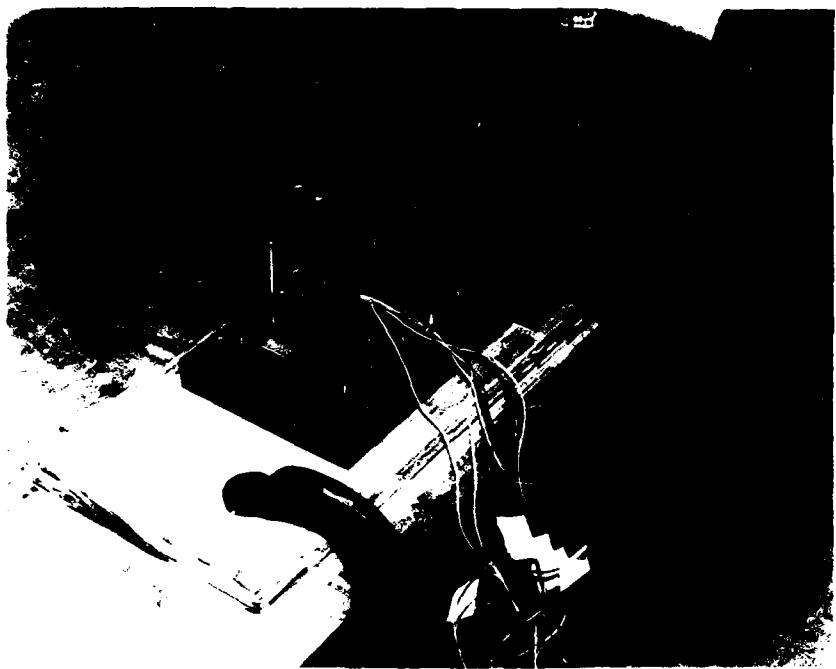
Figure 34(a).   Unassembled Compression Fixture.
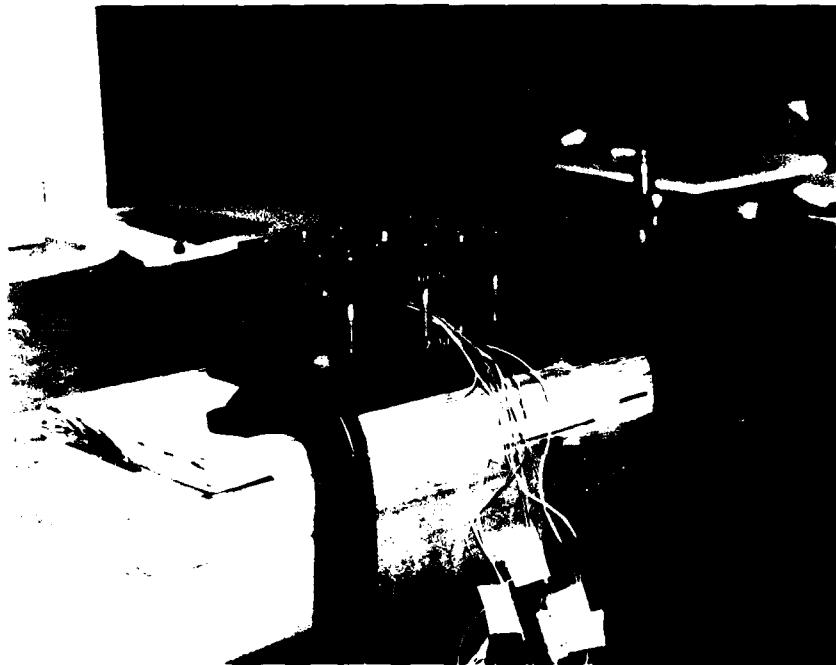


Figure 34(b).   Assembled Compression Fixture.

103

determining basic properties, five obstensibly identical

tests of each type of specimen were assumed to provide a

good average of material property data. For the ultimate

strength tests, four specimens with gages at the hole and at

far field were tested along with three specimens having only

a far field gage. It was desired to provide as much data as

possible for this phase. For the remaining phase, three

tests for each type of specimen were assumed to give a

statistically accurate account of results. In all phases,

extra specimens were manufactured in the event of poor

results. Occasionally in this type of testing, strain gages

fail or tab adhesive fails prior to failure of the specimen.

## D.  Basic Property Tests

To determine the basic property data of APC-2, the

basic property specimens were gaged at their centers and

tested under static loading at room temperature. The goal

of these tests was to provide sets of values from which the

computer program could derive the nonlinear values of $E_1^T$, $E_1^C$, $E_2^T$, $E_2^C$, $G_{12}$, $\nu_{12}^T$, and $\nu_{12}^C$. The tests were listed in

Table 1 of Chapter II, along with their corresponding curves

and the basic property derived from the data. Note that the

$[\pm45]_{4S}$ laminate was used for determining the $\tau_{12}$ vs.

$\gamma_{12}$ data. According to ASTM Standards [31], the tensile

coupon of $\pm45$ laminas yields shear stress-strain results

from the following equations:

104

Table 5. Summary of Testing Program

Basic Property Tests (Specimens with no hole)

| Specimen Type/Test | Number of Specimens | Number of Gages | Type of Gage * |
|---|---|---|---|
| $0^\circ$ Tension | 6 | 12 | 1 |
| $0^\circ$ Compression | 5 | 10 | 1 |
| $90^\circ$ Tension | 9 | 18 | 2 |
| $90^\circ$ Compression | 8 | 16 | 1 |
| $\pm45^\circ$ Tension | 6 | 12 | 2 |
| Totals | 34 Specimens Tested | | |

Ultimate Strength Tests (Specimens with a 0.4" dia hole)

| Specimen Type | Test Symbol | Number of Specimens | Number of Gages | Type of Gage * |
|---|---|---|---|---|
| $[0_{16}]$ | 0T | 3 | 6 | 2 |
| | | 3 | 6 | 3 |
| $[90_{16}]$ | 90T | 3 | 6 | 2 |
| | | 4 | 8 | 3 |
| $[\pm45]_{4S}$ | SH | 3 | 6 | 2 |
| | | 4 | 8 | 3 |
| $[0/-45/90/-45]_{2S}$ | Q1 | 3 | 6 | 2 |
| | | 4 | 8 | 3 |
| $[0/-45/90]_{2S}$ | Q2 | 3 | 6 | 2 |
| | | 4 | 8 | 3 |
| Totals | | 15 | 30 | 2 |
| | | 19 | 38 | 3 |
| | | 34 Specimens Tested | | |

Continued.

105

Table 5 (Continued).   Summary of Testing Program

Failure Progression Tests   (Specimens with 0.4" dia hole)

| Specimen Type | Test Symbol | Number of Specimen at Percentage | | |
|---|---|---|---|---|
| | | # 1 | # 2 | # 3 |
| $[0_{16}]$ | 0T | 3 | 3 | 2 |
| $[90_{16}]$ | 90T | 3 | 3 | 3 |
| $[\pm45]_{4S}$ | SH | 3 | 3 | 3 |
| $[0/+45/90/-45]_{2S}$ | Q1 | 3 | 3 | 3 |
| $[0/+45/90]_{2S}$ | Q2 | 3 | 3 | 3 |
| Totals | | 15 | 15 | 14 |

44 Specimens Tested

* Types of Strain Gages

| Reference Number | Type of Gage | Number Applied | Remarks |
|---|---|---|---|
| 1 | CEA-03-062UR-350 | 190 | |
| 2 | CEA-03-125UR-350 | 38 | Far field gage. |
| 3 | WK-03-060WR-350 | 40 | Stacked rosette at hole. |

106

$$\tau_{12} = P_x / 2 \; b \; d \qquad\qquad (50)$$

$$\gamma_{12} = \varepsilon_x - \varepsilon_y \qquad\qquad (51)$$

where

$P_x$ = load in the specimen longitudinal axis

b = specimen width

d = specimen thickness

$\tau_{12}$, $\gamma_{12}$, $\varepsilon_x$, and $\varepsilon_y$ have been defined previously.

Note that Eqs. (50) and (51) are derived for the $\pm 45°$ laminate through the use of a coordinate transformation. Taking Eq. (51), for example, to get the desired shear strain in the material axis system, one would use this transformation equation:

$$\begin{Bmatrix} \varepsilon_1 \\ \varepsilon_2 \\ \gamma_{12} \end{Bmatrix} = \begin{bmatrix} \cos^2\theta & \sin^2\theta & 2\sin\theta\cos\theta \\ \sin^2\theta & \cos^2\theta & -2\sin\theta\cos\theta \\ -\sin\theta\cos\theta & \sin\theta\cos\theta & \cos^2\theta - \sin^2\theta \end{bmatrix} \begin{Bmatrix} \varepsilon_x \\ \varepsilon_y \\ \gamma_{xy} \end{Bmatrix}$$

With $\theta = +45°$ or $-45°$, Eq. (51) is realized.

To obtain the desired stress-strain data sets which were entered into the computer program of this study, the stress and strain values derived from each test were plotted on a single graph and an average stress-strain curve was determined. For example, to determine $\sigma_1$ vs. $\varepsilon_1$, six curves were plotted of the axial stress ($\sigma_1 = \sigma_x = P / A$) versus the maximum strain ($\varepsilon_1 = \varepsilon_x$) read from the strain rosette for the 0-degree tension specimens. All six experimental

$\sigma_1$ vs. $\varepsilon_1$ curves were output on one plot, and a curve that was based on least squares fit was plotted through the six experimental curves. Values of $\sigma_1$ vs. $\varepsilon_1$ were then taken from this curve and tabulated. These basic property curves are presented in Chapter V with other test results.

Other values were tabulated as well. To determine the Poisson ratios, both the tension and compression curves of $\sigma_1$ vs. $\varepsilon_1$ and $\sigma_1$ vs. $\varepsilon_2$ were plotted on one graph and values of $\varepsilon_2$ and $\varepsilon_1$ were chosen. Dividing $\varepsilon_1$ into $\varepsilon_2$ yielded the desired results. Additionally, the engineering elastic constants were needed to give the computer program values of basic properties from which to start. The constants were the initial values of basic properties. The engineering elastic constants derived from these tests were compared with others' findings and found to be accurate. The tabulated values of nonlinear material properties, along with the elastic engineering constants were entered into data files for the analysis portion of this thesis.

## E.  Ultimate Strength Tests

To determine laminate stress-strain responses to ultimate tensile load, the 0T, 90T, SH, Q1, and Q2 specimens were tested under tension. All seven specimens of each of the five types of lay-ups were instrumented with a (CEA-03-125UR-350) strain rosette away from the hole, the far field gage, to determine strain to failure for the laminate. Four of the seven specimens were instrumented

with a "stacked" rosette (WK-03-062UR-350) at the side of
the hole. (See Figure 28 in Section B of this chapter.)
The use of a stacked rosette allows one to determine the
strain in a much smaller area. Because of the extremely
large stress gradients at the hole (See Figure 21 in Section
III C), use of a rosette with three grids spread apart, as
in Figure 25, would produce meaningless results.

Refering to the finite element model of the specimen
geometry, the small stacked rosette was centered on the
second element from the hole on the transverse centerline of
the specimen. The rosette approximately covered the area of
that element. The far field gage was placed on a group of
elements where stresses were assumed to be uniform.
Figure 35 shows this strain gage placement with respect to
the finite element mesh.

For each of the five types of laminates, specimens were
subjected to tension until they failed. The loads and
strains throughout the test and at failure were recorded.
Results from the small rosette at the hole, as well as from
the gage at far field, were used for comparison to the
computer analysis. The tensile stresses at failure were
averaged to obtain average failure stresses. These average
stresses were not only compared to analytical findings, but
they were also used to accomplish the final phase of
testing.

FAR FIELD STRAIN GAGE

STACKED GAGE AT THE HOLE.
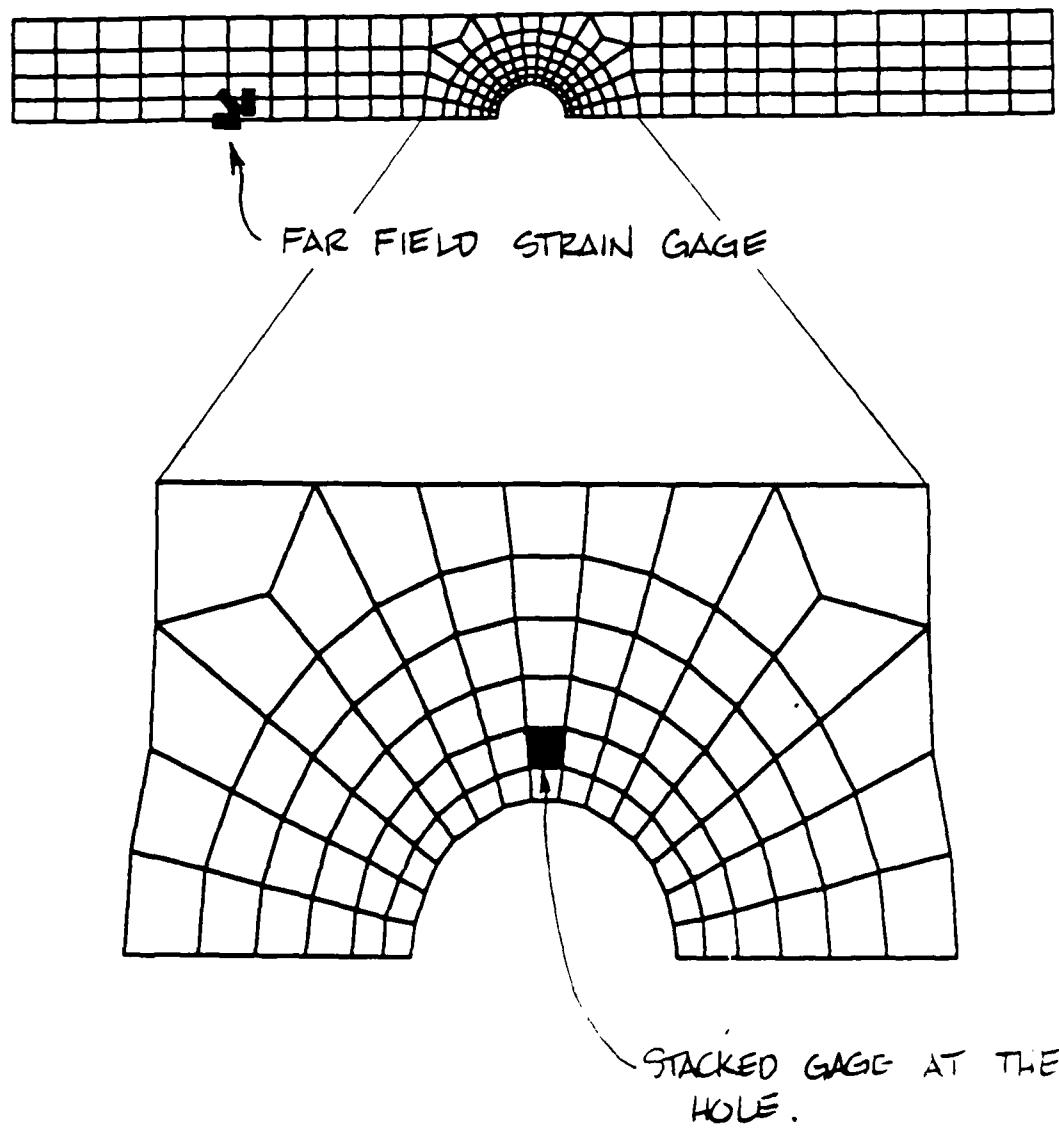
FIGURE 35. STRAIN GAGE PLACEMENT WITH RESPECT TO FINITE ELEMENT MESH.

A videotape was made of all the tests to ultimate strength. From repeated viewing, one could see and hear occurrences that were not noticed during the test. Also, stills (photographs) were taken of various frames which showed the initiation and progression of failure, as well as deformations and the ultimate breaking of the specimen.

F. Failure Progression Tests

To determine the initiation and growth of ply failure in laminates with a 0.4-inch diameter hole, 0T, 90T, SH, Q1, and Q2 specimens were tested under tension. For three percentages of the average failure stresses, three specimens of each lay-up were tested. The specimens were placed in the grips of the Instron test machine and loaded to a predetermined load. This load was derived by multiplying the predetermined stress percentage by the cross-sectional area of each specimen.

For each average failure stress determined above, three percentages of failure load were chosen. For each of the five laminates, the results of the ultimate strength tests were studied. The stress-strain curves were examined, and the videotape was viewed repeatedly. From this post-failure analysis, the percentages of failure stress were chosen and are listed in Table 6. These percentages were based on occurrences during the failure process that warranted investigation. It was hoped that testing to these

111

Table 6. Percentages of Average Failure Stress
(to which each laminate was tested)

| Specimen | Percentage | # 1 | # 2 | # 3 |
|----------|-----------|-----|-----|-----|
| 0T | | 50 | 80 | 90 |
| 90T | | 80 | 90 | 95 |
| SH | | 70 | 85 | 95 |
| Q1 | | 80 | 90 | 95 |
| Q2 | | 80 | 90 | 95 |

percentages would render visible results through the
technique of stereo X-ray.

G.  Enhanced Stereo X-Ray

Once laminates had been loaded to a percentage of
failure stress, they were taken to the Air Force Materials
Laboratory for analysis.  There the growth of ply failure
was photographed using the techniques of stereo x-ray.  To
determine which plies failed in a laminate under tension
around the hole, each set of three specimens was subjected
to 'opaque penetrant enhanced, three-dimensional,
x-radiaography' [32].  By using this technique one can see
failure through the entire laminate thickness and, ideally,
pick out the extent to which each ply has' failed.  This
visual analysis requires some education and acclamation for
the person who has never performed stereo viewing of
composites.

At the facilities of the Non-Destructive Evaluation
Branch of the Materials Lab, all 44 specimens were
photographed using the techniques of Reference [32].
The specimens were penetrated with an x-ray opaque fluid and
then photographed onto x-ray film in two images.  The right
image was shot first while a thin plate of lead was placed
over the left side of the film.  Then the left side of the
the x-ray was shot with the lead plate on the right side.
This set-up is shown in Figure 36.  Once the film was
developed and stereo x-rays were completed, the analysis of
the images began.  This analysis involved using a stereo
viewer with a magnifying lens and picking out the damage
progression.

With the experimentation described in this chapter,
along with the methods for evaluating failure in specimens,
results were obtained.  These results are presented next.
It was hoped that this combination of experiment and
analysis would give a complete picture of how APC-2
laminates fail under tension around a hole, and whether or
not the computer analysis used can accurately predict this
behavior.
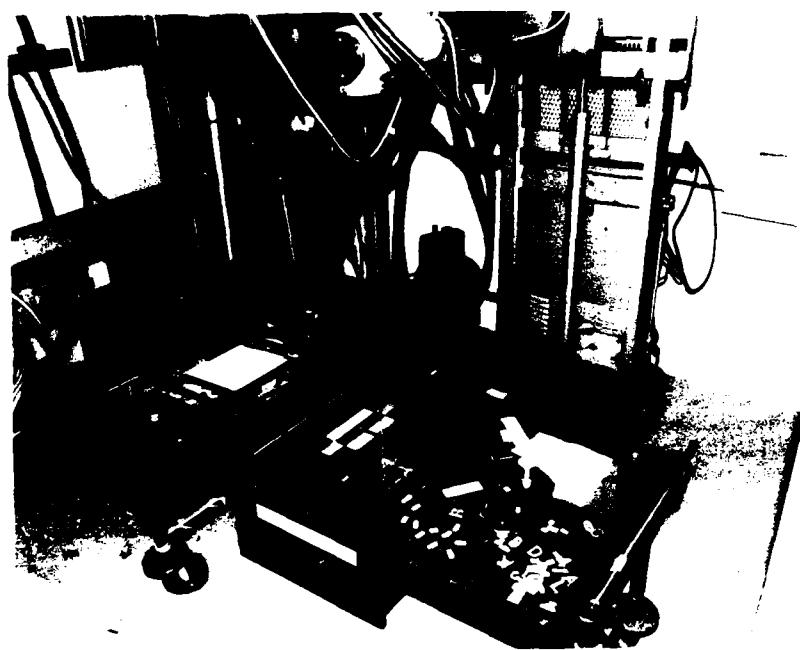
Figure 36.   Equipment Set-Up for Stereo X-Ray Procedure.

114

# V. Results and Discussion

This chapter presents and discusses the analytical and experimental results of this thesis. The computer program embodying the concepts of Chapter II and applied in Chapter III was used to determine the theoretical responses of $[0_{16}]$, $[90_{16}]$, and $[\pm45]_{4S}$ Gr/PEEK laminates subjected to in-plane uniaxial loads. These responses were then compared to the experimental results of Chapter IV. The experimental study of the two quasi-isotropic laminates follows the analytical-experimental study of the unidirectional and angle-ply laminates. But first, the basic property results are presented showing best fit curves and listing the data that was input to the computer program.

## A. Results of Basic Property Tests

The results of each test conducted during this phase of the experimentation are listed in Tables 7 through 11. For each table, remarks are included for completeness. Note that the average failure stresses shown in the tables represents the strength of Gr/PEEK under simple loading conditions.

Table 7.   Basic Property Tests of 0-deg Tension Specimens

| Test Number | X-Sect Area | Failure Load (lbs.) | Failure Stress (psi) |
|---|---|---|---|
| 1101 | 0.04988 | 14,900. | 298,700. |
| 1002 | 0.04988 | 15,700. | 314,900. |
| 1003 | 0.0498 | 14,380. | 288,800. |
| 1004 | 0.05013 | 15,400. | 307,200. |
| 1005 | 0.05107 | 13,850. | 271,200. |
| 1006 | 0.0498 | 15,400. | 309,200. |

Average Failure Stress =   298,300.


Table 8.  Basic Property Tests of 0-deg Compression Specimens

| Test Number | X-Sect Area | Failure Load (lbs.) | Failure Stress (psi) | Notes |
|---|---|---|---|---|
| 5501 | 0.06083 | —— | | A |
| 5502 | 0.05917 | 9,439. | 159,500. | |
| 5503 | 0.05933 | 10,701. | 180,350. | |
| 5504 | 0.05992 | 9,850. | 164,400. | B |
| 5505 | 0.05941 | 11,360. | 191,200. | |

Average Failure Stress =   173,900.

Notes:

A.  A tab to one of the strain gages was lost, and the specimen was scapped.

B   Slippage of the grip on the tab occurred.  Test was redone.  First load was 5,604 lbs.  Second and ultimate load was 11,161 lbs.

116

Table 9.  Basic Property Tests of 90-deg Tension Specimens

| Test Number | X-Sect Area | Failure Load (lbs.) | Failure Stress (psi) |
|---|---|---|---|
| 2001 | 0.07884 | 1,200. | 15,220. |
| 2002 | 0.08108 | 1,183. | 14,590. |
| 2003 | 0.08008 | 1,134. | 14,160. |
| 2004 | 0.08208 | 1,209. | 14,730. |
| 2005 | 0.08325 | 1,210. | 14,530. |
| 2006 | 0.07992 | 920. | ——— |
| 2007 | 0.08116 | 990. | 12,200. |
| 2008 | 0.083 | 560. | ——— |
| 2009 | 0.08192 | 1,092. | 13,330. |

Average Failure Stress =   14,110.

Table 10.  Basic Property Tests of 90-deg Compression Specimens

| Test Number | X-Sect Area | Failure Load (lbs.) | Failure Stress (psi) | Notes |
|---|---|---|---|---|
| 4601 | 0.06208 | ——— | ——— | A |
| 4502 | 0.06225 | 2,113. | 33,940. | |
| 4503 | 0.06217 | 2,101. | 33,790. | |
| 4504 | 0.06233 | 2,144. | 34,400. | |
| 4505 | 0.06004 | 2,082. | 34,680. | |
| 4506 | 0.06008 | 1,999. | 33,270. | |
| 4507 | 0.06016 | 1,987. | 33,030. | |
| 4508 | 0.05933 | 2,036. | 34,320. | |

Average Failure Stress =   33,920.

Notes:

A.  Data obtained in this test was not useable.

### Table 11. Basic Property Tests of Shear Specimens

| Test Number | X-Sect Area | Failure Load (lbs.) | Duration of Test (min.) | Failure Stress (psi) | Notes |
|---|---|---|---|---|---|
| 3001 | 0.08317 | 4000. | 22.0 | —— | A |
| 3002 | 0.08159 | 4200. | 18.3 | —— | B |
| 3003 | 0.08200 | 4400. | 18.8 | —— | B |
| 3004 | 0.08300 | 4670. | 38.3 | 56,260. | |
| 3005 | 0.08400 | 4800 | 40.2 | 57,140. | |
| 3006 | 0.08400 | 4630. | 38.6 | 55,120. | |

Average Failure Stress = 56,170.

Notes:

A. This specimen was loaded twice. When it was realized the duration of the test was much longer than the other laminates, this first specimen was unloaded to check for slippage of the grips or the tabs. It was then reloaded at a faster rate (0.1 inches per min.).

B. These specimens were loaded at the rate of 0.1 inches per minute. However, it was realized that this load rate was too fast, and the load rate was switched back to 0.05 inches per minute for the rest of the specimens.

For the shear $[\pm45]_{4s}$ specimens, these results were significant:

(1) All of the coupons reached strains that were beyond the linear assumptions of this study. The average

strain was estimated to be at least 20%, based on measuring the final gage lengths of the failed specimens.

(2) Scissoring of the fibers occured in each specimen. Scissoring is a phenomenon where the fibers in an angle-ply laminate try to align themselves with the load. The graphite fibers in the ductile PEEK matrix accomplished much scissoring before ultimate failure.

Both of the above anomalies can be seen in the failed shear specimens of Figure 37.

The original stress-strain curves of these shear tests showed that a failure point needed to be defined before the actual failure of the specimen. On the original curve, after strains reached approximately 5.5 %, the slope of the curve began to flatten out and continue to about a 20% strain. It was believed that both the large strains indicative of thermoplastics and the scissoring effect of the angle-ply laminate were responsible for this apparent plasticity. As an initial estimate of reasonable failure, the data derived from the shear tests was cut off at a value near 5.5 percent strain. This value of strain is slightly above the approximate bound on linear assumptions in Reference [33]. Strains occurring beyond 5 or 6 percent approach phenomena described by the principles of large displacement theory, where partial second derivatives begin to enter the analysis.
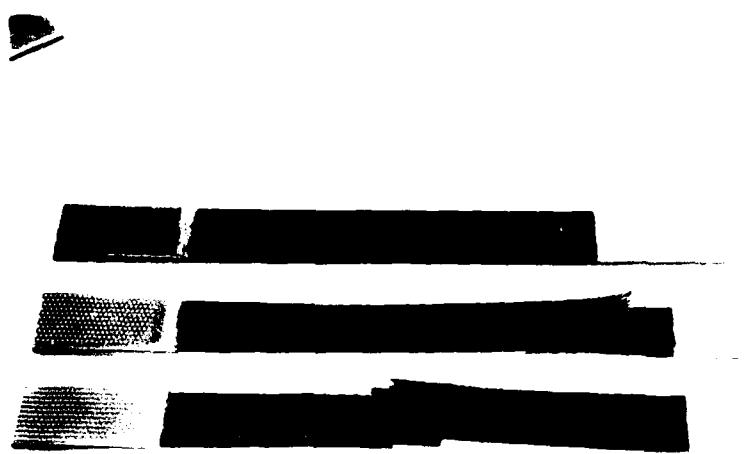
Figure 37.   Basic Property Shear Specimens
Before and After Testing.

120

The stress-strain curves of each of the basic property tests were plotted from experimental data as described in Chapter IV. From each set of stress-strain curves a best fit curve was determined. These best fit curves are shown in Figures 38 through 44.

From these seven curves, corresponding stress and strain values (or Poisson ratios and strain values) were picked off and tabulated. These values were the basic property input for the computer program as described in Chapter III. These basic properties of APC-2 Gr/PEEK are listed in Table 12.

As described in Chapter IV, initial values for the engineering properties must be input into the computer program for it to begin its analysis. For Young's modulus and the shear modulus, these initial values were simply the initial slopes of the basic property curves (stress/strain for the first data point). For the Poisson ratios, the initial values were extrapolated from the data above. These initial values are given as engineering elastic constants for APC-2 Gr/PEEK in Table 13.

B. Stress-Strain Responses of $[0_{16}]$, $[90_{16}]$, and $[\pm 45]_{4S}$ Laminates

As described in Chapter IV, 0T, 90T, and SH laminates with holes were tested under tension to their failure load. Also tested to ultimate strength were the quasi-isotropic

121
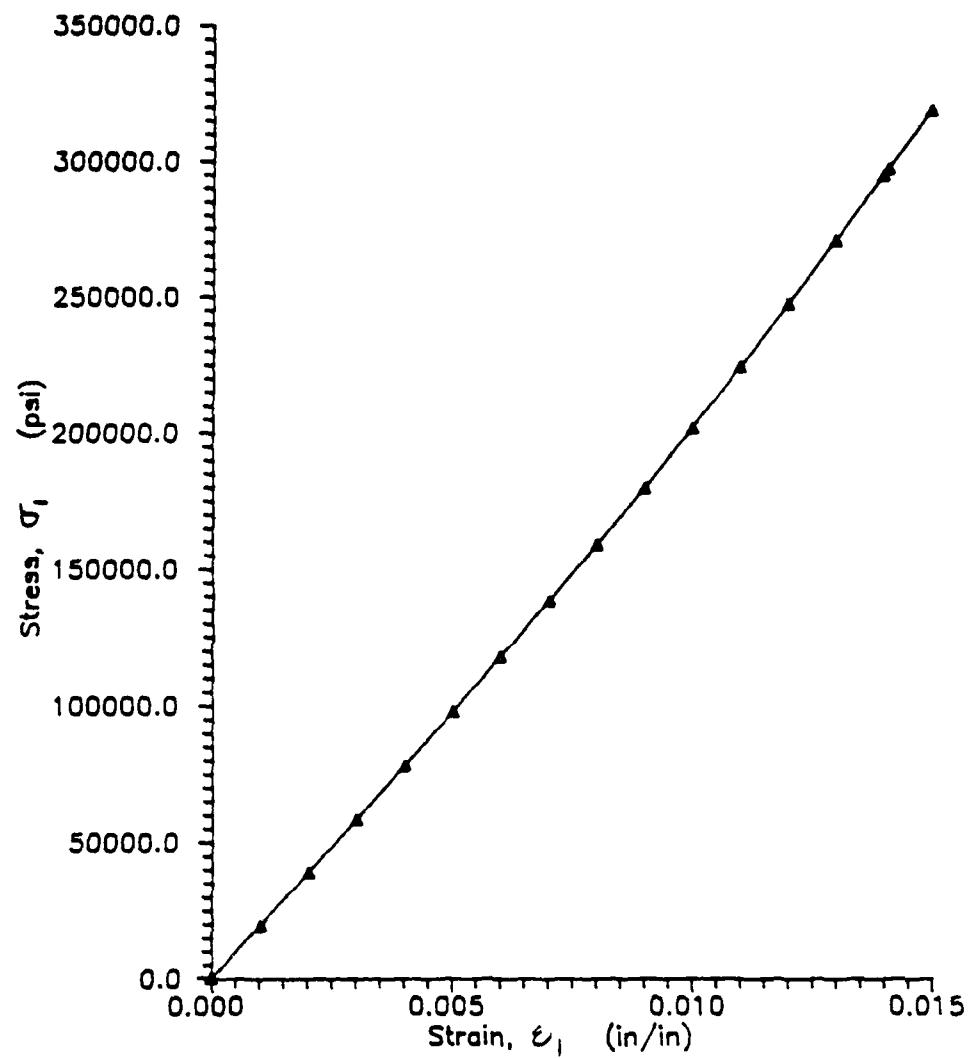
FIGURE 38. BASIC PROPERTY CURVE:
0-DEGREE TENSION FOR $E_1^T$
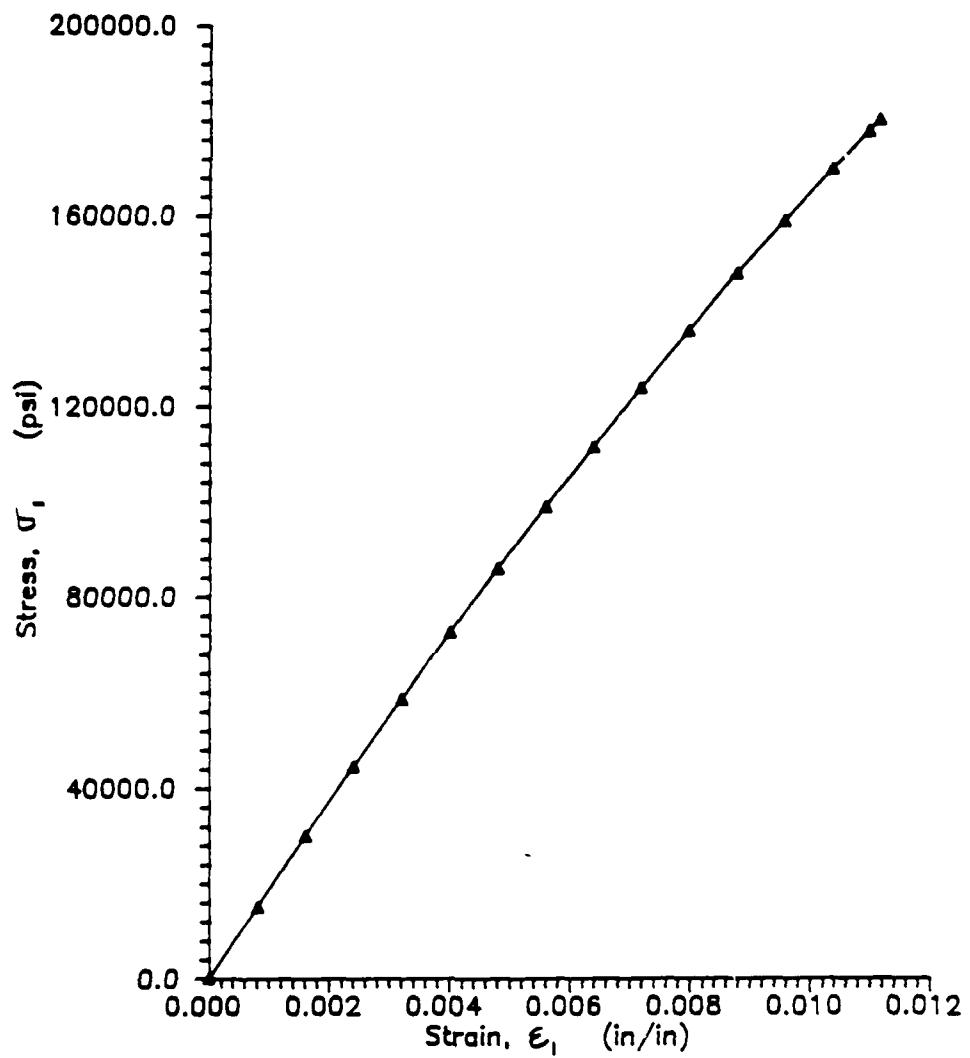
FIGURE 39. BASIC PROPERTY CURVE:

O-DEGREE COMPRESSION FOR $E_1^c$
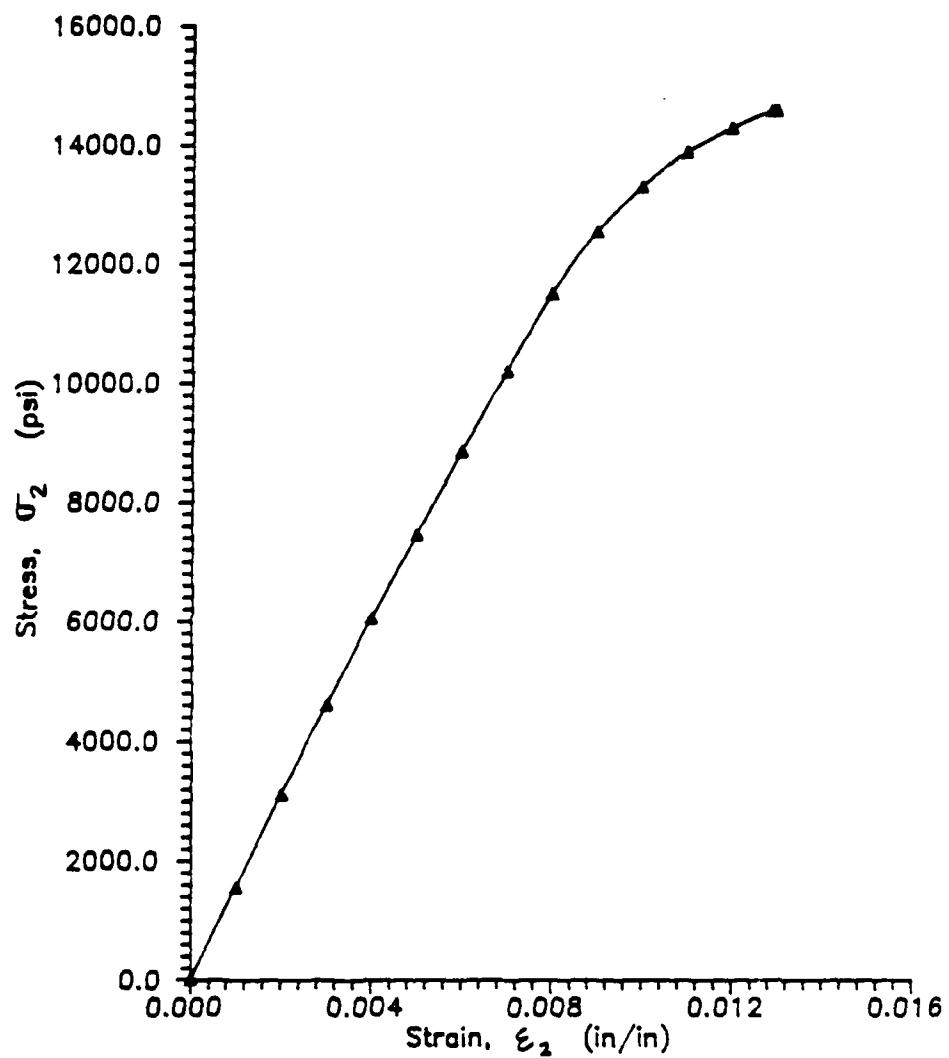
FIGURE 40. BASIC PROPERTY CURVE:
90-DEGREE TENSION FOR $E_2^T$

124
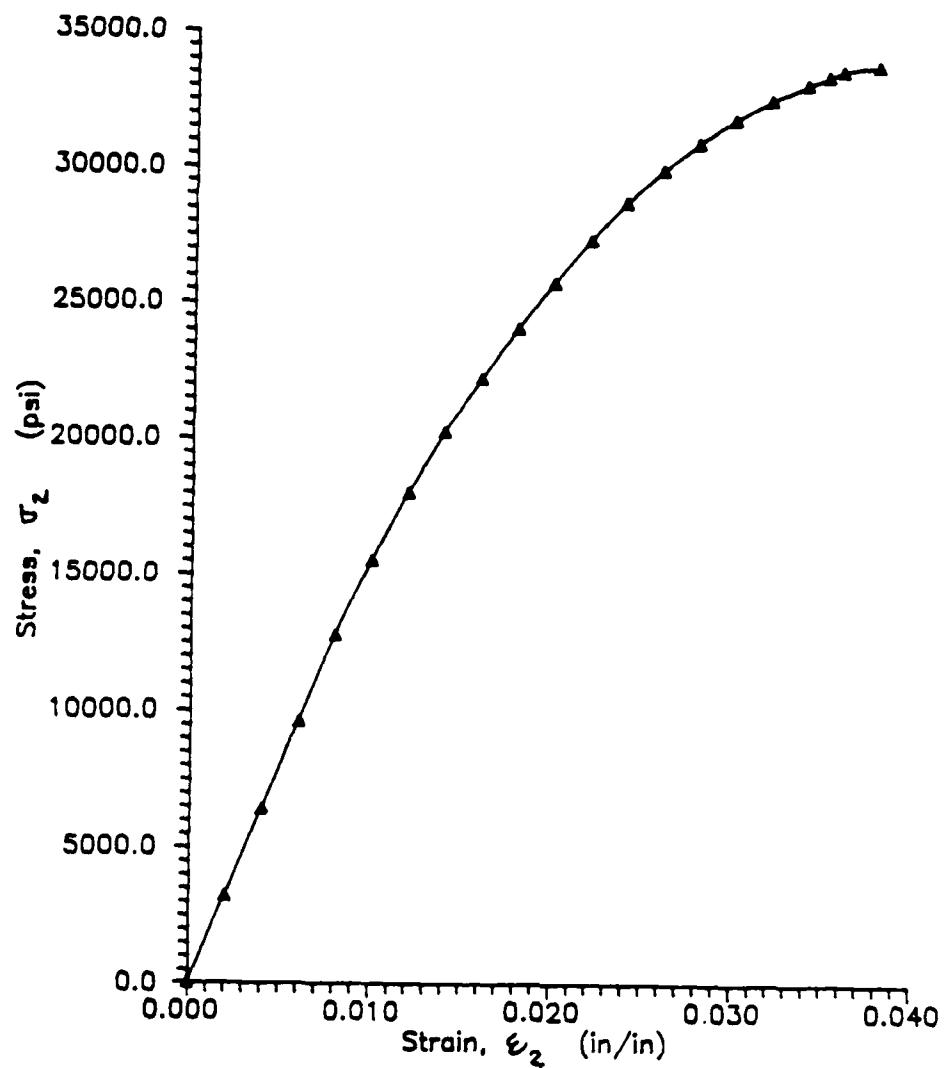
FIGURE 41. BASIC PROPERTY CURVE:
90-DEGREE COMPRESSION FOR $E_2^C$

125
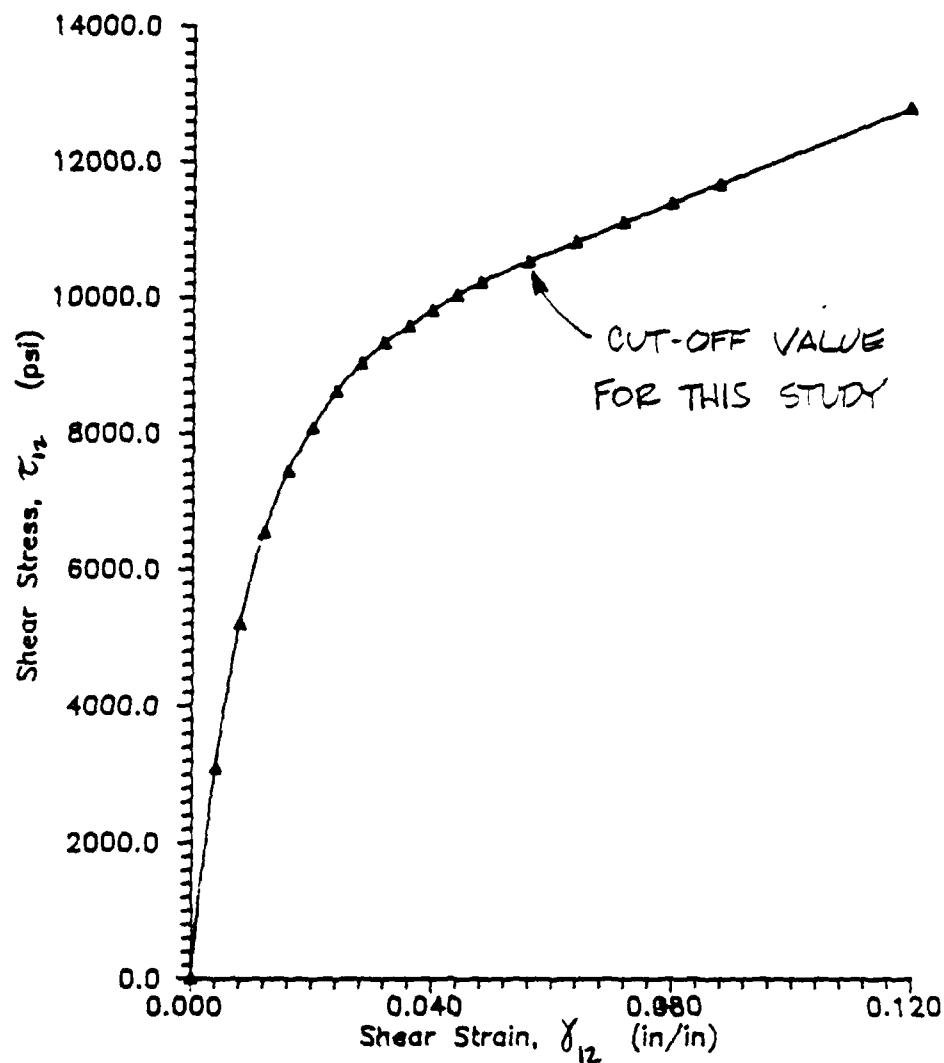
FIGURE 42. BASIC PROPERTY CURVE:
SHEAR SPECIMEN FOR $G_{12}$

126
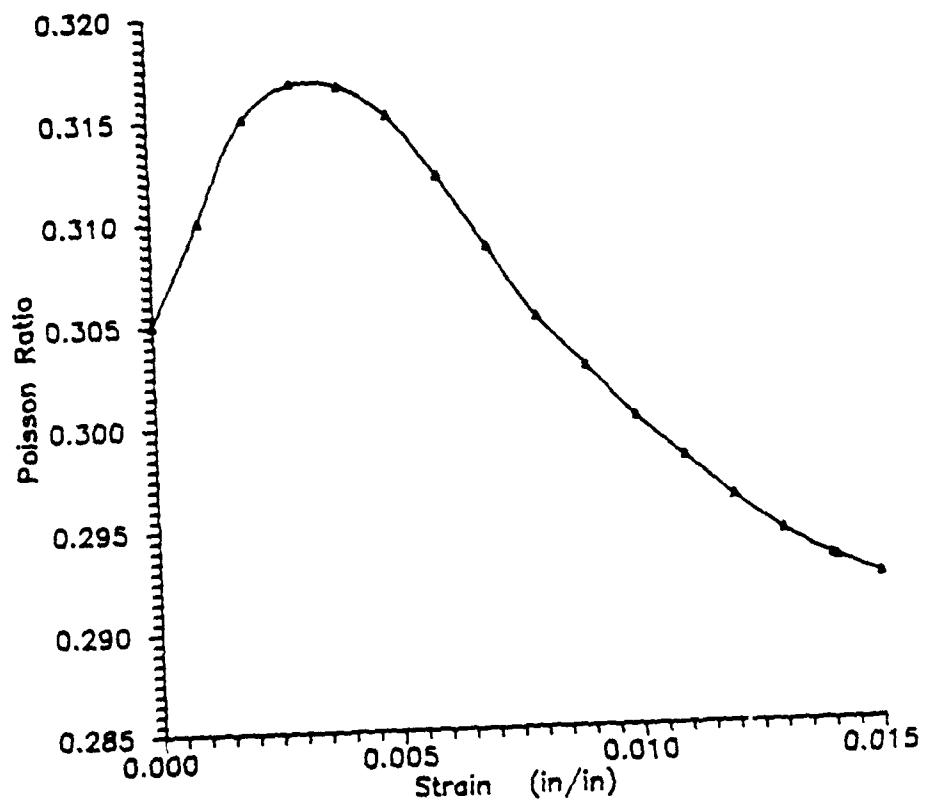
FIGURE 43. BASIC PROPERTY CURVE:

O-DEGREE TENSION YIELDS

$-\dfrac{\varepsilon_2}{\varepsilon_1}$ VS $\varepsilon_1$ FOR $\nu_{12}^T$

127
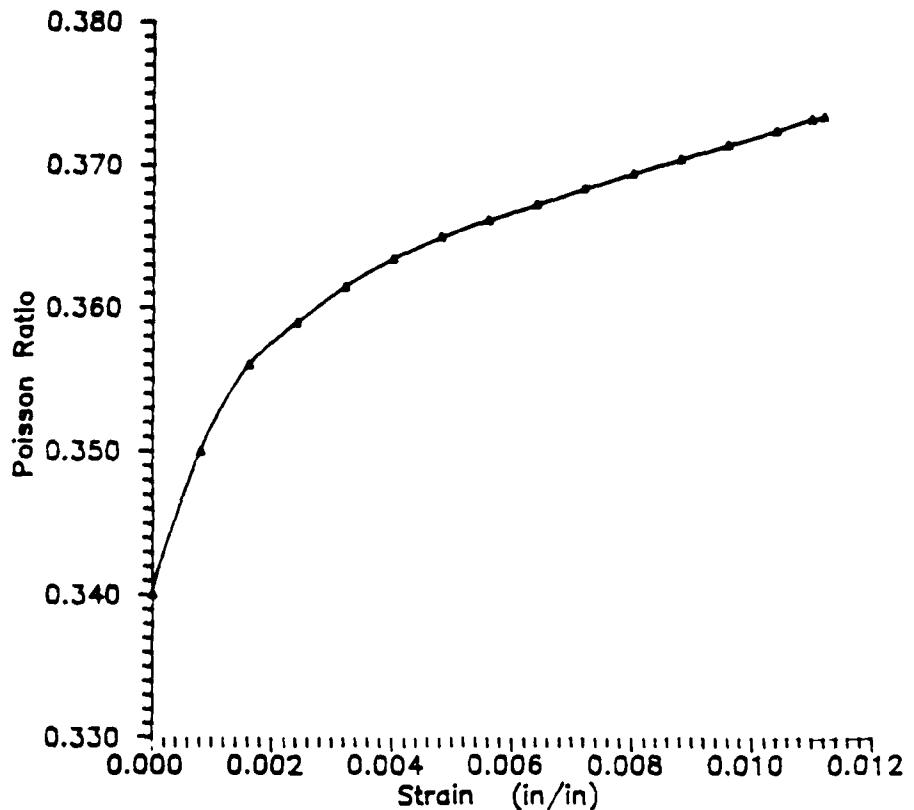
FIGURE 44. BASIC PROPERTY CURVE:
O-DEGREE COMPRESSION YIELDS
$-\dfrac{\varepsilon_2}{\varepsilon_1}$ VS. $\varepsilon_1$ FOR $\nu_{12}^{\,c}$

Table 12. Basic Material Properties of APC-2 Gr/PEEK
(Stress-strain data from basic property tests)

| 0° Tension | | | | 0° Compression | | |
|---|---|---|---|---|---|---|
| Strain (in/in) | Stress (ksi) | Poisson Ratio | | Strain (in/in) | Stress (ksi) | Poisson Ratio |
| 0.001 | 19.5 | 0.31 | | 0.0008 | 15.0 | 0.35 |
| 0.002 | 39.0 | 0.315 | | 0.0016 | 30.0 | 0.356 |
| 0.003 | 58.5 | 0.3167 | | 0.0024 | 44.5 | 0.359 |
| 0.004 | 78.1 | 0.3165 | | 0.0032 | 58.5 | 0.3615 |
| 0.005 | 97.8 | 0.315 | | 0.004 | 72.5 | 0.3635 |
| 0.006 | 118.0 | 0.312 | | 0.0048 | 86.0 | 0.365 |
| 0.007 | 138.5 | 0.3085 | | 0.0056 | 99.0 | 0.3662 |
| 0.008 | 159.0 | 0.305 | | 0.0064 | 111.5 | 0.3673 |
| 0.009 | 180.0 | 0.3025 | | 0.0072 | 124.0 | 0.3684 |
| 0.01 | 202.0 | 0.3 | | 0.008 | 136.0 | 0.3695 |
| 0.011 | 224.5 | 0.298 | | 0.0088 | 148.0 | 0.3705 |
| 0.012 | 247.5 | 0.296 | | 0.0096 | 159.0 | 0.3715 |
| 0.013 | 271.0 | 0.2943 | | 0.0104 | 170.0 | 0.3725 |
| 0.014 | 295.0 | 0.293 | | * 0.01101 | 178.0 | 0.3733 |
| * 0.0141 | 297.393 | 0.2929 | | | | |

| 90° Tension | | 90° Compression | | Shear | |
|---|---|---|---|---|---|
| Strain (in/in) | Stress (ksi) | Strain (in/in) | Stress (ksi) | Strain (in/in) | Stress (ksi) |
| 0.001 | 1.55 | 0.002 | 3.20 | 0.004 | 3.090 |
| 0.002 | 3.10 | 0.004 | 6.40 | 0.008 | 5.200 |
| 0.003 | 4.60 | 0.006 | 9.60 | 0.012 | 6.535 |
| 0.004 | 6.05 | 0.008 | 12.75 | 0.016 | 7.440 |
| 0.005 | 7.45 | 0.01 | 15.50 | 0.02 | 8.080 |
| 0.006 | 8.85 | 0.012 | 18.00 | 0.024 | 8.610 |
| 0.007 | 10.20 | 0.014 | 20.25 | 0.028 | 9.020 |
| 0.008 | 11.50 | 0.016 | 22.20 | 0.032 | 9.330 |
| 0.009 | 12.55 | 0.018 | 24.05 | 0.036 | 9.578 |
| 0.01 | 13.30 | 0.02 | 25.73 | 0.04 | 9.810 |
| 0.011 | 13.90 | 0.022 | 27.30 | 0.044 | 10.030 |
| 0.012 | 14.30 | 0.024 | 28.70 | 0.048 | 10.230 |
| * 0.0129 | 14.586 | 0.026 | 29.90 | * 0.056 | 10.540 |
| | | 0.028 | 30.90 | * | |
| | | 0.03 | 31.80 | | |
| | | 0.032 | 32.50 | | |
| | | 0.034 | 33.10 | | |
| | | * 0.0352 | 33.40 | | |

" * " denotes Ultimate Stress-Strain Values.

129

Table .3.    Engineering Elastic Constants for APC-2 Gr/PEEK

$$E_1^T = 19.5 \times 10^6 \qquad E_1^C = 18.75 \times 10^6$$

$$E_2^T = 1.55 \times 10^6 \qquad E_2^C = 1.6 \times 10^6$$

$$G_{12} = 0.8125 \times 10^6$$

$$\nu_{12}^T = 0.305 \qquad \nu_{12}^C = 0.34$$

specimens, but their results will be presented in a separate section.  For all tests, data was gathered in various forms with the goal of determining stress-strain response to ultimate strength of the laminates.  The results from this phase of experimentation are presented in this section.  As an overall view of the results, all 5 types of laminates are shown as failed specimens in Figure 45.  The results of the quasi-isotropic study are discussed in Section D of this chapter.  As described in Chapter III, the 0T, 90T, and SH laminates were also analyzed using a fully nonlinear ply-by-ply plane stress finite element technique.  These analytical studies of the laminates are presented in tandom with experimental results.

1.  [0_{16}] Unidirectional Specimens.  The general results of 6 tests to ultimate strength are listed in

TYPE

OT

90T

CH

Q1
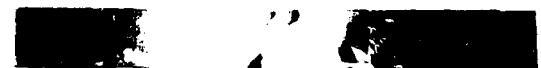
Q2

Figure 45.  Failed Specimens of all 5 Types of Laminates.

Table 14. Ultimate Strength Tests of $[0_{16}]$ Specimens

| Sample Number | X-Sect Area | Test Number | Failure Load (lbs.) | Failure Stress (psi) |
|---|---|---|---|---|
| A1-0T-0-01 | 0.04988 | 6001 | 14,900. | 159,100. |
| A1-0T-0-02 | 0.04988 | 6002 | 15,707. | 165,400. |
| A1-0T-0-03 | 0.0498 | 6003 | 14,380. | 153,350. |
| A1-0T-0-04 | 0.05013 | 6004 | 15,400. | 136,550. |
| A1-0T-0-05 | 0.05107 | 6008 | 13,850. | 133,450. |
| A1-0T-0-06 | 0.0498 | 6012 | 15,400. | 128,250. |

Average Failure Stress = 146,000.

Table 14. For these specimens, a repeatable and significant occurrence took place. At 40% of each specimen's failure load, splitting of the laminate occurred. It began at the sides of the hole and suddenly extended, parallel to the fibers, through the tab. Failure of each specimen was dominated by this phenomenon. A single specimen is shown in Figure 46. Notice that the top segment slipped out of the left tab at failure, and the bottom segment slipped out of the right tab. The middle segments were simply unloaded.

When the splitting occurred, nearly an instantaneous drop in measured load occurred. This can be seen in Figure 47 on the load-displacement curve. Each of the discontinuities (at approximately 6000 lbs.) represents one side of the specimen splitting.

Figure 46.  Failed  $[\emptyset_{16}]$  Specimen
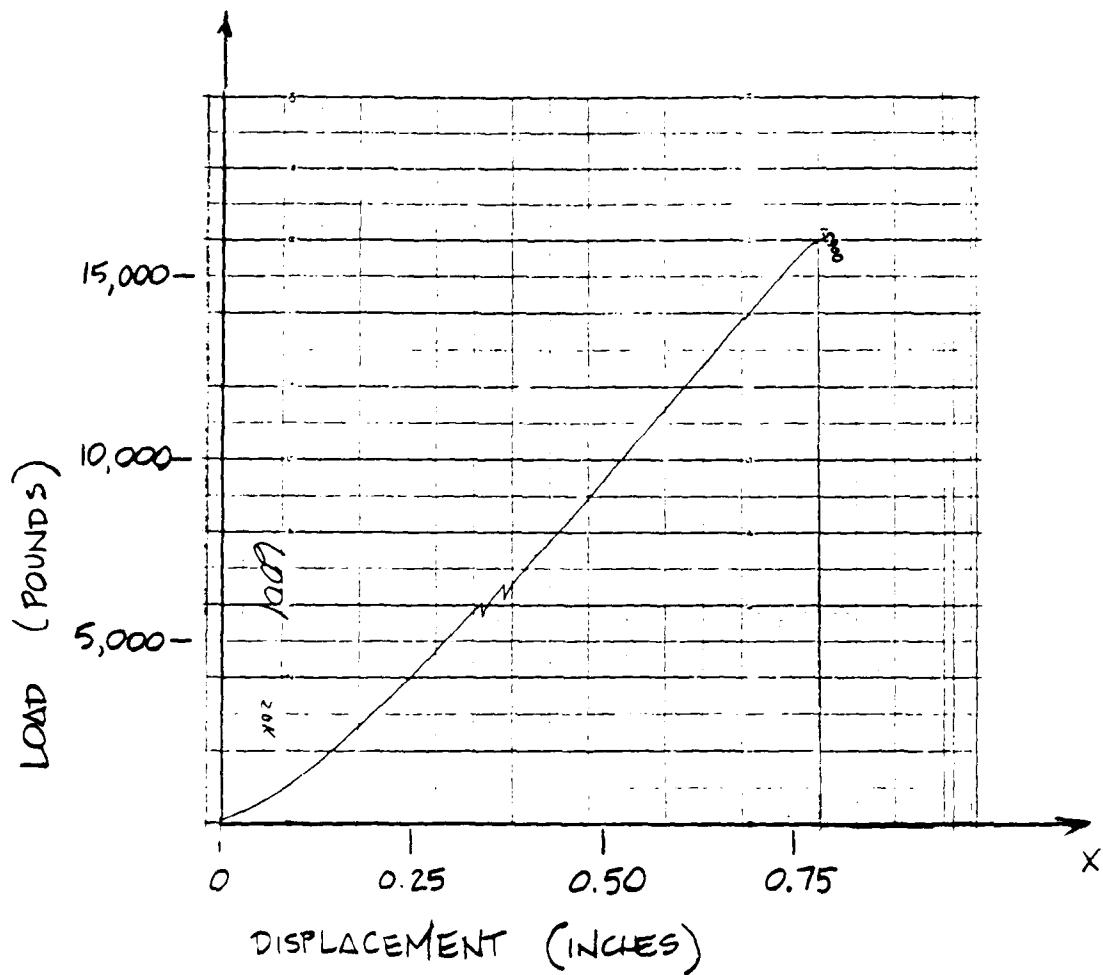
FIGURE 47. LOAD·DISPLACEMENT CURVE FOR
[$O_{16}$] TENSILE SPECIMEN

134

In analyzing this phenomenon, one could consider the sudden splitting as the ultimate failure of the laminate. Thus, 40% of failure load from Table 14 could be considered as the actual ultimate load on the specimen. Therefore, after 40% of the ultimate load, a different problem exists. The problem is one of two 0.4-inch-wide thin plates under a uniaxial tensile load, with an unloaded 0.4-inch wide segment in the center. As a comparison to the unnotched 0-degree basic property specimen, we could calculate the failure stress of one of the segments. However, these outer segments, with no stress risers in their geometry, never failed across their fibers. Instead, they slipped out of their tabs. Thus, direct comparison to ultimate strength in the 0-degree direction was not possible.

When the splitting occurred, the strain gages at both the hole and far field read discontinuous jumps in strain. For the gages at the hole, three of the four gages continued to read strain after the splitting, and these three readings were similar past 40% of the failure stress. The fourth gage most likely failed due to the shock of the splitting. These three sets of readings were averaged, and the average experimental curves are shown in Figure 48. Again, note the jumps in the readings. The analytical stress-strain curve is also plotted against the laboratory results. The stress-strain response was modeled accurately up to the occurrence of splitting, then to a good approximation beyond

135

FIGURE 48. $[0_{16}]$ RESPONSE AT HOLE

136
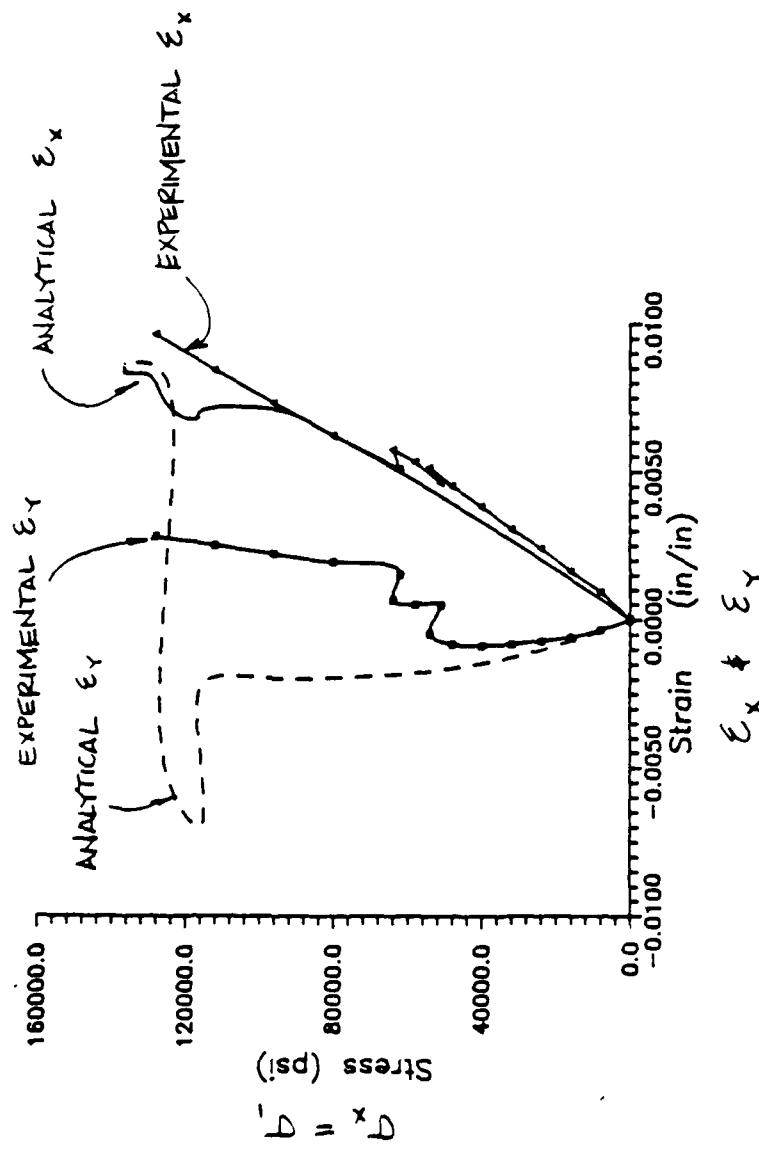
that load. The analytical discontinuities that occurred just before the element near the hole failed were a result of the element's strain response reacting to other elements failing next to it. The current version of the program contained only a gradual unloading scheme (see Section II G), and these strain responses were a result of this scheme. This unloading scheme produced some anomalies between experimental and analytical results for both types of unidirectional laminates, and these will be discussed in subsequent paragraphs. The general trend was accurate, however, and the model predicted failure of that area exactly within the range of experimental values.

After the splitting, most far field gages continued to read strain, but no readings were repeatable, as they were before the splitting. For six specimens, the far field stress-strain response is shown in Figure 49. Note the discontinuities. These results are reasonable since the gages were placed in the center of the specimen, which became unloaded after 40% of the ultimate load. Also shown on this plot is a superimposed analytical response. Note that the computer program accurately measured the stress-strain response until the splitting occurred. The splitting never reached the element measuring the far field response because of the gradual unloading scheme used in the program. Therefore, the element continued to output stress and strain values.
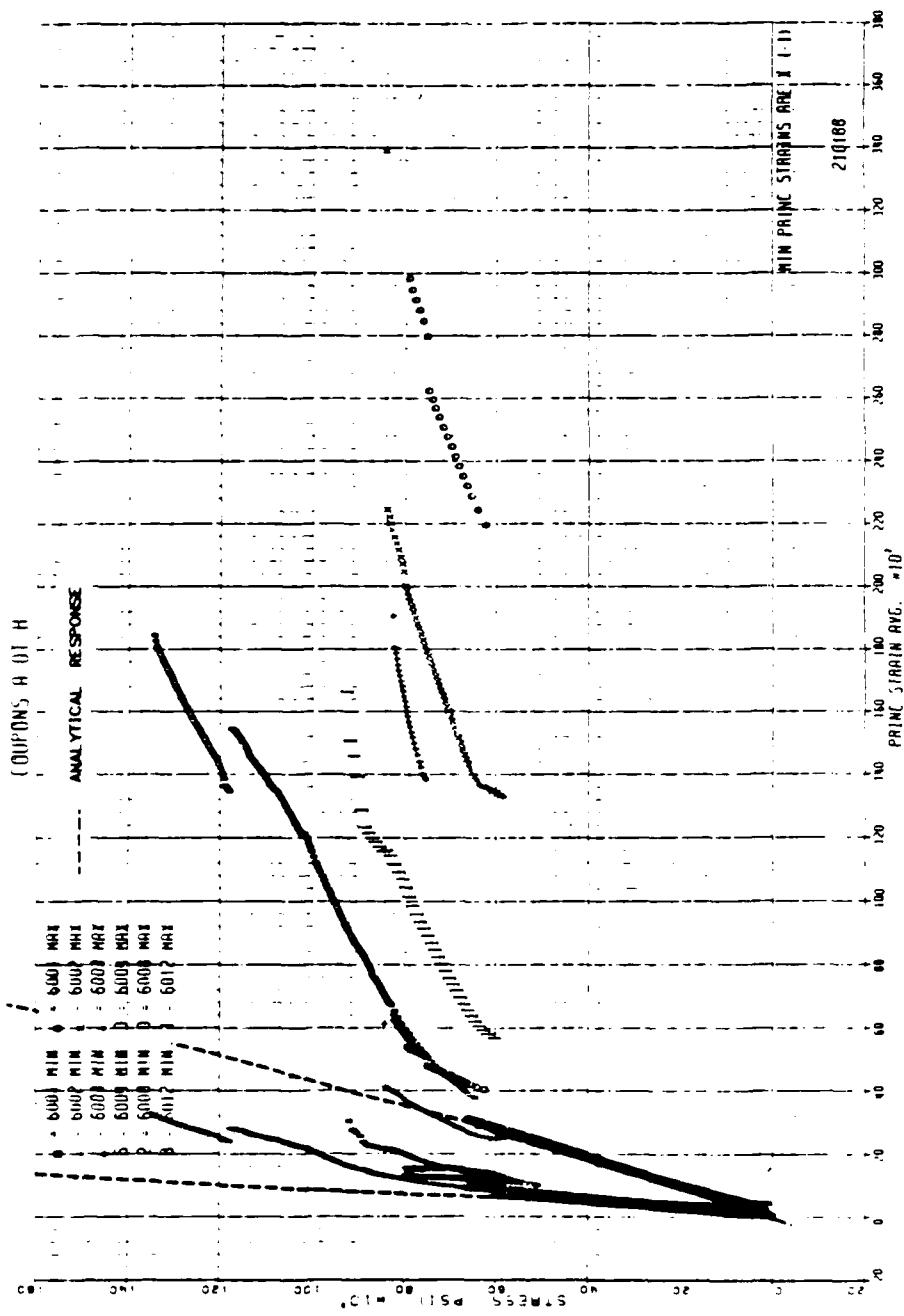
FIGURE 49. $[0_{16}]$ RESPONSE AT FAR FIELD

Note that for all the stress-strain plots of this section, the axes for the curves are the nominal stress on the laminate (load/area) versus the axial and transverse strains in the element.

2. $[90_{16}]$ <u>Unidirectional</u> <u>Laminates</u>. Seven specimens were tested to failure, and the general results of these tests are listed in Table 15.

For these specimens, a predictable failure mode occurred. The specimens simply failed at the most narrow part of their cross-sectional area. This type of failure is shown in the photograph of Figure 50.

For the strain gage near the hole, the average experimental stress-strain response is shown compared to the analytical response in Figure 51. Again, the model

Table 15. Ultimate Strength Tests of $[90_{16}]$ Specimens

| Sample Number | X-Sect Area | Test Number | Failure Load (lbs.) | Failure Stress (psi) |
|---|---|---|---|---|
| B2-90T-H-02 | 0.09815 | 7002 | 765. | 7794. |
| B2-90T-H-03 | 0.09815 | 7003 | 850. | 8660. |
| B2-90T-H-04 | 0.09815 | 7004 | 780. | 7947. |
| B2-90T-H-05 | 0.09840 | 7005 | 808. | 8211. |
| B3-90T-H-08 | 0.09720 | 7008 | 780. | 8025. |
| B4-90T-H-12 | 0.09720 | 7012 | 712. | 7325. |
| B4-90T-H-16 | 0.098646 | 7016 | 697. | 7066. |

Average Failure Stress = 7860.

Figure 50.  Failed  $[90_{16}]$  Specimen.
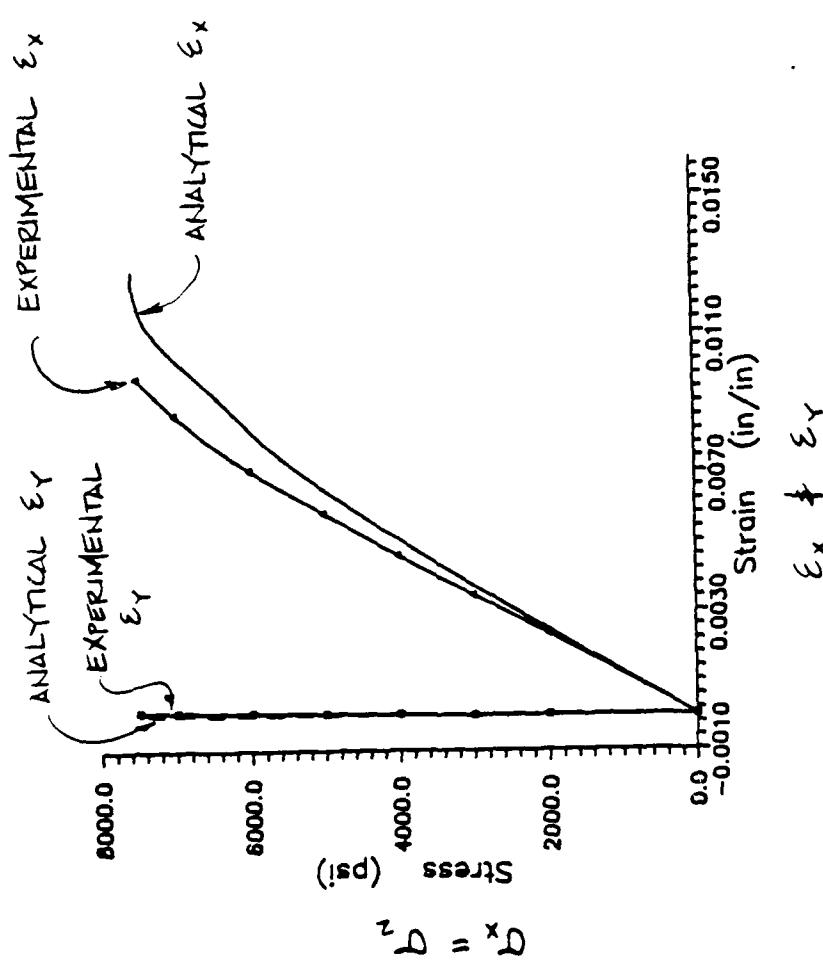
FIGURE 51. [90₁₆] RESPONSE AT HOLE

accurately predicted stress-strain behavior, and it exactly predicted the ultimate failure of the area next to the hole. Its prediction of 7,551 psi at failure fell within the range of experimental vaules of failure stress. Analytically, the strain response, $\varepsilon_x$, follows closely the basic property curve for 90-degree tension. The actual area failed with a stiffer response. The reason for this variance probably relates to the modeling of gradual failure versus the reality of sudden failure. This concept will be further discussed in the next section.

The stress-strain response is shown in Figure 52 for the far field gage. The analytical stress-strain response modeled the experimental response exactly as shown. However, beyond the experimental failure stress, the model still showed some stiffness, due to the unloading scheme. And after 40 load increments, which corresponded to a stress of 8840 psi, the model had not yet failed completely across the specimen, and the computer run was stopped.

3. [±45]$_{4s}$ Angle-Ply Laminates. Seven angle-ply laminates were tested to their ultimate strength, and the general test results are listed in Table 16. The failure of these specimens was characterized by high strain to failure, especially in the region of the hole. This high strain is apparent in the failed SH specimen shown in Figure 53. Note that significant necking occurred in the region of the

142
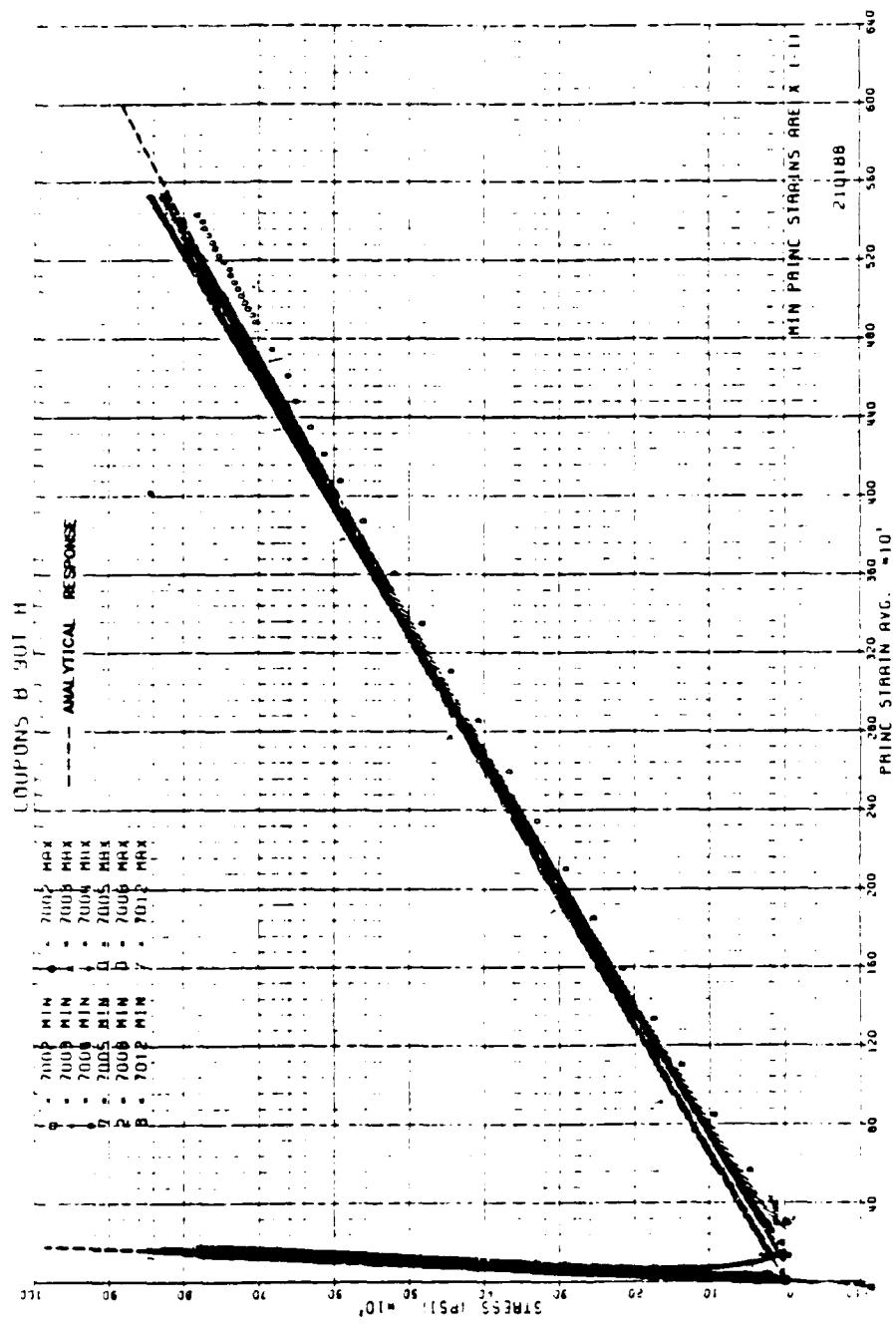
FIGURE 52. [90₁₆] RESPONSE AT FAR FIELD

143

Figure 53. Failed $[\pm45]_{4S}$ Specimen

Table 16.    Ultimate Strength Tests of [±45]$_{4s}$ Specimens

| Sample Number | X-Sect Area | Test Number | Failure Load (lbs.) | Failure Stress (psi) |
|---|---|---|---|---|
| C2-SH-0-01 | 0.09752 | 8001 | 2,628. | 26,948. |
| C2-SH-0-02 | 0.09865 | 8002 | 2,669. | 27,055. |
| C2-SH-0-03 | 0.09952 | 8003 | 2,630. | 26,427. |
| C2-SH-0-04 | 0.09993 | 8004 | 2,423. | 24,247. |
| C2-SH-0-08 | 0.0972 | 8008 | 2,352 | 24,198. |
| C2-SH-0-12 | 0.09856 | 8012 | 2,400. | 24,351. |
| C2-SH-0-16 | 0.09985 | 8016 | 2,650. | 26,540. |

Average Failure Stress =   25,680.

hole.    The holes itself also appears as an ellipse in the specimen of Figure 53, due to the high deformations.

For the gage at the hole, the very high strain which occurred in these specimens started early in the loading. As shown in the next section, a distinct failure region was growing at the sides of the holes.    When that region met the gage, the gage failed.    The stress at failure varied for each gage, but in all cases it was significantly below the failure stress of the entire laminate.    Taking the average failure stress corresponding to the strain gage at the hole, the failure of the region over which the gage was placed was about 45% of the average failure stress of the entire specimen.    The stress-strain curves for the area at the hole were averaged, and this average curve is plotted in

Figure 54 as shear stress on the specimen versus shear strain at the hole.

Analytically, the stress-strain response and ultimate failure of the element matched the actual response very well. This analytical response is also plotted in Figure 54. Note that the first analytical stress-strain values were output almost at the ultimate failure stress for the element. When the load increment was applied (which was one-tenth of the final displacement of the experimental specimen; see Section III D), the strain in the element at the hole was suddenly very large. If a smaller load increment was applied, the analytical stress-strain curve would have better matched the experimental response.

Note also in Figure 54 that the analytical ultimate failure stress predicted very closely the failure of the area near the hole. Thus, cutting off the shear basic property data at values corresponding to approximately 5.5% strain yielded accurate results.

The stress-strain curves of nominal shear stress versus the far-field shear strain (as defined in Section IV E) is shown in Figure 55. Note that repeatable data was obtained except for one errant strain reading. The analytical stress-strain behavior matched this experimental response very well, also shown in Figure 55; and this result met the goal of this test.

146
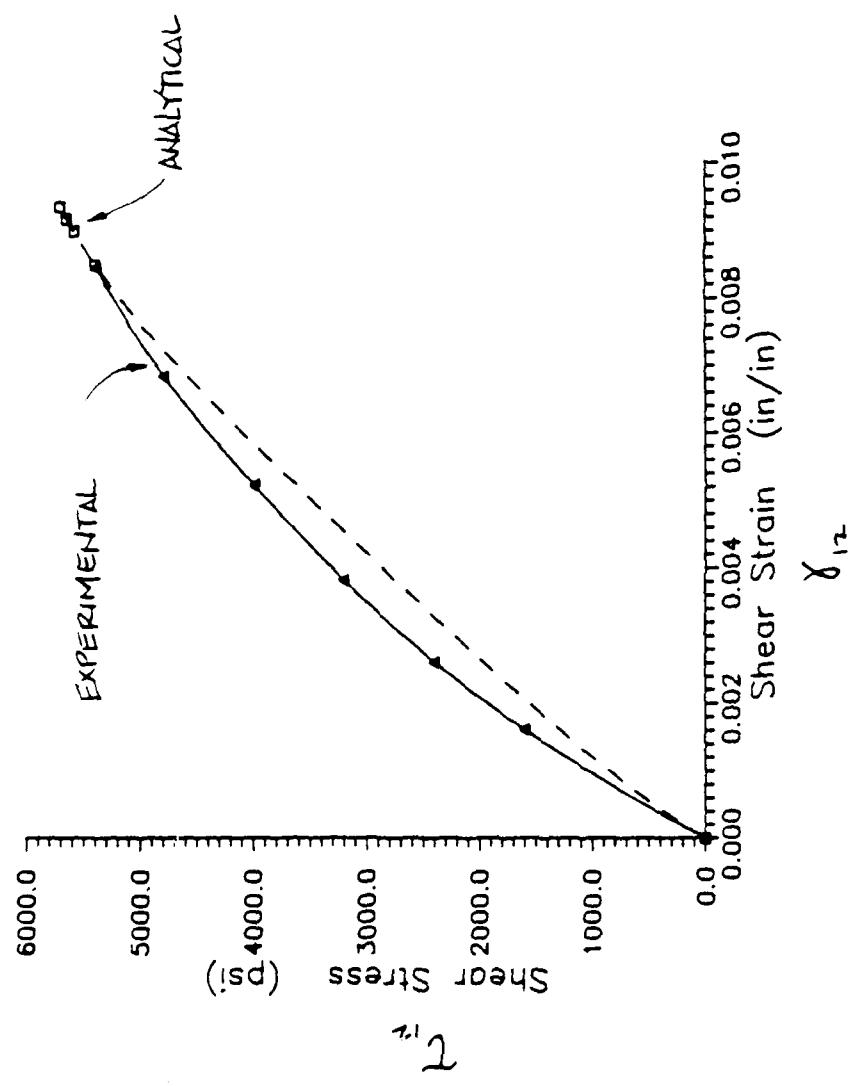
FIGURE 54. $[\pm 45]_{4s}$ RESPONSE AT HOLE
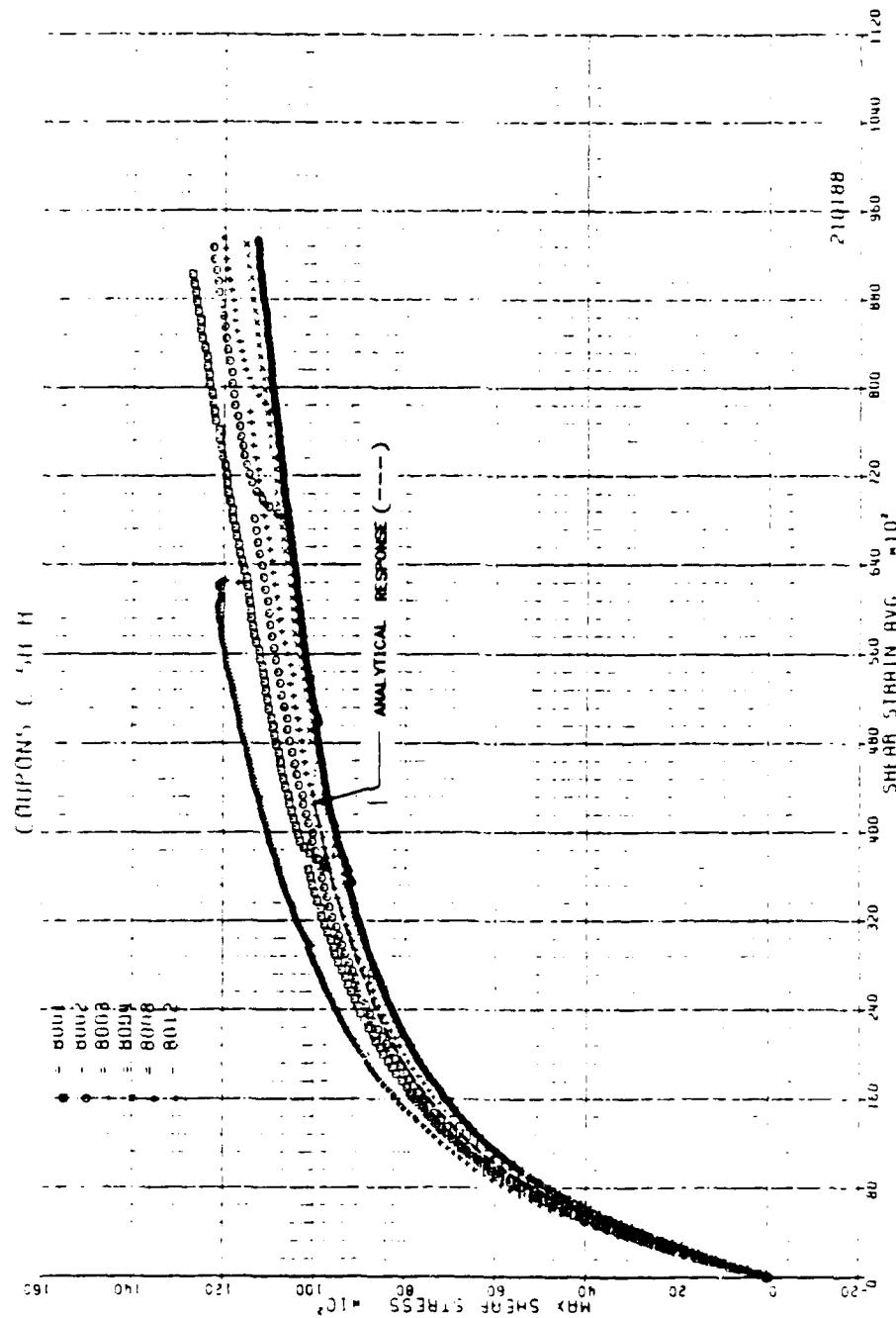
FIGURE 55. $[\pm 45]_{4S}$ RESPONSE AT FAR FIELD

148

Overall, the computer analysis provided good results in modeling the stress-strain behavior of the 0T, 90T, and SH laminates. Conclusions will be drawn for the results of this section in Chapter VI.

C. Results of the Failure Progression Study for $[0_{16}]$, $[90_{16}]$, and $[\pm45]_{4S}$ Laminates

The results of studying the initiation and progression of failure in the laminates were derived from:

    (1)   A videotape post-failure analysis.

    (2)   A stereo x-ray post-failure analysis, and

    (3)   A progressive-failure finite element technique.

Note that the specimens were subjected to x-ray only after loading. They were not x-rayed before loading to check for fabrication flaws.

1. Failure Progression in $[0_{16}]$ Unidirectional Specimens. As discussed in the previous section, splitting occurred for these specimens at 40% of their ultimate strength. This phenomenon thus dominated the experimental stress-strain behavior of this laminate.

The splitting and eventual failure was documented by the video camera, and 4 stills were taken for a representative specimen. Figure 56 shows the tensile coupon for test # 5002 at the beginning of the loading. For this test, one volt corresponded to 4.082 pounds. The splitting occurred at a reading of about 1.60 volts. After further loading,

149

the split is slightly perceptable at 3.50 volts (14.700
lbs.) in Figure 57. The ultimate load on the specimen is
shown in Figure 58 at 4.05 volts (16,500 lbs.), and the next
frame of the videotape provided the failed laminate, as
shown in Figure 59, implying sudden failure. The '-0.02'
indicates a sudden zero loading on the specimen.

The results of all tests to percentages of the average
failure stress are shown in Table 17. (The average failure
stress was 146,000; see Table 14.) A stereo x-ray was
taken of all 9 specimens. As expected, the only failure
region that is visible is the splitting along the fiber
direction. The effect of stereo viewing provided the

Table 17. Progressive Failure Tests of $[0_{16}]$ Specimens

| Sample Number | X-Sect Area | Test Number | %* | Load (kips) | Stress (ksi) | Actual % |
|---|---|---|---|---|---|---|
| A2-0T-H-05 | 0.10114 | 6005 | 50% | 7.417 | 73.334 | 50.2 |
| A2-0T-H-06 | 0.0996 | 6006 | 50 | 6.997 | 70.251 | 48.1 |
| A2-0T-H-07 | 0.09993 | 6007 | 50 | 7.598 | 76.033 | 52.1 |
| A3-0T-H-09 | 0.09504 | 6009 | 80% | 11.183 | 117.665 | 80.6 |
| A3-0T-H-10 | 0.09616 | 6010 | 80 | 11.228 | 116.764 | 80.0 |
| A3-0T-H-11 | 0.09832 | 6011 | 80 | 12.925 | 131.458 | 90.0 |
| A3-0T-H-13 | 0.09728 | 6013 | 90% | 12.126 | 124.650 | ** |
| A3-0T-H-14 | 0.09632 | 6014 | 90 | 12.044 | 125.042 | 85.6 |

\* This is the percentage where the test machine was
attempted to be stopped.

\** This specimen broke unexpectedly.
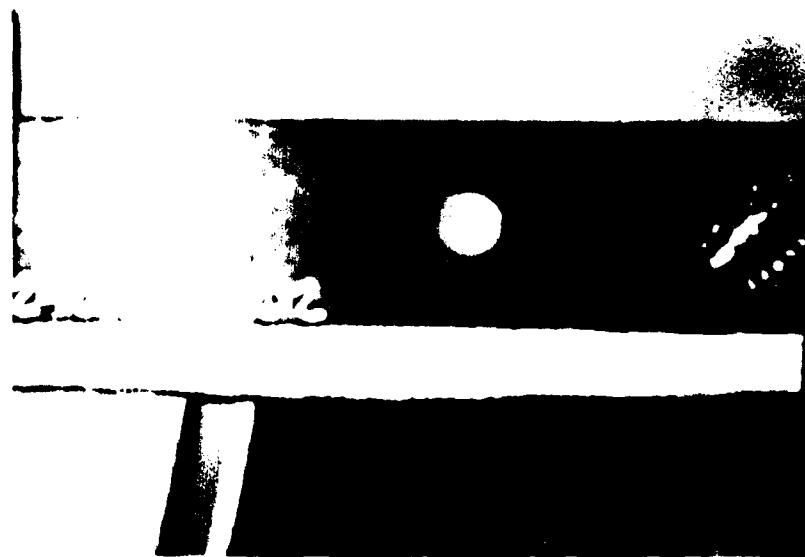
Figure 56.  [$\emptyset_{16}$]  Specimen at Beginning of Loading.
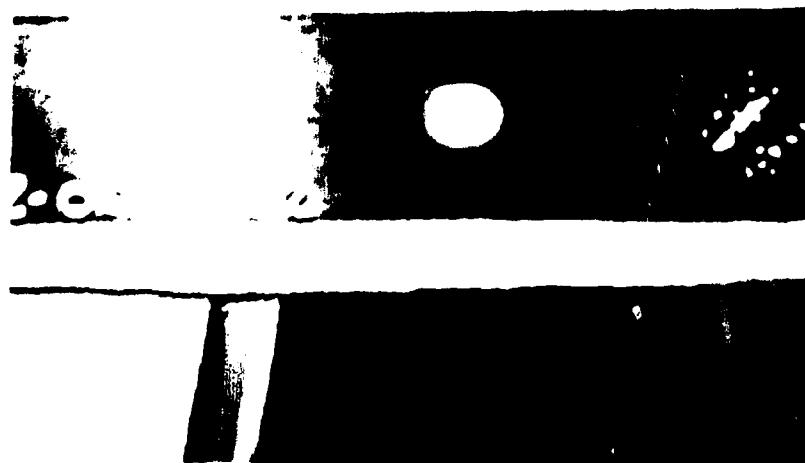


Figure 57.  [$\emptyset_{16}$] Specimen at 14,300 lbs.  Splitting Visible.
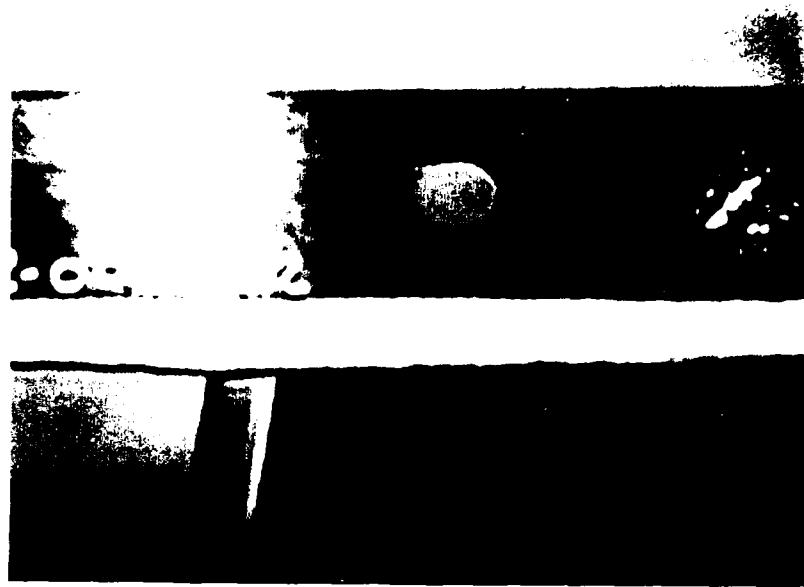
Figure 58. $[0_{16}]$ Specimen at Maximum Load of 16,500 lbs.



Figure 59. $[0_{16}]$ Specimen: Sudden Failure; Instant Unloading.

152

expected result that the splitting occurred perpendicular to the front face of the specimen and through the thickness. A typical specimen stressed almost to failure is shown in Figure 60. The stereo x-rays for the failed specimen of test # 6013 are shown in Figure 61.

For an analytical comparison to growth of failure, Figure 62 shows a similar progression to the experimental results. As shown, the failure began at the element that was most highly stressed and proceeded parallel to the fiber direction. However, the analytical result shows a failure region developing, instead of a single line of elements failing. The reason for this difference is in the unloading scheme of the computer program. The scheme in the current version of program provides only for gradual unloading, although the specimen modeled was a unidirectional element. (See Section II G.) Thus, as the elements failed, they were still modeled to have stiffness. (The program is currently being developed to handle instantaneous unloading.) The results of Figure 62, however, do show an accurate trend of failure progression.

Analyzing this specimen further, the failure of the first element in the mesh is a measure of the strain energy at the center of the element. If the strain energy is extrapolated to the edge of the element at the hole, the value of 55% of ultimate load would decrease to a value near 40%, which is our experimental result. Thus, the onset of
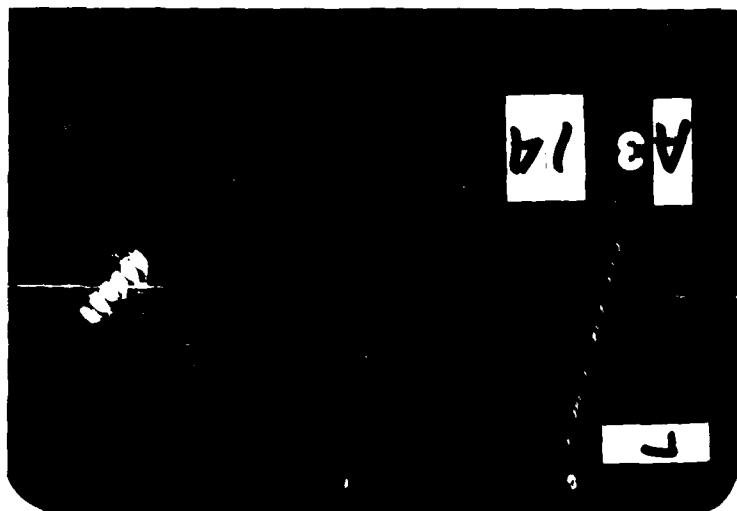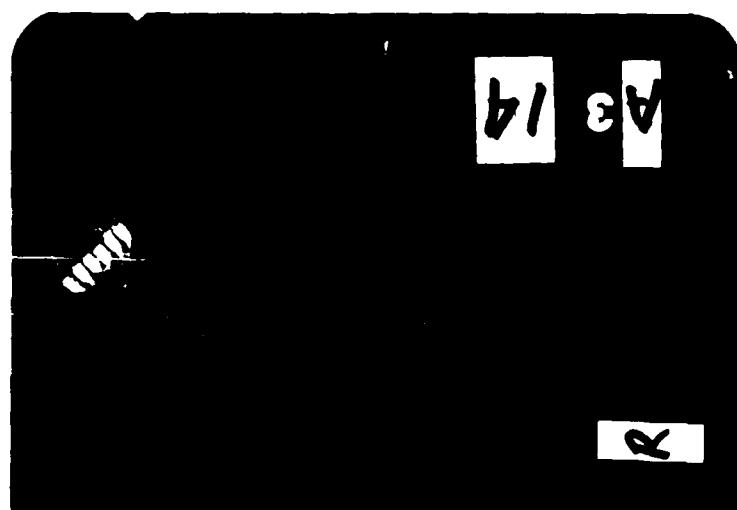
Figure 60.    Stereo X-Ray of $[0_{16}]$ Specimen at 95% of Average
Ultimate Stress.
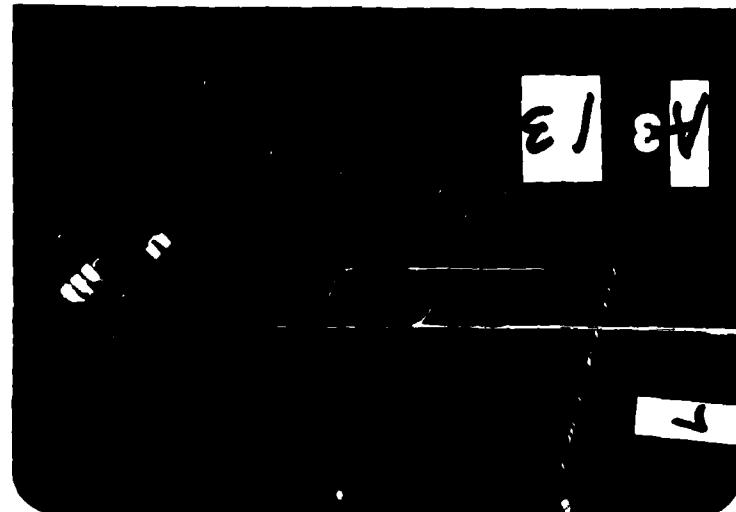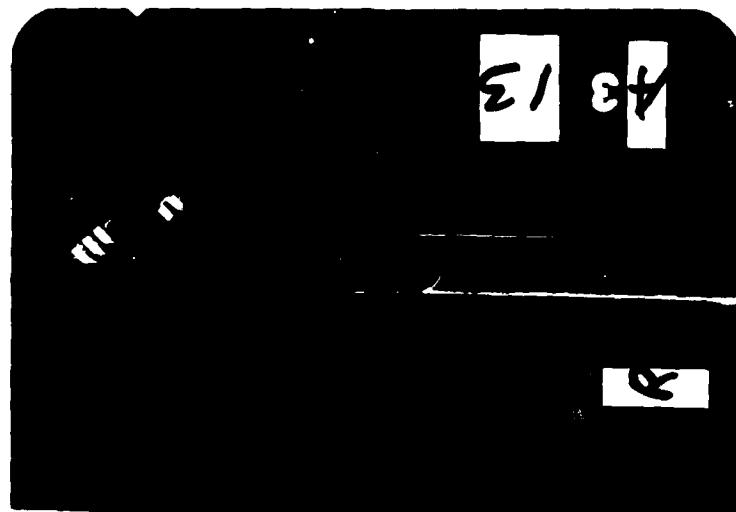
Figure 61.   Stereo X-Ray of Failed $[0_{16}]$ Specimen.
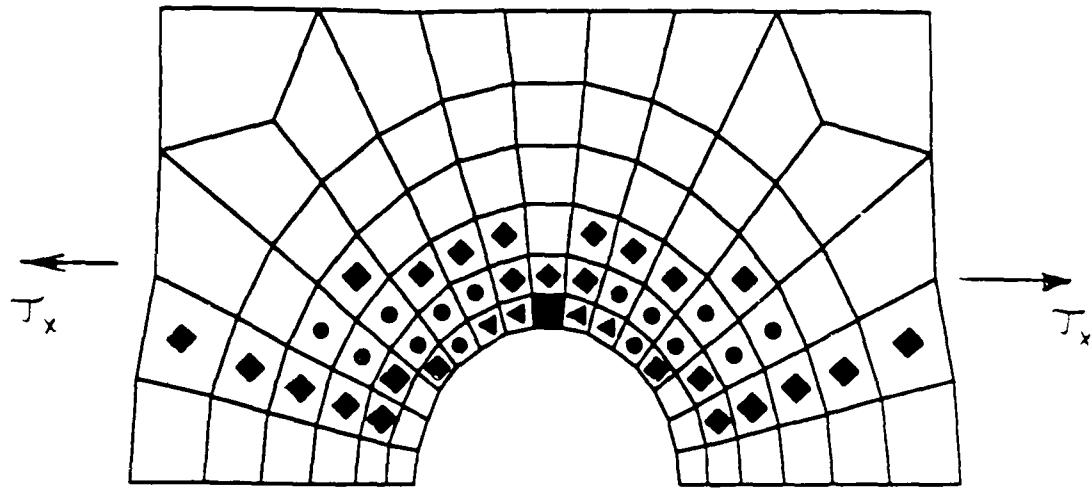
FIGURE 16.

$[O_{16}]$ ANALYTICAL FAILURE PROGRESSION

| KEY | % OF AVERAGE FAILURE STRESS |
|---|---|
| [SOLID SQUARE] | 55% – FIRST ELEMENT TO FAIL |
| ◀ | 80% |
| ● | 92% |
| ◆ | 110% |

failure in the 0-degree specimen could be predicted in this manner. From this analysis, the splitting of the entire laminate could be defined by the failure of the first element.

Thus, analytically, this problem has two bounds: (1) The definition of sudden splitting with failure of the first element, which models the actual failure, and (2) the gradual failure of the elements, which does not model reality but is an academic exercise. No interlaminar stresses exist in the 0-degree laminate, and this gradual failure scheme, or strain softening concept, does not apply.

2. <u>Failure Progression in 90° Unidirectional Specimens</u>. As implied in the previous section, the failure of these specimens was dominated by matrix failure beginning at the hole and extending to the edge of the laminate. However, the <u>progression</u> of this failure was barely noticeable in the post-failure analyses.

From the videotape, three loading 'scenes' of a typical test are shown in Figures 63 through 65. In Figure 63, a typical 90-degree specimen is shown at the beginning of loading. For these tests, one volt corresponded to a load of 408 pounds. In Figure 64, where the specimen is loaded to nearly 100% of its failure load, no failure region is shown. Then, after advancing one frame of the videotape, (where one frame equals 1/60 sec) the video picture shown in
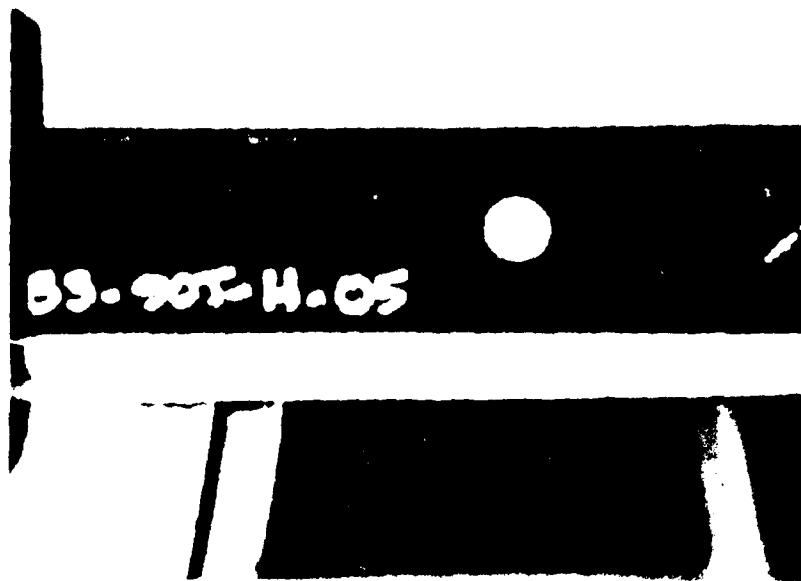
Figure 63.   [$90_{16}$] Specimen at Beginning of Loading.
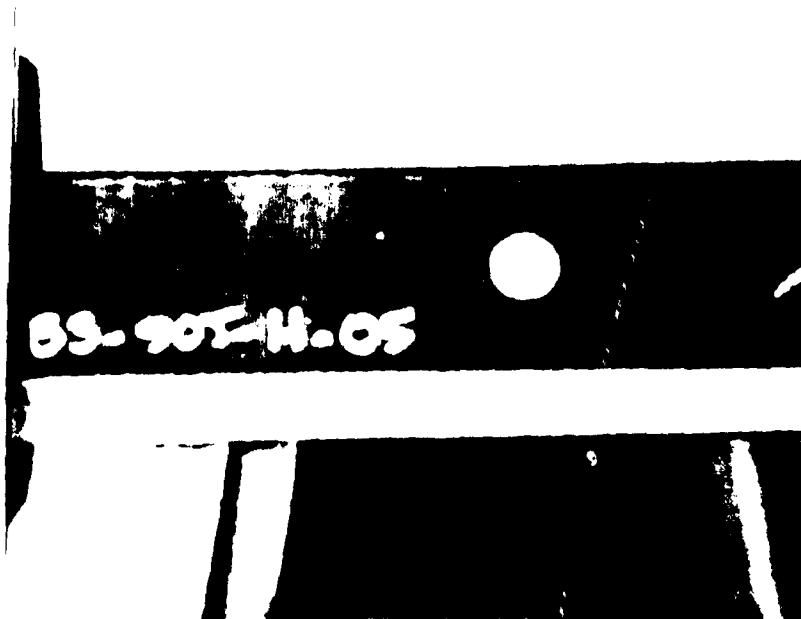


Figure 64.   [$90_{16}$] Specimen at 99.5% of Ultimate Load.

158

Figure 65.  Failed [$90_{16}$] Specimen.

Figure 65 rendered a failed specimen, again implying sudden failure.

The results of each test to a percentage of the average failure stress (7860 pounds) are presented in Table 18. These tests and the stereo x-rays provided further proof of sudden failure. A specimen loaded to approximately 90% of the average failure load showed little sign of being stressed. In Figure 66 the white regions shown could represent the beginning of a failure area, or they could simply be a hole defect caused by the drill. The specimen shown in Figure 67 has failed through the thickness but not exactly at the hole. This unexpected failure could have been initiated by flaws or notches from the fabrication of the hole.

Table 18. Progressive Failure Tests of $[90_{16}]$ Specimens

| Sample Number | X-Sect Area | Test Number | %[*] | Load (lbs.) | Stress (psi) | Actual % |
|---|---|---|---|---|---|---|
| B2-90T-H-01 | 0.09848 | 7001 | 80% | 639. | 6489. | 82.6 |
| B3-90T-H-06 | 0.09752 | 7006 | 80 | 625. | 6408. | 81.5 |
| B3-90T-H-07 | 0.09744 | 7007 | 80 | 632. | 6486. | 82.5 |
| B3-90T-H-09 | 0.09744 | 7009 | 90% | 697. | 7153. | 91.0 |
| B3-90T-H-10 | 0.096 | 7010 | 90 | 694. | 7229. | 92.0 |
| B3-90T-H-11 | 0.09624 | 7011 | 90 | 695. | 7222. | 91.9 |
| B4-90T-H-13 | 0.09752 | 7013 | 95% | 737. | 7557. | 96.2 |
| B4-90T-H-14 | 0.09865 | 7014 | 95 | 746. | 7562. | ** |
| B4-90T-H-15 | 0.0984 | 7015 | 95 | 735. | 7470. | 95.0 |

** This specimen in broke approximate 3 seconds after loading was halted.
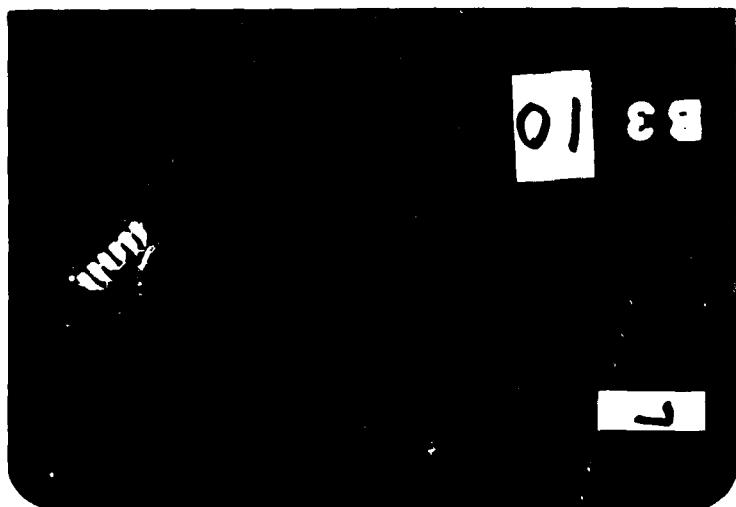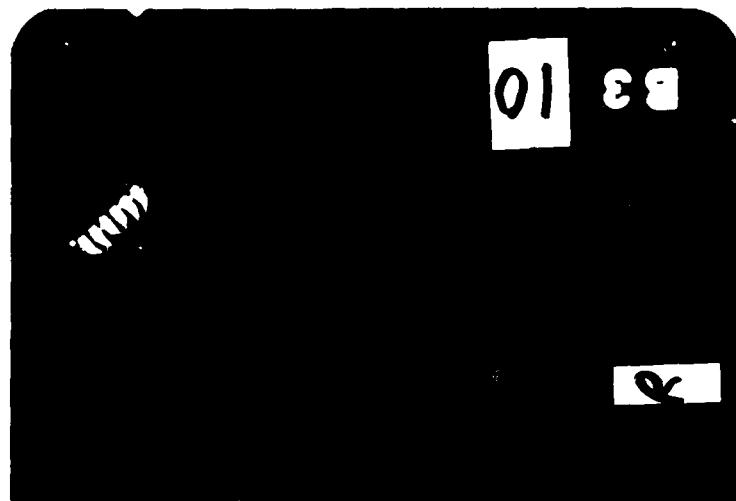
Figure 66.    Stereo X-Ray of $[90_{16}]$ Specimen Stressed to 92% of Average Failure Stress.

161
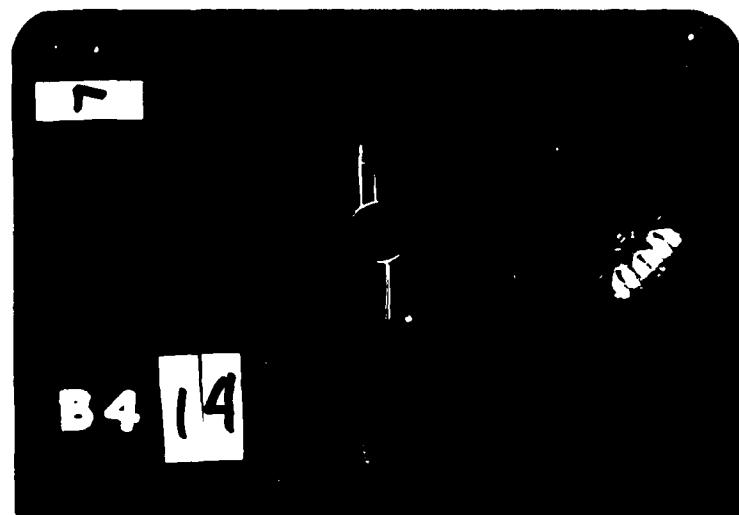
Figure 67. Stereo X-Ray of Failed $[90_{16}]$ Specimen.

Analytically, the progression of failure modeled by the computer program is shown in Figure 68. Again a region of failure developed instead of the failure of a row of elements across the specimen and parallel to the fibers. As in the 0-degree tests, the computer program used a gradual unloading scheme on this model. Thus, only the trend of failure progression is accurate.

As in the previous subsection, failure in the analytical model could be defined by failure of the first element. In this case, failure occurs in the element at the hole at 89% of the average ultimate stress. Extrapolating to the hole, the percentage is further reduced to approximately 86%. This prediction of sudden failure is lower than the actual result. However, the fibers in the 90-degree specimens may not have been exactly at 90°, thus raising the ultimate stress value. The stress concentration factor drops off significantly if the fibers are not at 90°. (See Figure 9 in Section II D.), and this may account for the difference in results.

3. Failure Progression in [±45]$_{4S}$ Angle-Ply Specimens. As mentioned in the last section, a distinct failure region grew at the hole during the loading of ±45-degree specimens. Physically, strain response was characterized by a necking of the specimen at the hole and the growth of a triangular region on either side of the hole. It seemed that when

163
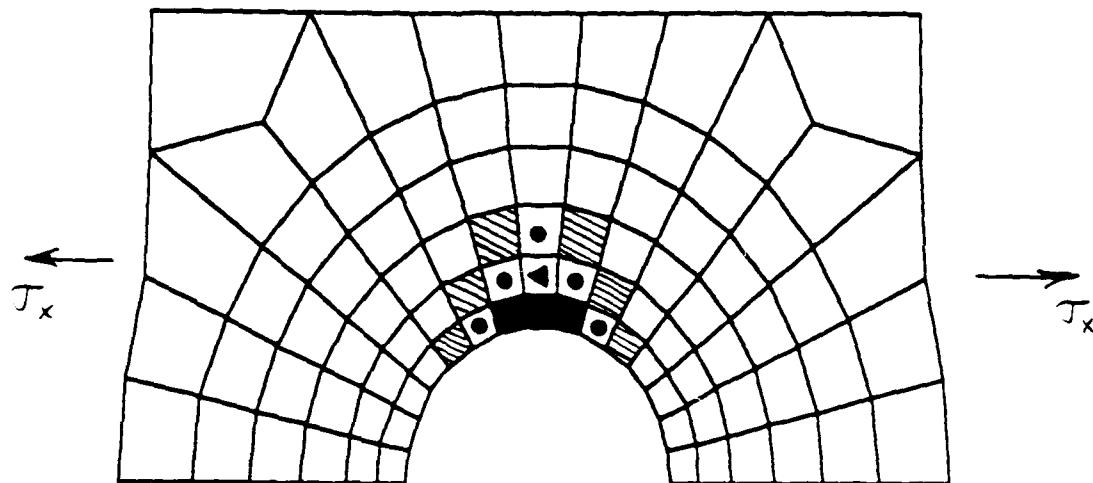
$[90_{16}]$ ANALYTICAL FAILURE RESPONSE

| KEY | % OF AVG. FAILURE STRESS |
|---|---|
| SOLID | 89 % |
| ◄ | 96 % |
| ● | 99 % |
| ⫽ | 103 % |

FIGURE 68.

these 'triangles' reached the midpoint between the hole and the edge, the specimen failed.

This progression of failure is shown in several photographs from the videotape. For a reference, Figure 69 shows the specimen at the beginning of loading. Note here that 1 volt equals 1020 pounds. Note also that the displacement of the specimen can be measured qualitatively by looking at the writing on the specimen at the left of the picture. The crosshead is moving left and pulling with it the left end of the specimen. The writing on the specimen is slowly moving out of view.

The next five photographs show a series of failure states. Figure 70 shows the initial region of failure and the initial necking of the specimen. Figure 71 shows a distinct triangle, and Figure 72 shows the development of reflective cracking toward the edge of the specimen. This seems to be a three-dimensional effect caused by the interlaminar stresses at the edges of the specimen. As will be shown, the computer program did not model this three-dimensional phenomenon. Continuing the loading, Figure 73 represents the maximum load (2,660 lbs.) on this specimen. Finally, Figure 74 shows the specimen failure after the load dropped off to 2570 lbs.

The results of the tests to percentages of average failure stress (25,680 lbs.) are listed in Table 19. The stereo x-rays from each of these tests yield results similar

Figure 69.    $[\pm 45]_{4S}$ Specimen at Beginning of Loading.



Figure 70.    $[\pm 45]_{4S}$ Specimen at 1950 lbs.
(73% of ultimate load.)

Figure 71. $[\pm 45]_{4S}$ Specimen at 2350 lbs. (88% of Ultimate).



Figure 72. $[\pm 45]_{4S}$ Specimen at 2540 lbs. (95% of Ultimate).

Figure 73. $[\pm 45]_{4S}$ Specimen at 2662 lbs. (Maximum Load).



Figure 74. Failed $[\pm 45]_{4S}$ Specimen. Load dropped to 2570 lbs.

Table 19.  Progressive Failure Tests of $[\pm45]_{4s}$ Specimens

| Sample Number | X-Sect Area | Test Number | %[*] | Load (kips) | Stress (ksi) | Actual % |
|---|---|---|---|---|---|---|
| C2-SH-H-05 | 0.09848 | 8005 | 70% | 1.773 | 18.004 | 70.1 |
| C2-SH-H-06 | 0.09873 | 8006 | 70 | 1.750 | 17.725 | 69.0 |
| C2-SH-H-07 | 0.09848 | 8007 | 70 | 1.755 | 17.821 | 69.4 |
| C2-SH-H-09 | 0.09512 | 8009 | 85% | 2.076 | 21.825 | 85.0 |
| C2-SH-H-10 | 0.096 | 8010 | 85 | 2.095 | 21.823 | 85.0 |
| C2-SH-H-11 | 0.09632 | 8011 | 85 | 2.102 | 21.823 | 85.0 |
| C3-SH-H-13 | 0.09744 | 8013 | 95% | 2.377 | 24.394 | 94.3 |
| C3-SH-H-14 | 0.09728 | 8014 | 95 | 2.373 | 24.394 | 94.3 |
| C3-SH-H-15 | 0.09712 | 8015 | 95 | 2.369 | 24.393 | 95.0 |

to those of the videotape, but with some new insights.
Figure 75 shows an x-ray of a specimen loaded to 70%
of its probable failure load.  The beginning of necking is
evident, and the hole appears slightly elliptical.  Also,
the beginning of the triangular region of failure is
slightly visible.  Figure 76 shows an x-ray of a specimen
loaded to 85% of its failure load, and the failure region is
more evident.  Figure 77 shows a specimen close to failure.

The stereo effect of viewing these pairs of x-rays
showed that the tips of the triangle exist in the middle of
the specimen lay-up.  Close to the hole, failure is
occurring through the thickness, but it tapers off to the
center of the laminas.  Also, this failure region does not
appear to be that of delamination, but instead each line
shown is series of short parallel cracks along the fibers.
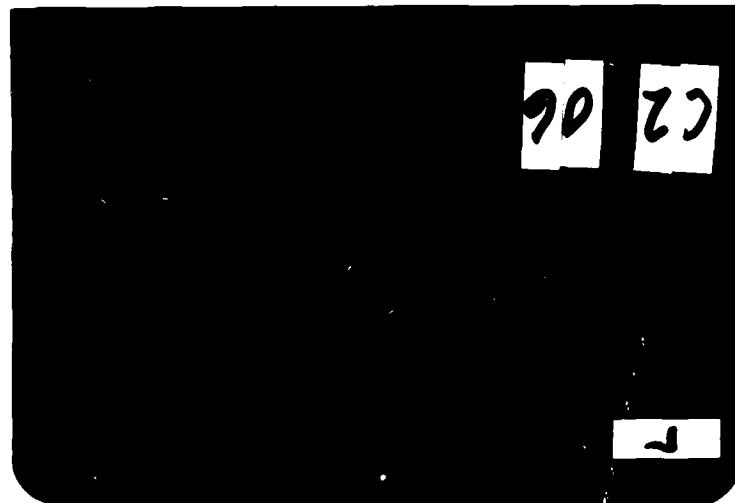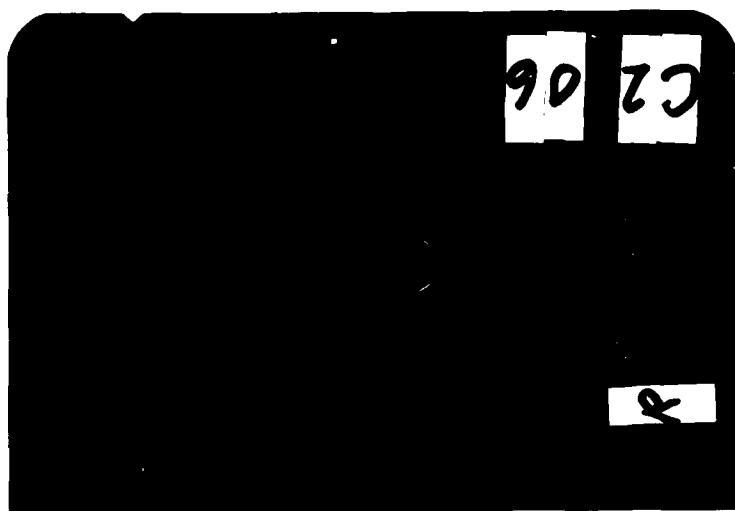
Figure 75.   Stereo X-Ray of $[\pm45]_{4S}$ Specimen Loaded to 70% of its Ultimate Load.

170
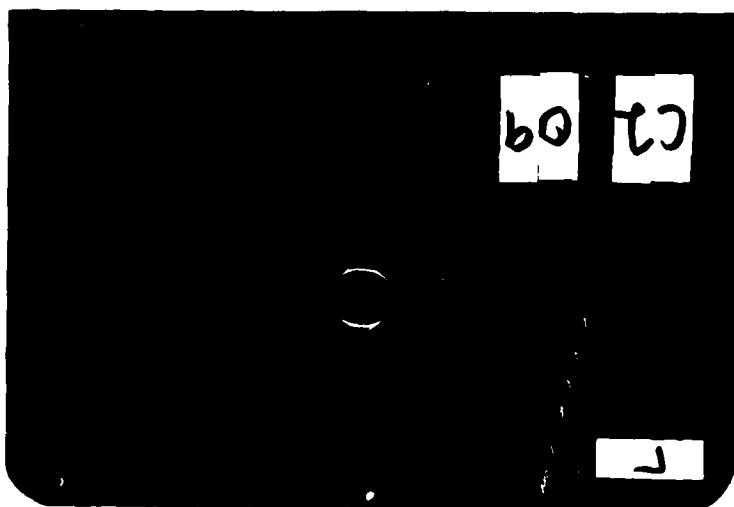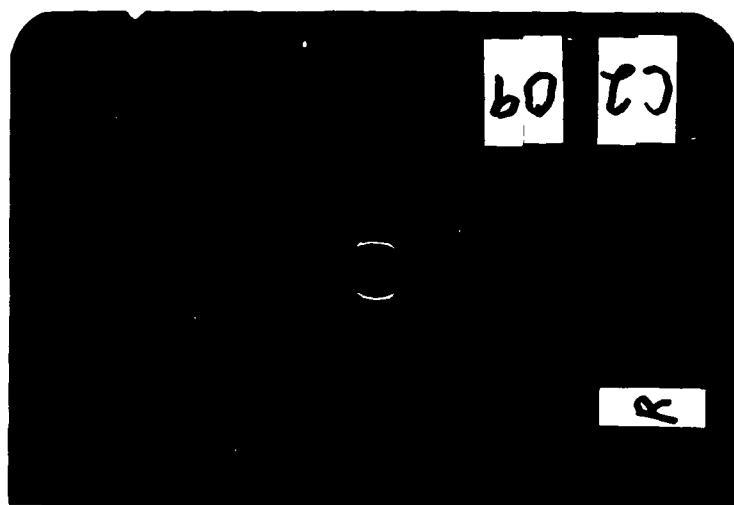
Figure 76.   Stereo X-Ray of $[\pm 45]_{4S}$ Specimen Loaded to 85% of its Ultimate Load.
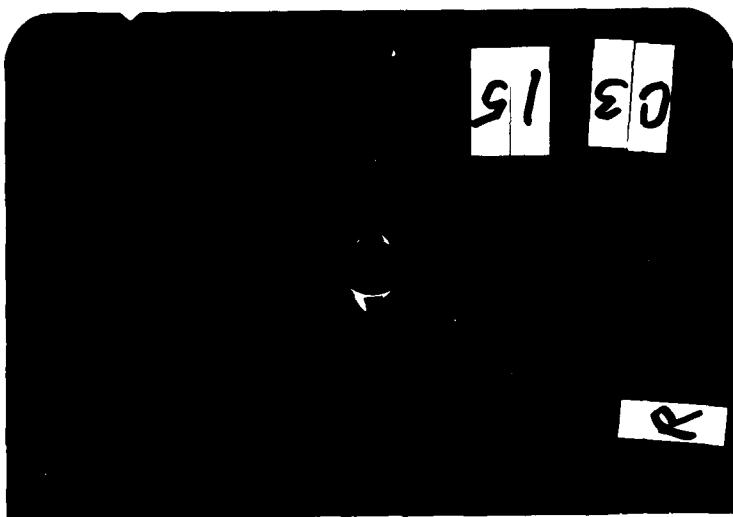
Figure 77.  Stereo X-Ray of $[\pm 45]_{4S}$ Specimen Loaded to 95% of its Ultimate Load.

Further evident in these x-rays were minute cracks extending along the fibers from the hole to the edge of the specimen. These occurred in various layers, but they apparently did not degrade the laminate. Also evident in these x-rays is that the edges appear to be failing where the necking is occurring.

For the computer model of the failure process, a similar region of failure was shown. This analytical progression of failure is shown in Figure 78. Note that the triangular regions shown in the video stills and in the stereo x-rays are not reflected in the analytical failure progression. A possible explanation for the V-shape of the analysis is that in the experimental specimen, the three-dimensional edge effects, caused by interlaminar stresses, restrict the V-shape from occurring; and a triangular region is formed. Thus, the computer model provides an accurate account of the failure process in a two-dimensional format, but it cannot measure three-dimensional effects.

D. Results of the Quasi-isotropic Study

As described in Chapter IV, the two types of quasi-isotropic laminates, $[0/+45/90/-45]_{2s}$ and $[0/\pm45/90]_{2s}$, were tested for experimental comparison of stress-strain responses. Also, an experimental investigation of the initiation and progression of ply failure was conducted.

173
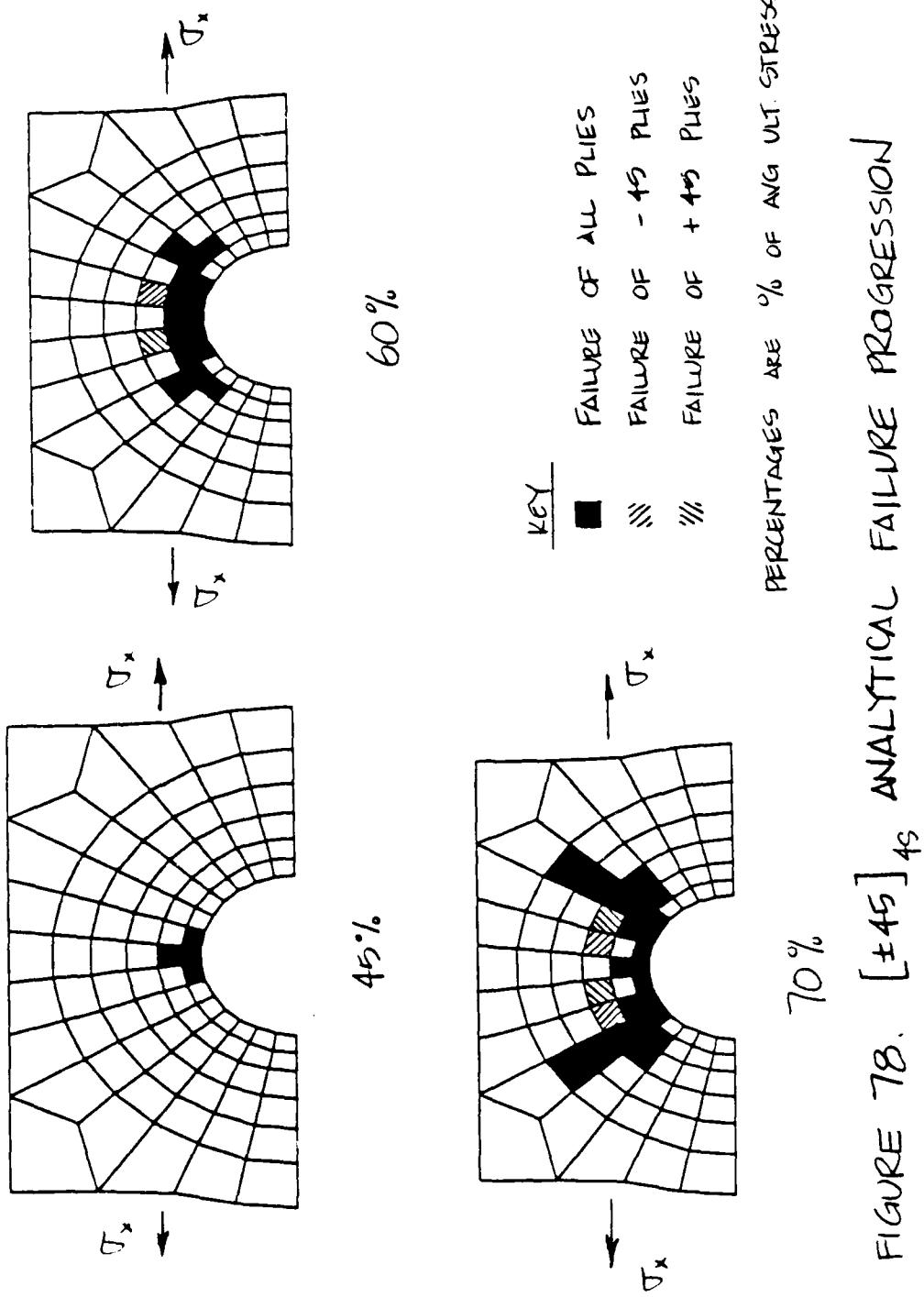
FIGURE 78. $[\pm 45]_{4S}$ ANALYTICAL FAILURE PROGRESSION

KEY

■ FAILURE OF ALL PLIES

▨ FAILURE OF -45 PLIES

▨ FAILURE OF +45 PLIES

PERCENTAGES ARE % OF AVG ULT STRESS

45%

60%

70%

1.0

4.5  2.8  2.5
3.2  2.2
3.6
4.0  2.0

1.1

1.8

1.25  1.4  1.6
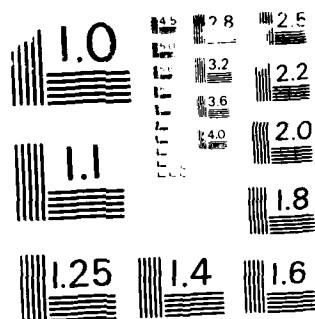
MICROCOPY RESOLUTION TEST CHART
NATIONAL BUREAU OF STANDARDS-1963

Again, the purpose of this test was to compare experimental behavior of the laminate and to draw conclusions about their potential for delamination based on comparisons to similar Gr/Ep specimens in Reference [23].

1.    Results of Tests to Ultimate Strength.  The results of all tests to failure of the [0/+45/90/-45] (Q1) and [0/±45/90] (Q2) tensile coupons are listed respectively in Tables 20 and 21.  Note that the average failure stresses are identical, considering the range of all failure stresses.  A failed specimen of each laminate is shown in Figures 79 and 80.  Note here that the failure surfaces are also very similar.  The only difference seems to be that the Q1 specimens (designated D1) show a more ±45-degree dominated failure; and alternatively the Q2 (E1) specimens show a more 90-degree dominated failure.

This difference in failure surfaces proved to be negligible when the stress-strain curves of the two quasi-isotropic specimens were compared.  Figures 81 and 82 show the far field response to tensile loads for the Q1 and Q2 specimens, respectively.  Note that if these curves were mapped together there would be no discernable difference in the responses.

Figures 83 and 84 show the experimental stress-strain response at the holes of the Q1 and Q2 specimens.  Note

Table 20.   Failure Tests of $[0/+45/90/-45]_{2S}$   Specimens

| Sample Number | X-Sect Area | Test Number | Failure Load (lbs.) | Failure Stress (psi) |
|---|---|---|---|---|
| D1-Q-H-01 | 0.09383 | 9001 | 3,986. | 42,480. |
| D1-Q-H-02 | 0.09255 | 9002 | 4,000. | 43,220. |
| D1-Q-H-03 | 0.09472 | 9003 | 4,240. | 44,760. |
| D1-Q-H-04 | 0.09504 | 9004 | 4,160 | 43,770. |
| D1-Q-H-08 | 0.09352 | 9008 | 3,964. | 42,390. |
| D1-Q-H-12 | 0.09376 | 9012 | 4,084. | 43,560. |
| D2-Q-H-16 | 0.09391 | 9016 | 4,292. | 45,700. |

Average Failure Stress = 43,700.

Table 21.   Failure Tests of $[0/\pm45/90]_{2S}$   Specimens

| Sample Number | X-Sect Area | Test Number | Failure Load (lbs.) | Failure Stress (psi) |
|---|---|---|---|---|
| E1-Q-H-01 | 0.09383 | 1201 | 3,714. | 39,580. |
| E1-Q-H-02 | 0.09496 | 1202 | 4,265. | 44,910. |
| E1-Q-H-03 | 0.09584 | 1203 | 4,391. | 45,820. |
| E1-Q-H-04 | 0.09632 | 1204 | 4,330. | 44,950. |
| E1-Q-H-08 | 0.09352 | 1208 | 3,936. | 42,090. |
| E1-Q-H-12 | 0.09496 | 1212 | 4,020. | 42,330. |
| E2-Q-H-16 | 0.09391 | 1216 | 4,154. | 44,230. |

Average Failure Stress = 43,420.

(By assuming that test #1201 is a bad test, the average failure stress would be 44,050 psi.)

Figure 79.   Failed [0/45/90/-45]$_{2S}$ Specimen



Figure 80.   Failed [0/±45/90]$_{2S}$ Specimen

177
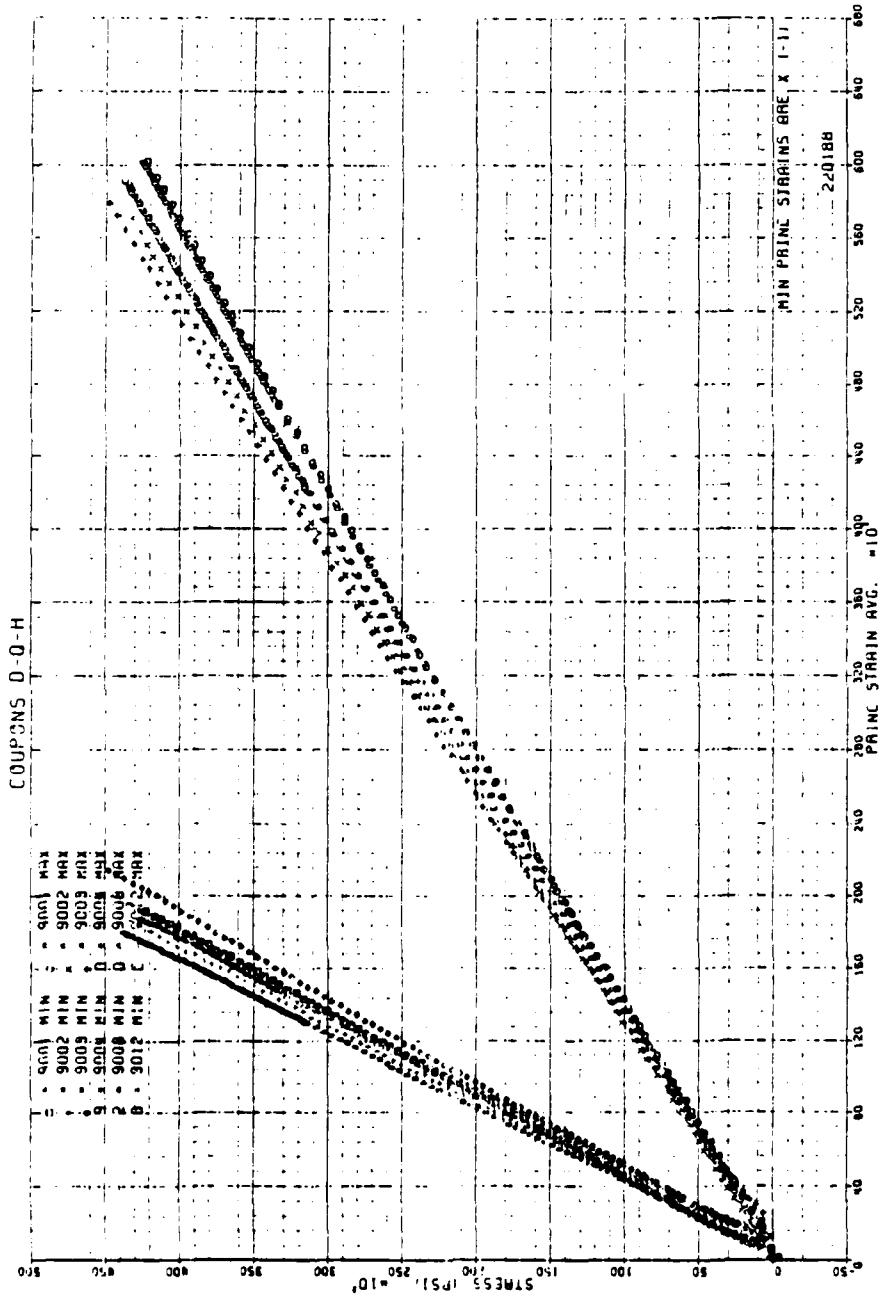
FIGURE 81. STRESS-STRAIN RESPONSE AT FAR FIELD FOR $[0/45/90/-45]_{2s}$ SPECIMENS.

178
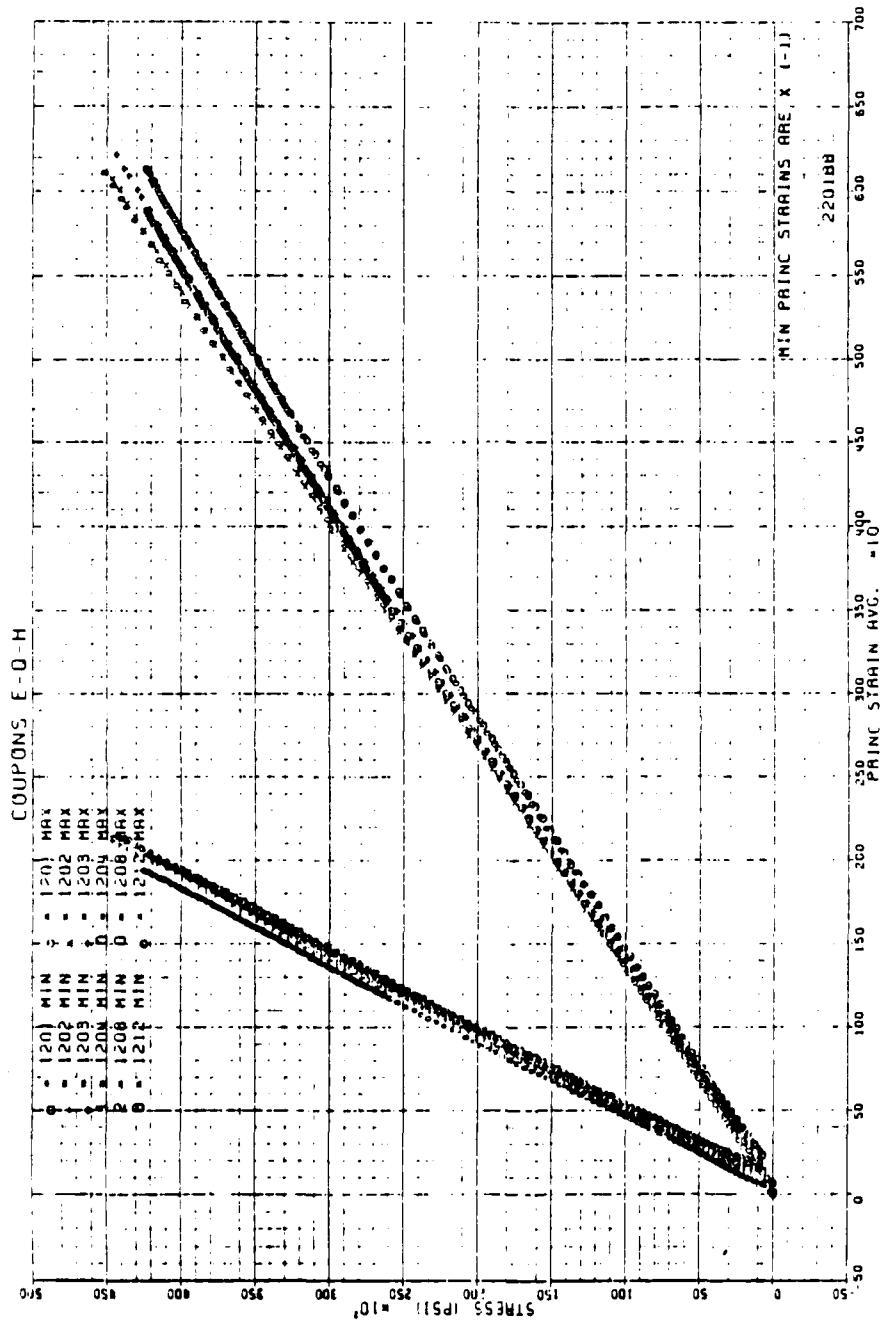
FIGURE 82. STRESS-STRAIN RESPONSE AT FAR FIELD FOR $[0/\pm45/90]_{2S}$ SPECIMENS.

179
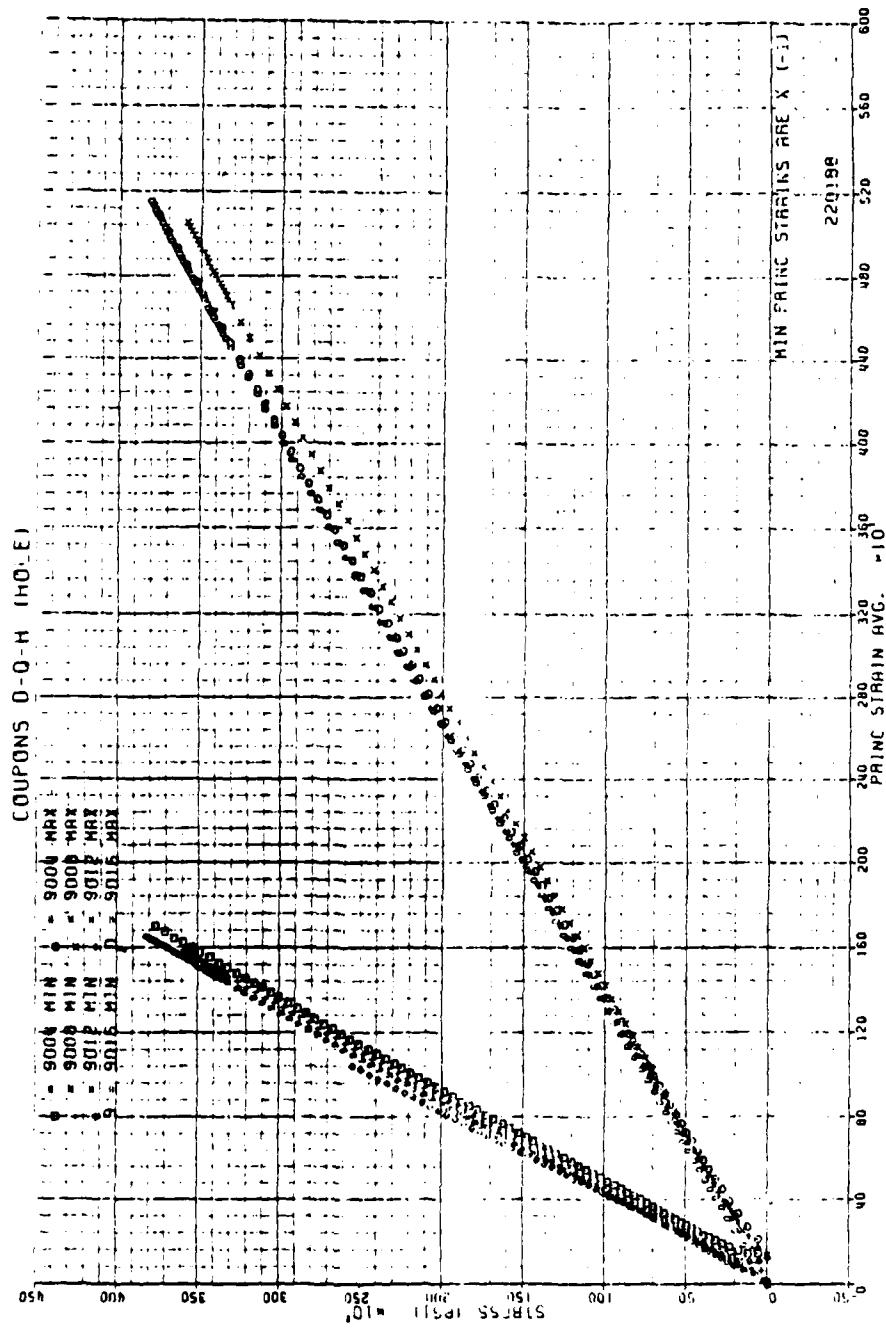
FIGURE 83. STRESS-STRAIN RESPONSE AT HOLE FOR $[0/45/90/-45]_{2S}$ SPECIMENS.
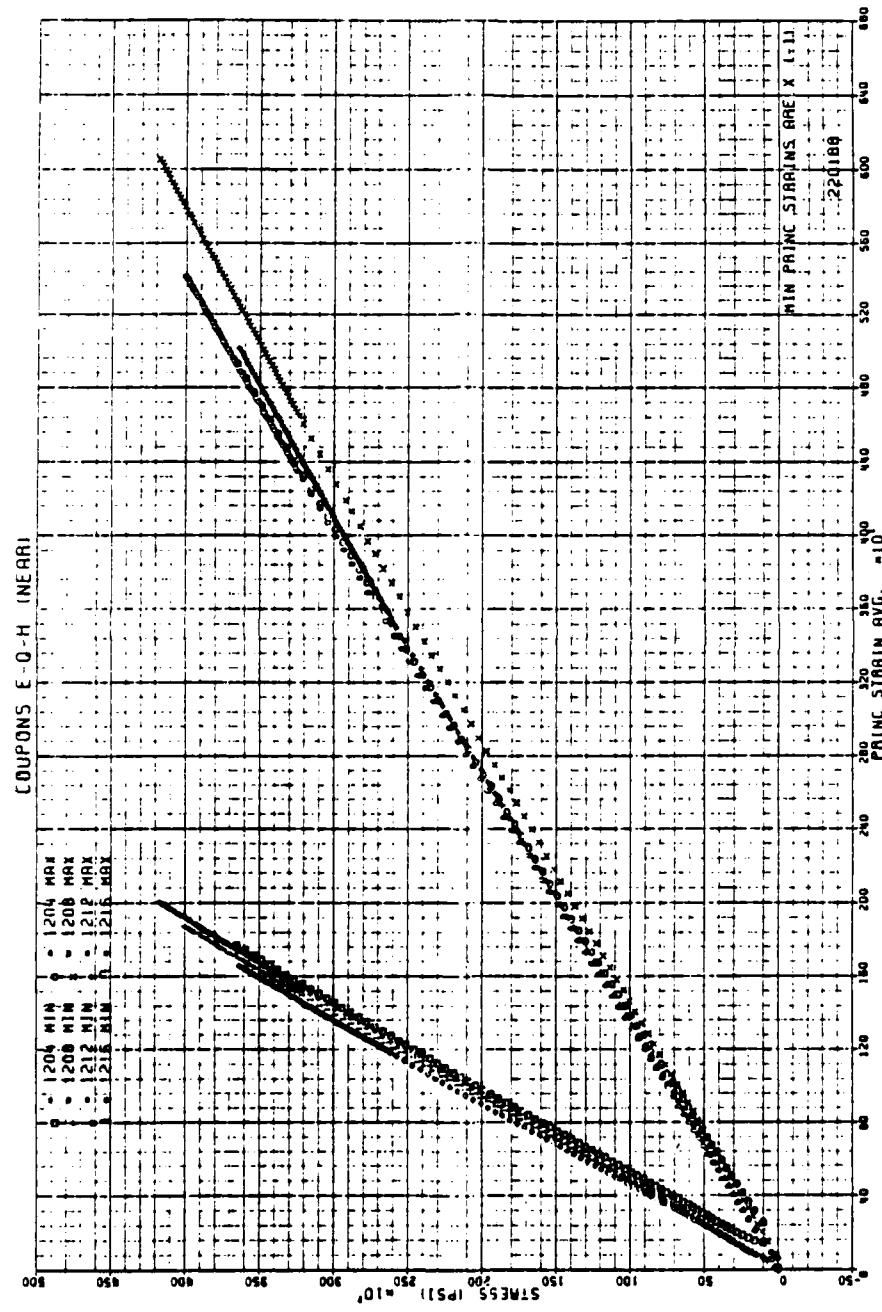
FIGURE 84. STRESS-STRAIN RESPONSE AT HOLE FOR [0/±45/90] SPECIMENS.

again that the responses of each laminate are nearly identical.

2. _Results of Failure Progression Study_. For the quasi-isotropic laminates tested to ultimate strength, the videotape post-failure analysis was conducted. Also, a stereo x-ray post-failure analysis was conducted on specimens subjected to percentages of their average failure stresses.

Typical photographs were taken off the videotape. For the Q1 specimen, a series of failure states is shown in Figures 85 through 88. Likewise, a group of photographs is shown in Figures 89 through 92 that represents progressive failure of the Q2 specimen. For both tests, the voltmeter read 1 volt for every 2,041 pounds. Notice that failure for both specimens does not begin to show through the specimen until late in the loading.

Q1 and Q2 laminates were tested to percentages of their ultimate loads, according to Chapter IV, and the results of these tests are listed in Tables 22 and 23.

Each specimen tested was subjected to stereo x-ray and typical results are shown in Figures 93 through 95 for the Q1 specimen and in Figures 96 through 98 for the Q2 specimen. For the Q1 specimen, at 80% of the average failure load, only a few 45-degree cracks were evident, and these were mostly in the middle plane. See Figure 93.

Figure 85.   [0/45/90/-45]$_{2S}$ Specimen at Beginning of Loading.
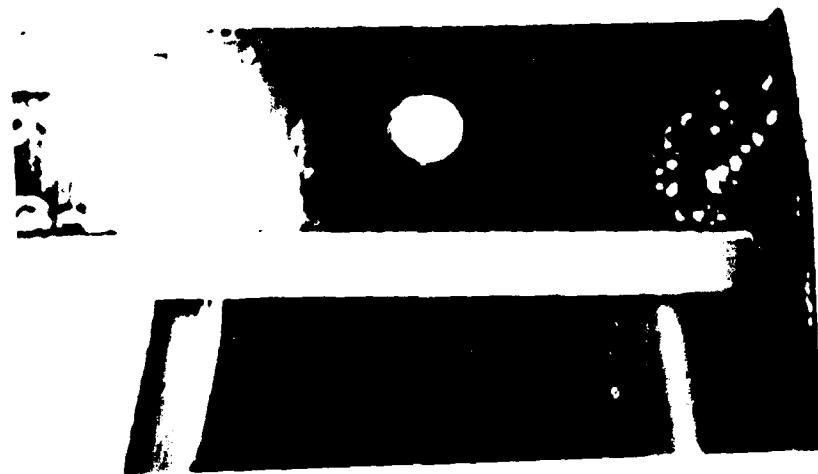


Figure 86.   [0/45/90/-45]$_{2S}$ Specimen at 4020 lbs. (95% of Ultimate Load).

183
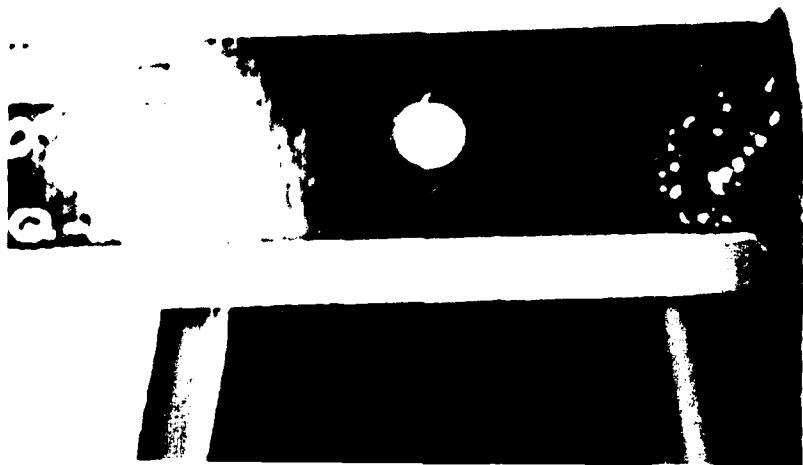
Figure 87.  $[0/45/90/-45]_{2S}$ Specimen at 4200 lbs.  (99% of Ultimate Load).



Figure 88.  Failed $[0/45/90/-45]_{2S}$ Specimen.
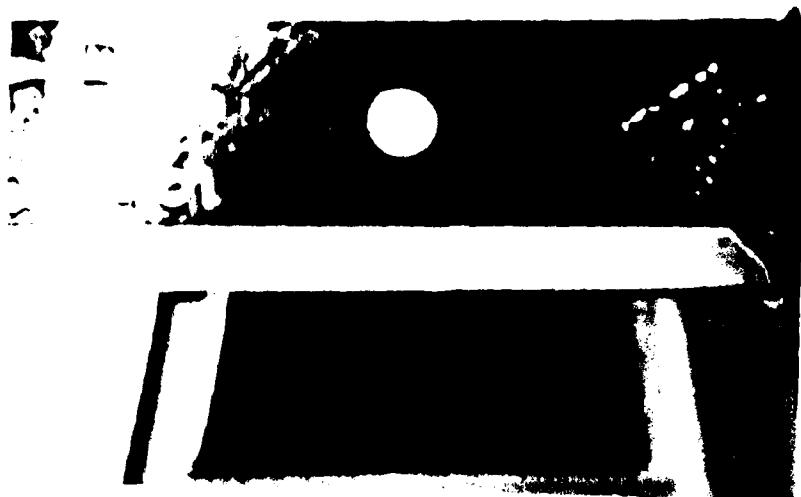
Figure 89. $[0/\pm45/90]_{2S}$ Specimen at Beginning of Loading.
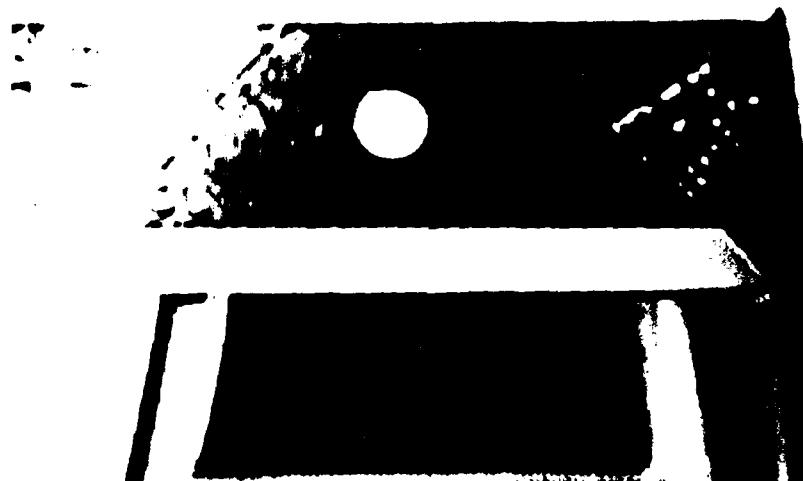


Figure 90. $[0/\pm45/90]_{2S}$ Specimen at 3670 lbs. (99% of Ultimate Load).
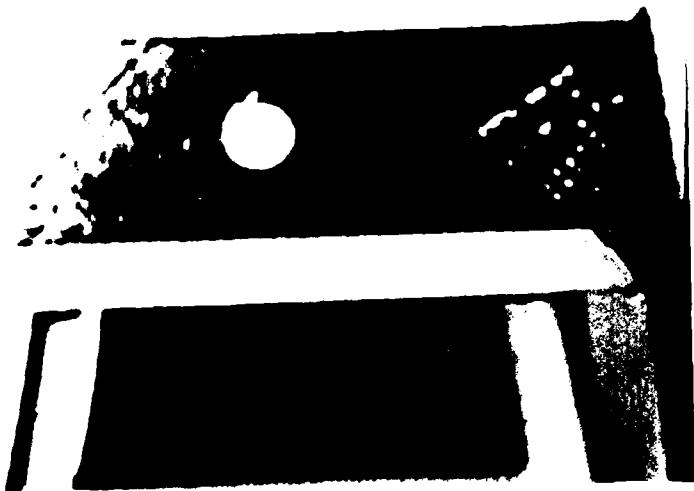
Figure 91. $[0/\pm45/90]_{2S}$ Specimen at Max. Load of 3715 lbs.



Figure 92. Failed $[0/\pm45/90]_{2S}$ Specimen.

Table 22.  Progressive Failure Tests of Q1 Specimens

| Sample Number | X-Sect Area | Test Number | %* | Load (kips) | Stress (ksi) | Actual % |
|---|---|---|---|---|---|---|
| D1-Q-H-05 | 0.09368 | 9005 | 80% | 3.317 | 35.408 | 81.0 |
| D1-Q-H-06 | 0.09512 | 9006 | 80 | 3.368 | 35.408 | 81.0 |
| D1-Q-H-07 | 0.09616 | 9007 | 80 | 3.374 | 35.087 | 80.3 |
| D1-Q-H-09 | 0.09263 | 9009 | 90% | 3.651 | 39.415 | 90.2 |
| D1-Q-H-10 | 0.0936 | 9010 | 90 | 3.702 | 39.551 | 90.5 |
| D1-Q-H-11 | 0.09383 | 9011 | 90 | 3.697 | 39.401 | 90.2 |
| D2-Q-H-13 | 0.09015 | 9013 | 95% | 3.729 | 41.364 | 94.7 |
| D2-Q-H-14 | 0.09143 | 9014 | 95 | 3.809 | 41.660 | 95.3 |
| D2-Q-H-15 | 0.09232 | 9015 | 95 | 3.838 | 41.573 | 95.1 |

Table 23.  Progressive Failure Tests of Q2 Specimens

| Sample Number | X-Sect Area | Test Number | %* | Load (kips) | Stress (ksi) | Actual % |
|---|---|---|---|---|---|---|
| E1-Q-H-05 | 0.096 | 1205 | 80% | 3.317 | 34.552 | 79.6 |
| E1-Q-H-06 | 0.09624 | 1206 | 80 | 3.368 | 34.996 | 80.6 |
| E1-Q-H-07 | 0.09616 | 1207 | 80 | 3.374 | 35.087 | 80.8 |
| E1-Q-H-09 | 0.09383 | 1209 | 90% | 3.651 | 38.911 | 89.6 |
| E1-Q-H-10 | 0.09368 | 1210 | 90 | 3.702 | 39.518 | 91.0 |
| E1-Q-H-11 | 0.09616 | 1211 | 90 | 3.697 | 38.447 | 88.5 |
| E2-Q-H-13 | 0.09143 | 1213 | 95% | 3.729 | 40.785 | 93.9 |
| E2-Q-H-14 | 0.09135 | 1214 | 95 | 3.809 | 41.697 | 96.0 |
| E2-Q-H-15 | 0.09232 | 1215 | 95 | 3.838 | 41.573 | 95.7 |
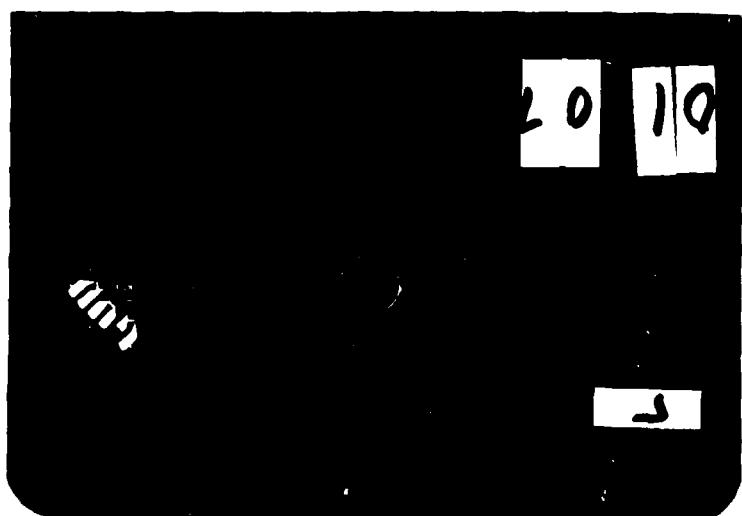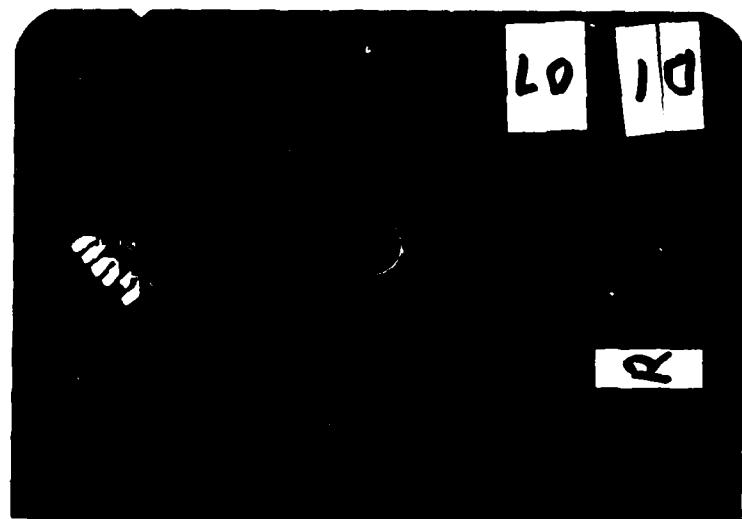
Figure 93. Stereo X-Ray of $[0/45/90/-45]_{2S}$ Specimen at 80% of Ultimate Failure Load.
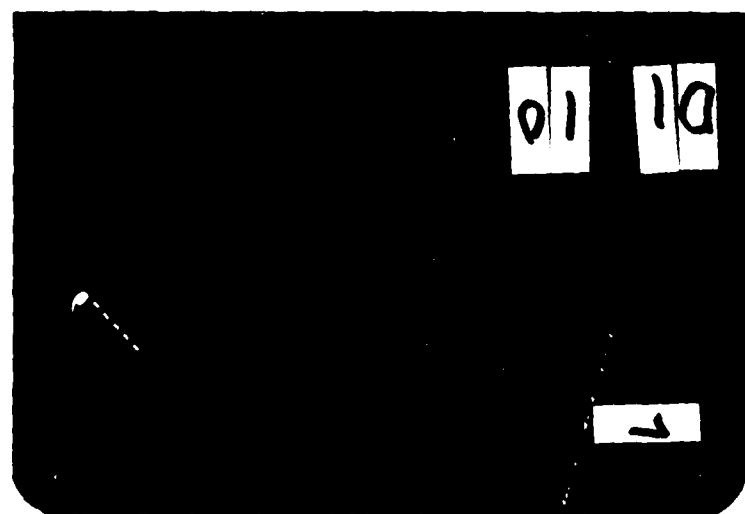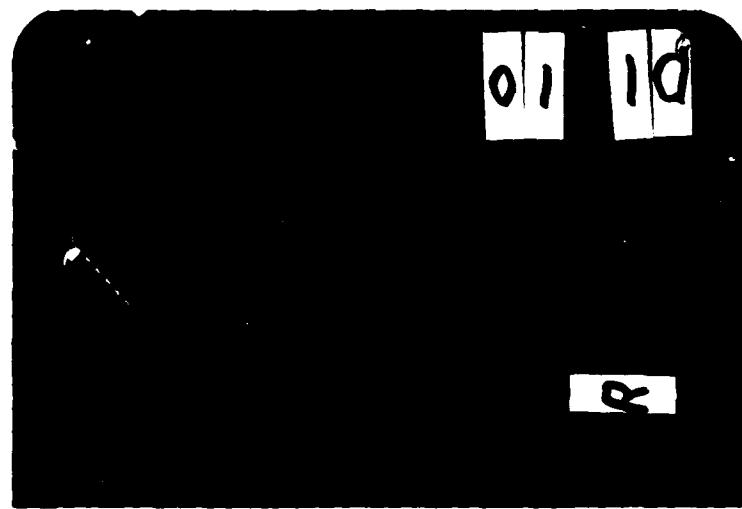
Figure 94.    Stereo X-Ray of $[0/45/90/-45]_{2S}$ Specimen at 90% of Ultimate Failure Load.
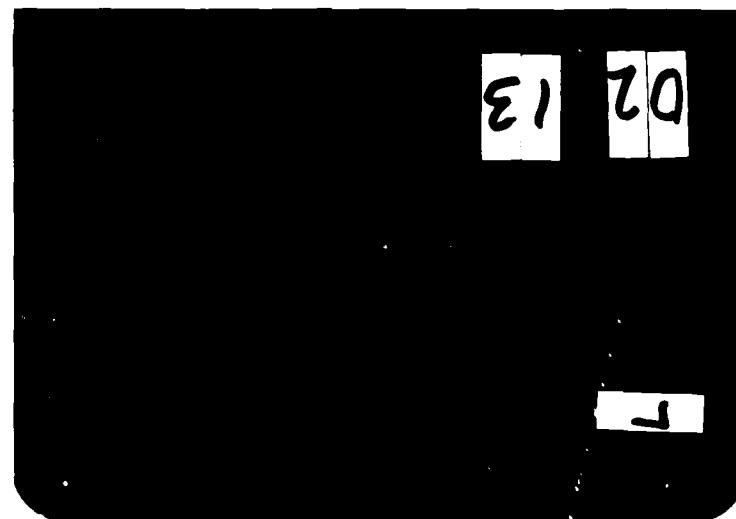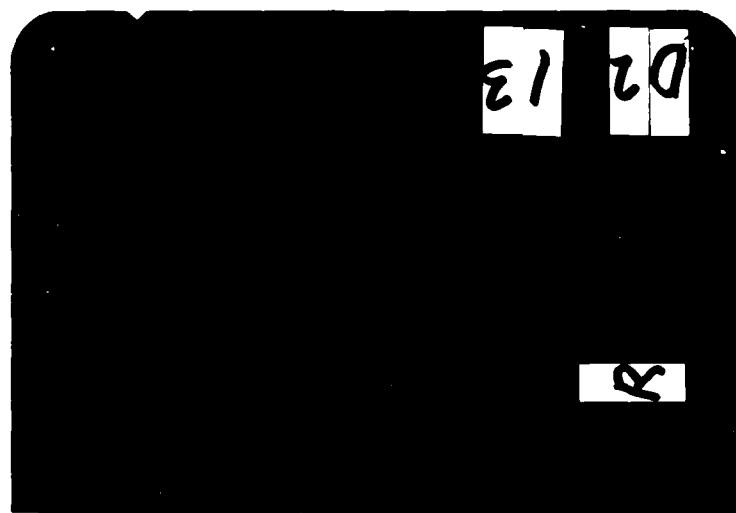
Figure 95.   Stereo X-Ray of $[0/45/90/-45]_{2S}$ Specimen at 95% of Ultimate Failure Load.
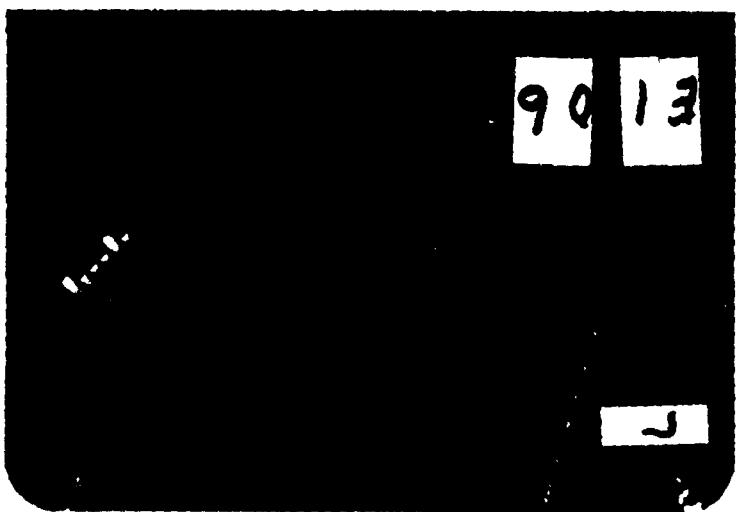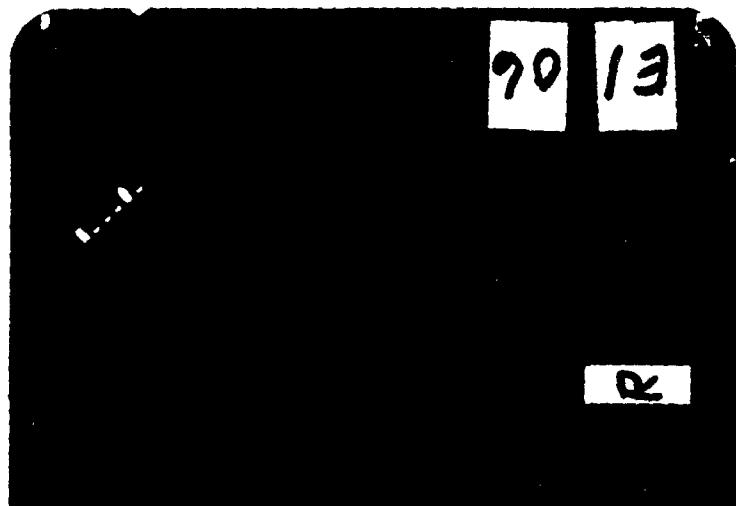
Figure 96. Stereo X-Ray of $[0/\pm45/90]_{2S}$ Specimen at 80% of Ultimate Failure Load.

Figure 97.　Stereo X-Ray of $[0/\pm45/90]_{2S}$ Specimen at 90% of Ultimate Failure Load.
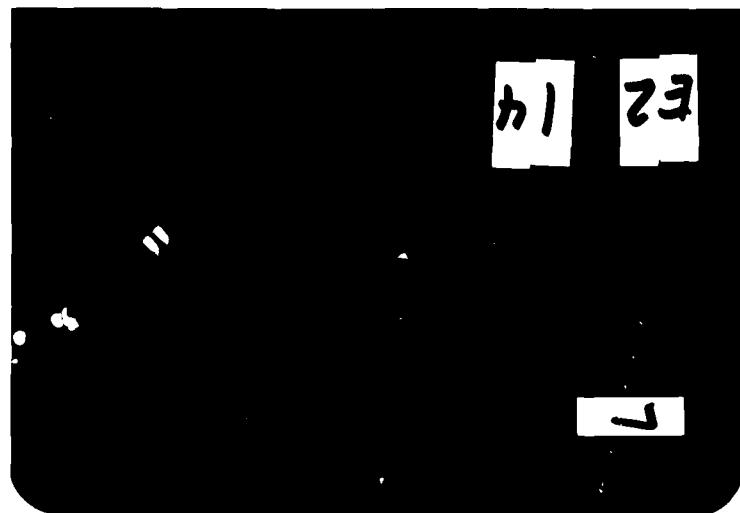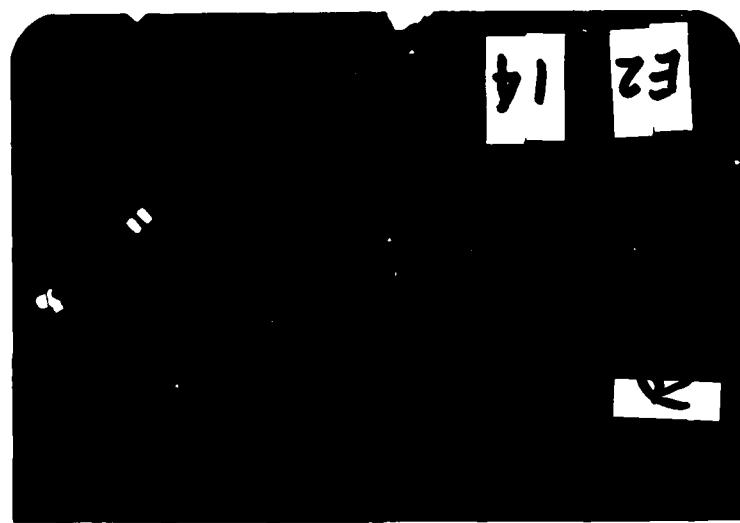
Figure 98. Stereo X-Ray of $[0/\pm45/90]_{2S}$ Specimen at 95% of Ultimate Failure Load.

Further loading to 90% produced a slight failure region as shown in Figure 94. Upon magnification, the entire hole showed cracks all the around which resembled the rays of the sun in 90 and 45 degree directions (with some 0-degree cracking as well). Still further loading to 95% produced the result shown in Figure 95. This region appeared to be dominated by short cracks in the matrix in the ±45-degree and 90-degree directions through the thickness. Another interesting note is that whenever a crack extended out from the hole, it was criss-crossed by short cracks of other laminas.

For the Q2 specimen loaded to 80% of its failure load, only slight cracks were evident all the way around the hole, along with a few single long cracks in the 90-degree and ±45-degree directions. A specimen loaded to 90% of the average failure load began to show significant cracking in the 90-degree direction on one side only, and it appeared in the back of the specimen. A specimen further loaded to 95% shows developed failure regions on both sides of the hole and through the thickness for all laminas.

As a final note for the x-rays of the quasi-isotropic study (as well as for those of the other laminates) failure of the composite for most specimens seemed to start at the bottom of the specimen. The specimens were fabricated, drilled, and gaged consistently; therefore there must have been consistent damage to the hole to produce consistent

failure initiation at the bottom of the hole. More on this
and other points of the failure progression studies will be
discussed next in Chapter VI.

## VI.  Conclusions

Based on the results of this thesis and on comparisons to past studies, many conclusions can be drawn.  Much was learned during the course of this thesis, and not all of it was directly related to the objectives first listed in Chapter I.  However, only conclusions relating to those objectives will be discussed in this chapter, and the appendices that follow will present other information gained in this study.

### A.  Conclusions on the Derivation of Basic Properties

The following conclusions were noteworthy for this phase of experimentation:

1.  The material response of Gr/PEEK is highly nonlinear, especially in shear.

2.  The strains measured in the shear specimen far exceeded the limits of linear strain theory.  Large displacements took place.  But these displacements were a combination of the ductility of the matrix and the scissoring of the fibers.  As the fibers turned from 45° toward 0° the specimen gained strength.  Therefore, a point on the original experimental shear stress-strain curve between the small strains and the scissoring was assumed to equal failure of the laminate.  The point that was chosen yielded very good results.

3. Ideally, a convergence study should be done to correlate the cut-off point of shear stress-strain basic property values to the ultimate strength of the ±45-degree tension specimen with the hole. This procedure would use the experimental results of the ±45-degree test specimen with the hole and relate the analysis with a given range of cut-off points in the data.

4. Standard strain gages, which were accurate up to approximately 4%, were used for this thesis. For Gr/PEEK basic property specimens, 'high elongation' gages should be used to measure strain on test specimens. For the shear specimens, the gages failed before the specimen. And for a high temperature study, given the nature of thermoplastics, much more strain will develop in all basic property specimens during testing.

5. Comparisons to Gr/Ep [19] were made and the basic properties of Gr/PEEK were found to be similar in the 0-degree direction, about 2 times more ductile in 90-degree tension, similar in 90-degree compression, and more than 2 times more ductile in shear.

6. The basic properties of 0-degree tension were dominated by the fibers, as expected. The basic property curve was concave up. This 'wool thread' effect is a property of graphite fibers, and it was shown in previous

studies as well. (The wool thread analogy is referenced to a remark by Sandhu, in a conversation with him.)

7. As a final conclusion on the properties of Gr/PEEK, to accurately predict an elastic response of Gr/PEEK, a nonlinear form of the stress-strain constitutive relations must be used.

B. Conclusions on the Behavior of Gr/PEEK Unidirectional and Angle-Ply Laminates.

For the $[0_{16}]$, $[90_{16}]$, and $[\pm45]_{4S}$ specimens, several conclusions can be drawn:

1. Experimentally, the stress-strain responses of the $[0_{16}]$ test specimens were dominated by the discontinuity of splitting along the fibers. These specimens failed in two distinct parts: (a) sudden splitting longitudinally from the hole to the ends of the specimen and (b) sudden failure apparently involving tab failure of the two outside segments of the specimen.

2. Computer analysis of $[0_{16}]$ specimens matched the experimental stress-strain response up to the splitting of the specimen. The initiation of failure was accurately predicted. The progression of failure, however, was overestimated due to the use of a gradual unloading scheme which attempts to model interlaminar stresses. Since no interlaminar stresses exist in a unidirectional laminate. Therefore, to model reality, the failing elements should

have been given zero stiffness instantly. The trend of
failure was demonstrated, but the ultimate failure of the
model would have occurred quickly with an instantaneous
unloading scheme. (This program is still developmental;
the instantaneous unloading option will be available soon for
future work.)

3. Experimentally, the stress-strain response of the
$[90_{16}]$ specimens was almost linear, and it culminated with
catastrophic failure in the transverse direction.

4. Computer analysis of the $[90_{16}]$ specimens
accurately modeled the stress-strain response. Initiation
of failure was slightly underestimated, but small deviations
in the 90-degree orientation may have affected the
correlation. Progression of failure was overestimated as in
the 0-degree specimens due to the gradual unloading scheme.
However, the trend of failure was demonstrated.

5. Experimentally, the failure of $[\pm45]_{4S}$ is gradual,
and it is one that can be observed as failure progresses.
It is characterized by high strains to stress. Shear
stresses contribute to almost all of the failure in the
specimen.

6. The stress-strain response of the $[\pm45]_{4S}$
specimens was modeled accurately. Both initiation and
progression of failure in the specimen was predicted very
well. The point of cut-off for the basic properties proved

to be accurate. However, three-dimensional effects that were present in the experiment were not modeled by the analysis. The use of the gradual unloading scheme works well with this angle-ply laminate.

## C. Conclusions on the Quasi-isotropic Study

Based on the results presented in Chapter V, the tendency of the $[0/\pm45/90]_{2S}$ Gr/PEEK specimens to delaminate is not as great as that of Gr/Ep. In Reference [23], the delamination moment coefficient (DMC) for this lay-up was critical for Gr/Ep, due to the existance of two 90-degree plies in the middle of the lay-up. The DMC for the $[0/45/90/-45]_{2S}$ for Gr/Ep was far from critical due to the 45-degree plies in the center. But considering that both lay-ups of Gr/PEEK produced the same stress-strain behavior, the tougher PEEK material is more resistant to delamination.

## D. General Conclusions

1. A good method for the prediction of the onset of failure in composite laminates is Sandhu's fully nonlinear-elastic finite element program with its Strain Energy Failure Criterion. The prediction of the onset of failure proved to be accurate in this study.

2. For prediction of growth of failure this program yields an accurate trend.

3. An instantaneous unloading scheme should be considered for unidirectional specimens.

4. A gradual unloading scheme works well for multi-directional laminates, but the program does not measure three-dimensional effects.

5. In general, the use of progressive-ply-failure finite element analysis is a viable procedure for predicting the failure characteristics of composite laminates with stress concentrations. It has been shown that the incremental constitutive relations, in conjunction with the failure criterion proposed by Reference [5], provide suitable analytic means for predicting the behavior of unidirectional and angle-ply laminates under general stress states using only the lamina property data obtained under simple load conditions. This technique has the potential for improved accuracy, and could be extended to the study of multidirectional laminates with some additional work.

6. Experimentally, the failure progression due to tensile loading for all laminates was often aided by extra stress concentrators from the drilling of the hole. Fabrication damage should have first been checked by subjecting unstressed specimens to stereo x-ray for comparison to the failure progression results. Future projects should consider this procedure.

7.  In studying the failure behavior of composites,
visual post-failure techniques are important.  With the
videotape, photographs from the videotape, and with the
stereo x-rays, failure phenomena were more closely
correlated than could have been obtained with only the
results from strain gages.

E.  Closing

This thesis has accomplished the objectives that were
listed in Chapter I.  It has completed a comprehensive
experimentation program that may help guide future
experimentation in related areas such as high temperature
applications.  Also, this study has shown that the computer
program provides good results but requires optimization to
include various unloading schemes.

The author hopes that the information presented in this
thesis may contribute a small increment to the advancement
of materials technology and the development of future
composite material applications.

## Appendix A

## Progression of Study

This appendix describes the logistics effort involved
in accomplishing an AFIT thesis sponsored by the Flight
Dynamics Laboratory. Much prior planning was required for
this thesis to be accomplished. Work began with the
ordering of materials from manufacturers. In addition to
the composite panels used to fabricate the specimens, the
supply of strain gages and tab material also required
advanced planning. For this study, the time between placing
the order and having specimens ready to instrument was about
six months. For a typical AFIT student whose thesis program
only lasts nine months, this lead time can severely affect
the amount of work that can be reasonably accomplished in an
experimental thesis. Thus, the following sequence of events
is chronicled for the future AFIT student who wishes to do a
study using experimental facilities at Wright-Patterson AFB.

Once the prospectus was accepted, the material that was
chosen (Gr/PEEK) had to be manufactured in the desired
lay-ups. In April 1987, there were two potential choices.
The Gr/PEEK material could have been ordered from a reputable
manufacturer, or it could have been manufactured at the
Structures Test Facility (Bldg. 65) of the Flight Dynamics
Laboratory. The press with which Gr/PEEK is manufacutered

was not due to arrive to Bldg. 65 until June 1987, and the
personnel who would make the material had yet to be trained.
Therefore, the choice to order from the manufacturer was
made, and an order was placed in May with a promised due
date of late August. The company which supplied the
material was Imperial Chemical Industries (ICI),
headquartered in England. The material was ordered from the
Fiberite Corporation in Orange, California, which is a
subsidiary of ICI. The order form was obtained from Mr.
Nick Yardich of the Aero/Astro Department of AFIT; and it
included the sizes, quantities, and lay-ups of the material
desired. It was submitted to AFIT/ENY, which ordered the
material through Base Supply.

To determine the quantities of panels needed, a test
plan was written in which the number of specimens to be
tested was sketched within the sizes of available panels.
This test plan became the guide to follow for all groups
involved with this experimentation.

This test plan was accomplished with the help of Dr.
Palazotto of AFIT/ENY and Dr. Sandhu of AFWAL/FIBCA.
Addressed to AFWAL/FIBC, the test plan described
experimentation which involved five different groups
within FIB, the Structures Division of the Flight Dynamics
Library. While the panels were being manufactured, the test
plan was finalized, and each group involved met to discuss

the logistics of the program. An outline of the test plan follows.

The test plan was in letter format, and the first section listed general program information about the project. The first page contained the following text:

FROM: AFIT/ENY (Lt R. John Martin, 54731)            29 SEP 87

SUBJECT: Test Plan for Master's Degree Thesis

TO: AFWAL/FIBC (Mr. G.R. Holderby)

1. Program Information

|   |   |   |
|---|---|---|
| a. | Organization | AFIT/ENY |
| b. | Project Number | 24010366 |
| c. | Project Title | 'Study of Ply Failure in Thermoplastic Composites' |
| d. | Security Classification | Unclassified |
| e. | Project Engineer | Lt Martin |
| f. | Project Advisor | Dr. Anthony Palazotto, AFIT/ENY |
| g. | Project Sponsor | Dr. R.S. Sandhu, AFWAL/FIBCA |
| h. | Instrumentation Engineer | Mr. J. Pappas |
| j. | Test Engineer | Mr. Stalnaker/ Mr. Bates |
| k. | USAF Fabrication Engineer | Lt Felker |
| l. | Test Location | AFWAL/Structures Test Facility, Bldg. 65, Area B, WPAFB |

Next came a description of the test plan, which included many diagrams and figures explaining the testing that was to take place. The general test plan began by stating objectives. The remaining portion was devoted to the technical description of the project. The following subjects were addressed by this technical description:

1. Material

2. Stacking Sequence of Specimens

3. Panels

4. Specimens

5. Testing

6. Report


With the test plan submitted, the panels arrived in October 1987, two months after they had been promised. They were taken to the Non-Destructive Evaluation Branch for inspection by C-scan. After it was determined that each panel contained no significant flaws, the panels were taken to Bldg. 65 to the Composites Group which fabricated the samples.

Panels were cut into subpanels, which were then tabbed. Once tabbing was complete, the subpanels were cut into specimens according to the test plan. Specimens were drilled as necessary to create a 0.4-inch hole at their centers. The process of fabricating the specimens from the manufacturer's panels took a total of a month and a half. As specimens were completed, they were taken from the Composites Group to the Instrumentation Group for the application of strain gages.

The Instrumentation Group accomplished the tedious task of 'gaging' each specimen. The strain gages used were three types of Micro-Measurements Precision Strain Gages:

1. CEA-03-125UR-350
2. CEA-03-062UR-350
3. WK-03-060WR-350

The CEA gages were strain gage rosettes which contained three separate grids as shown in Figure 25 of Chapter IV. The WK gages were stacked rosettes, i.e., the three grids were stacked on one another to achieve more pinpointed measurements of strain. The '03' is a measure of the coefficient of thermal expansion of the strain gage material which must be compatible with that of the material being gaged. The third set of alpha-numeric set of characters tells the size and type of gage. For example, '060' is one dimension of the grids, i.e., 0.060 inches. 'WR' indicates a stacked rosette. The '350' indicates the resistance in ohms at room temperature for which the gage is designed. Test equipment used in this thesis was set up for 350 ohms. Any other resistance in a gage would have caused a major reconfiguration of the equipment.

Applying strain gages requires a skill level attained only through training and experience. The technicians in the Instrumentation Group followed a multi-step process and demonstrated excellent workmanship. Strain gaging the specimens took about four weeks to accomplish, but this time period was partly concurrent with the testing of specimens.

From the instrumentation group, the specimens were taken downstairs in Bldg. 65 to be tested. Total testing time also took about four weeks. The technicians and

engineers accomplishing this testing were extremely helpful and provided enthusiastic support for this project.

Data from the tests were extracted by the computers in Bldg. 65. The engineers gathering this data were also very supportive of this thesis. From this data came much of the experimental results used in this thesis.

As a final note, the author feels that much was learned just by participating in all the phases of the experimentation process. Getting a hands-on education not only helped get the work done, but it allowed for better understanding of the results when it came to writing the thesis.

## Appendix 2

## Processing of Thermoplastic Prepreg

Since thermoplastic composites have a semicrystalline matrix, they require different processing procedures than the thermoset matrix composites. The manufacturing of laminates involves the stacking of layers of prepeg, placing into a press, heating to above the melting temperature of the matrix under low pressure, applying a consolidation pressure, and cooling rapidly to control the degree of crystallinity to ensure consistent properties [34].

A prepeg is a thin layer (0.00525 inches) of the composite material. A laminated panel is made up of several plies of prepeg tape. A single lamina is produced by cutting pieces of the prepeg in the desired orientation (see Figure 99 [34]), aligning and butting the pieces together and spot welding each seam (see Figure 100 [34]).

Once the desired number of laminae have been made, a 'prelam stack' of eight plies is prepared by tacking together each ply in the desired stacking sequence. A laminate panel is made up of one or more of these prelam stacks [34].

The prelaminated panel is then placed into a mold cavity. The mold cavity is a picture frame of stainless steel with thickness 0.10-0.15 inches less than the finished consolidated panel. See Figure 101. This frame is
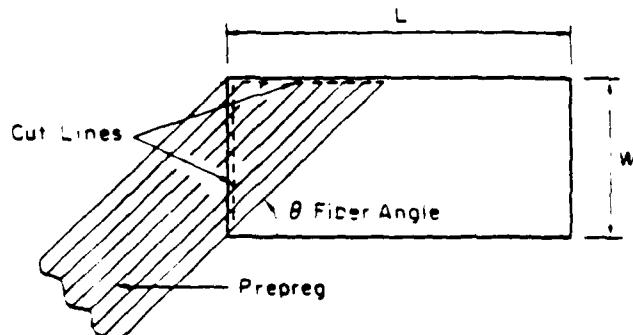
FIGURE 99. CUTTING A PREPREG LAYER TO A DESIRED FIBER ORIENTATION.
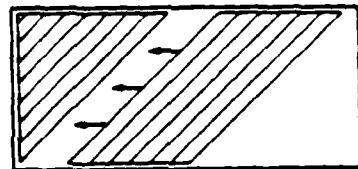


FIGURE 100. WELDING PIECES OF PREPREG TOGETHER.
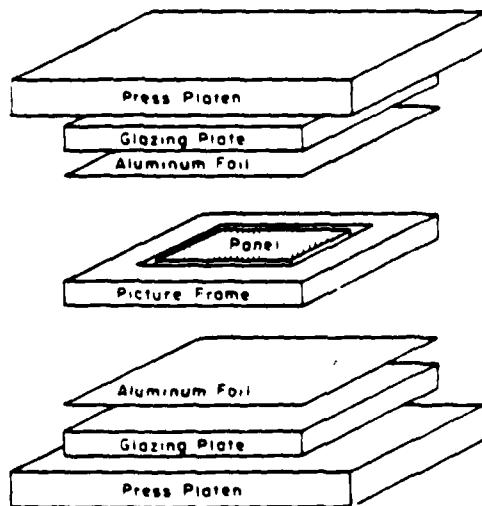


FIGURE 101. MOLD STACK USED FOR THERMOPLASTIC PROCESSING.

surrounded by layers of high temperature aluminum foil, stainless steel glazing plates, and the press platen. The glazing plate and the aluminum foil are pretreated with a mold-release agent [34].

The press platens are electrically heated and are equipped with temperature control. The pressures required for contact and consolidation are achieved by computer-controlled hydraulic pistons connected to the top press platen.

To achieve the proper cooling rate, one alternative is to use a two-stage process where the mold stack is removed from the hot press after consolidation and placed in a cold press for cooling. Another alternative is to keep the mold stack in the press and cool the press platens internally with an air-water mixture coolant system with the appropriate relation between air and water pressure to produce the cooling rate required.

The lamination/consolidated process can be summarized in the following steps:

1. Preheat the press platens to the melt temperature.

2. Place the mold stack between the platens and apply a contact pressure of 70 psi. Heat the stack for 5 minutes per each prelam stack with a maximum of 30 minutes

(3) Apply a consolidation pressure of 200 psi for 5 minutes.

(4) Cool the panel at a minimum of 50°F per minute to achieve the proper degree of crystallinity. The cooling pressure should be 300 psi.

(5) Remove the mold stack from the press after 5 minutes.

(6) Carefully remove the panel from the mold.

# Bibliography

1. Demuts, E. and P. Sharpe. "Tougher Advanced Composite Structures." Presented at AIAA/ASME/ASCE/AHS 28th Structures, Structural Dynamics and Material Conference, Monteray, CA, April 1987.

2. Fiberite Corporation, a subsidiary of Imperial Chemical Industries (ICI). APC-2 PEEK/Carbon Fibre Composite. Manufacturer's Data Sheets 1 through 8. Orange, CA, 1986.

3. Jones, R. M. Mechanics of Composite Materials. Washington, D.C.: Scripta Book Company, 1975.

4. English, L. K. "Fabricating the Future with Composite Materials." Materials Engineering, 4, No. 9 (September 1987), 15-45.

5. Sandhu, R. S. "Ultimate Strength Analysis of Symmetric Laminates." Technical Report AFFDL-TR-73-137, AD 779927, Air Force Flight Dynamics Laboratory, Wright-Patterson AFB, OH, February 1974.

6. Sandhu, R.S. "Nonlinear Behavior of Unidirectional and Angle Ply Laminates." Journal of Aircraft, 13, No.2 (February 1976), 104-111.

7. Sandhu, R.S., G.P. Sendeckyj, and R.L. Gallo. "Modeling of the Failure Process in Notched Laminates." Recent Advances in Mechanics of Composite Materials. IUTAM Symposium on Mechanics of Materials. (16-19 Aug 82) Zvi Hashin and Carl Herakovich, Eds. Virginia Polytechnical Institute: Pergamon Press, 1983, pp. 179-189.

8. Sandhu, R.S., R.L. Gallo, and G.P. Sendeckyj. "Initiation and Accumulation of Damage in Composite Laminates." Composite Materials: Testing and Design (Sixth Conference), ASTM STP 787, I.M. Daniel, Ed., American Society for Testing and Materials, 1982, pp. 163-182.

9. Whitney, J.M., I.M. Daniel, and R.B. Pipes. Experimental Mechanics of Fiber Reinforced Composite Materials. Society for Experimental Mechanics (SEM) Monograph No. 4, Revised Edition. Brookfield Center, CT: SEM, 1984.

10. Awerbuch, J. and M. S. Madhukar. "Notched Strength of Composite Laminates: Predictions and Experiments -- A Review." Journal of Reinforced Plastics and Composites. Vol.4, January 1985.

11. Witt, W.P. III, A.N. Palazotto, and H.T. Hahn. "Numerical and Experimental Comparison of the Notch Tip Stresses in a Laminated Plate." AIAA Journal, Vol.17, No. 5 (1978), pp. 500-506.

12. Tan, S.C. "Tensile and Compressive Notched Strength of PEEK Matrix Composite Laminates." Journal of Reinforced Plastics and Composites. Vol. 6 (July 1987), pp. 253-267.

13. Ramey, J. E. Coparison of Notch Strength Between Gr/PEEK (APC-1 and APC-2) and Gr/Epoxy Composite Material at Elevated Temperature. MS thesis, AFIT/GAE/ AA/85D-12. School of Engineering, Air Force Institute of Technology (AU), Wright-Patterson AFB, OH, December 1985.

14. Fan, T.C. and J.Knapp. "Properties of Composites." SAMPE (Society for the Advancement of Material and Process Engineering) Quarterly, Vol. 18, No. 4 (July 1987), pp. 16-19.

15. Hahn, H.T. and S.W. Tsai "Nonlinear Elastic Behavior of Unidirectional Composite Laminae." Journal of Composite Materials, Vol. 7, (January 1973), pp. 102-108.

16. Nahas, M.N. "Survey of Failure and Post-Failure Theories of Laminated Fiber-Rienforced Composites." Journal of Composites Technology and Research, Vol. 8, No. 4 (Winter 1986), pp. 138-153.

17. Rowlands, R.E. "Strength (Failure) Theories and Their Experimental Correlation." Handbook of Composites, G.C. Sih and A.M. Skudra, Eds. Vol. 3, Ch. 2, Elsevier Science Publishers B.V., 1985, pp. 71-125.

18. Sendecky, G.P., M.D. Richardson, and J.E. Pappas. "Fracture Behavior of Thornel 300/5208 Graphie-Epoxy Laminates -- Part 1: Unnotched Laminates." Composite Reliability, ASTM STP 580, pp. 528-546.

19. Cron, Steven M. Improvement of End Boundary conditions for Off-Axis Tension Specimen Use. MS Thesis, AFIT/ GAE/AA/85D-3. School of Engineering, Air Force Institute of Technology (AU), Wright-Patterson AFB, OH, December 1985.

20. Carpenter, J.F. "Thermal Analysis and Crystalization Kinetics of High-Temperature Thermoplastics." SAMPE Journal. Vol. 24, No. 1 (January/February 1988).

21. Palazotto, A.N. Class handouts and notes in MECH 541, Mechanics of Composite Materials. School of Engineering, Air Force Institute of Technology (AU), Wright-Patterson AFB, OH, January 1987.

22. Sandhu, R.S. and G.P. Sendeckyj. "On Delamination of $(\pm\theta_m/90_{n/2})_s$ Laminates Subjected to Tensile Loading." Technical Report AFWAL-TR-87-3058, Air Force Wright Aeronautical Laboratory, Wright-Patterson AFB, OH, July 1987

23. Sandhu, R.S. "Analytical-Experimental Correlation of the Behavior of $0°$, $\pm45°$, $90°$ Family of AS/3501-5 Graphite Epoxy Composite Laminates under Uniaxial Tensile Loading." Air Force Flight Dynamics Laboratory, AFFDL-TR-79-3064, May 1979.

24. Cook, R. D. Concepts and Applications of Finite Element Analysis. New York: John Wiley and Sons, 1981.

25. Petit, P. H. "Ultimate Strength of Laminated Composites." Air Force Materials Laboratory, FZM-4977, December 1969.

26. Sandhu, R. S. "A Survey of Failure Theories of Isotropic and Anisotropic Materials." Technical Report AFFDL-TR-72-71, AD 756889, Air Force Flight Dynamics Laboratory, Wright-Patterson AFB, OH, January 1972.

27. Peterson, R.E. Stress Concentration Factors. New York: John Wiley and Sons, 1974, p. 150.

28. Sandhu, R. S. and K. J. Singh. "Reduced Integration for Improved Accuracy of Finite Element Approximations." Computer Methods in Applied Mechanics and Engineering. Vol. 14 (1978), pp. 23-37.

29. Carnahan, B., H.A. Luter, and J.O. Wildes. Applied Numerical Methods. New York: John Wiley and Sons, Inc., 1969.

30. Rolfes, R.L. "Compressive Properties of Oriented Fiber Composites with the Prototype Compression Fixture (1983)." Technical Manual AFWAL-TM-85-222 FIBC, Air Force Wright Aeronautical Laboratories, Wright-

Patterson AFB, OH, August 1985.

31. "Standard Practice for Inplane Shear Stress-Strain
    Response of Unidirectional Reinforced Plastics (ASTM D
    3518, Reapproved 1982)." ASTM Standards and Literature
    References for Composite Materials. Philadelphia:
    ASTM, 1987.

32. Rummel, W.D., T. Tedrow, and H.D. Brinkerhoff.
    "Enhanced X-Ray Stereoscopic NDE of Composite
    Materials." Technical Report AFWAL-TR-80-3053, Air
    Force Wright Aeronautical Laboratories, Wright-Patterson
    AFB, OH, June 1980.

33. Bathe, K. Finite Element Procedures in Engineering
    Analysis. Englewood Cliffs, New Jersey: Prentice
    Hall, 1982, pp. 301-304.

34. Carlsson, L.A. and R. Byron Pipes. Experimental
    Characterization of Advanced Composite Materials.
    Englewood Cliffs, New Jersey: Prentice-Hall, 1987.

<u>VITA</u>

Born in Atlanta, Georgia on 18 January 1962, Robert
John Martin grew up in Raleigh, North Carolina.  He
graduated from Athens Drive High School in 1980 and attended
North Carolina State University on an Air Force ROTC
Scholarship.  Graduating Summa Cum Laude with a Bachelor of
Science in Civil Engineering in 1984, he was commissioned
into active duty and served as a Civil Design Engineer at
March AFB, Riverside, California until May 1986.  He then
began his studies toward a Master of Science in
Astronautical Engineering, with studies in Space Facilities,
at the Air Force Institute of Technology.

First Lieutenant Martin is the son of Mr. and Mrs.
Robert L. Martin of Raleigh, North Carolina.  Mrs. Martin is
a free lance artist.  Mr. Martin is a Professional Engineer,
and he is currently the Associate Director of the North
Carolina Institute for Transportation Research and Education
of The University of North Carolina.

<div style="text-align: right;">

Permanent Address:  305 Merwin Rd.
Raleigh, NC  27606

</div>

| REPORT DOCUMENTATION PAGE | | | | *Form Approved*<br>*OMB No 0704-0188* |
|---|---|---|---|---|

| 1a. REPORT SECURITY CLASSIFICATION<br>UNCLASSIFIED | 1b RESTRICTIVE MARKINGS | | | |
|---|---|---|---|---|

| 2a. SECURITY CLASSIFICATION AUTHORITY | 3 DISTRIBUTION/AVAILABILITY OF REPORT |
|---|---|
| 2b. DECLASSIFICATION/DOWNGRADING SCHEDULE | Approved for public release;<br>distribution unlimited. |

| 4 PERFORMING ORGANIZATION REPORT NUMBER(S)<br><br>AFIT/GA/AA/88M-2 | 5 MONITORING ORGANIZATION REPORT NUMBER(S) |
|---|---|

| 6a. NAME OF PERFORMING ORGANIZATION<br><br>School of Engineering | 6b OFFICE SYMBOL<br>*(If applicable)*<br>AFIT/ENY | 7a NAME OF MONITORING ORGANIZATION |
|---|---|---|

| 6c. ADDRESS *(City, State, and ZIP Code)*<br><br>Air Force Institute of Technology<br>Wright-Patterson AFB, OH 45433-6583 | 7b ADDRESS *(City, State, and ZIP Code)* |
|---|---|

| 8a. NAME OF FUNDING/SPONSORING<br>ORGANIZATION (Continued)<br>Structural Concepts Branch | 8b OFFICE SYMBOL<br>*(If applicable)*<br>AFWAL/FIBC | 9 PROCUREMENT INSTRUMENT IDENTIFICATION NUMBER |
|---|---|---|

| 8c. ADDRESS *(City, State, and ZIP Code)*<br><br>Wright-Patterson AFB, OH 45433 | 10 SOURCE OF FUNDING NUMBERS | | | |
|---|---|---|---|---|
| | PROGRAM<br>ELEMENT NO<br>62201F | PROJECT<br>NO<br>2401 | TASK<br>NO<br>03 | WORK UNIT<br>ACCESSION NO<br>66 |

| 11 TITLE *(Include Security Classification)*<br><br>A Study of Failure Characteristics in Thermoplastic Composite Material |
|---|

| 12. PERSONAL AUTHOR(S)<br>Robert John Martin, 1Lt, USAF |
|---|

| 13a. TYPE OF REPORT<br>MS Thesis | 13b TIME COVERED<br>FROM _____ TO _____ | 14. DATE OF REPORT *(Year, Month, Day)*<br>88 March | 15 PAGE COUNT<br>235 |
|---|---|---|---|

| 16 SUPPLEMENTARY NOTATION |
|---|

| 17 COSATI CODES | | | 18. SUBJECT TERMS *(Continue on reverse if necessary and identify by block number)* |
|---|---|---|---|
| FIELD | GROUP | SUB-GROUP | Composite Materials, Gr/PEEK, APC-2, Test Method, |
| 11 | 04 | | Finite Element Analysis, Nonlinear Analysis, |
| 13 | 13 | | Failure Criteria. |

19. ABSTRACT *(Continue on reverse if necessary and identify by block number)*


Thesis Advisor: Dr. Anthony N. Palazotto

| 20 DISTRIBUTION/AVAILABILITY OF ABSTRACT<br>☒ UNCLASSIFIED/UNLIMITED ☐ SAME AS RPT ☐ DTIC USERS | 21 ABSTRACT SECURITY CLASSIFICATION<br>UNCLASSIFIED | |
|---|---|---|
| 22a NAME OF RESPONSIBLE INDIVIDUAL<br>ANTHONY N. PALAZOTTO, PROFESSOR | 22b TELEPHONE *(Include Area Code)*<br>513-255-3517 | 22c OFFICE SYMBOL<br>AFIT/ENY |

**DD Form 1473, JUN 86**          *Previous editions are obsolete.*          SECURITY CLASSIFICATION OF THIS PAGE

8a. (Continued)
   Structures Division
   Flight Dynamics Laboratory
   Air Force Wright Aeronautical Laboratory
   Air Force Systems Command

ABSTRACT: Space facilities in the next decade will require applications of highly advanced materials which have properties exhibiting excellent fracture toughness and high strength-to-weight ratios. The recently introduced thermoplastic composite material, graphite polyetherether-ketone (Gr/PEEK) APC-2, promises lower costs, lower part weight, and higher operating temperatures. This new class of organic material has fracture toughness properties superior to those graphite epoxy. This thesis examines the failure characteristics of Gr/PEEK through an experimental investigation and through the application of fully nonlinear ply-by-ply finite element technique. Laminates investigated were 0 and 90° unidirectional lay-ups and ±45° angle-ply lay-ups. An experimental investigation was also done on [0/45/90/-45] and [0/±45/90] quasi-isotropic lay-ups to study failure characteristics.

The experimental investigation of Gr/PEEK APC-2 involved the testing of 34 tension and compression coupons to derive basic material properties for use with the finite element program. To investigate failure characteristics experimentally, 79 tensile specimens were manufactured with 0.4-inch diameter holes. A portion of these unidirectional, shear, and quasi-isotropic specimens where tested at room temperature for ultimate strength. The remaining specimens were tested to percentages of average failure stress to investigate the initiation and progression of laminate failure. To supplement the test results, two post-failure analyses were conducted. Videotapes were made of each test to ultimate strength. Also stereo x-rays were taken of each test specimen subjected to a percentage of failure load.

For comparison to experimental results, a fully nonlinear progressive-ply-failure finite element program was employed. The models of stress-strain responses and growth of failure were found to closely approximate the results of the experimentation.

This investigation provided further data on the application of tensile loads to Gr/PEEK containing circular discontinuities. This study also proved that a nonlinear finite element program can closely approximate progressive ply failure in a Gr/PEEK laminate. The excessive nonlinearity of this material proved the need for using nonlinear techniques when analyzing laminates of Gr/PEEK. Furthermore, this research reinforced the proposition that the thermoplastic matrix does produce a reliable composite that should be considered for use on aircraft, spacecraft, and space facilities.

DATE
FILMED
58